THE UNIVERSITY OF CHICAGO

THE GUT MICROBIOME SHAPES THE TUMOR MICROENVIRONMENT BY TUNING INNATE IMMUNITY

A DISSERTATION SUBMITTED TO

THE FACULTY OF THE DIVISION OF THE BIOLOGICAL SCIENCES

AND THE PRITZKER SCHOOL OF MEDICINE

IN CANDIDACY FOR THE DEGREE OF

DOCTOR OF PHILOSOPHY

COMMITTEE ON CANCER BIOLOGY

BY

JESSICA LYNN FESSLER

CHICAGO, ILLINOIS

MARCH 2021

TABLE OF CONTENTS

LIST OF FIGURES

LIST OF TABLES

Supplementary Files

Supplementary tables may be found online.

Table S1. Baseline patient characteristics in responders vs. non-responders.
Table S2. Significant 16S results.
Table S3. Complete BLAST search results.
Table S4. Agreement between different sequencing and taxonomic assignment methods for significant bacterial species.
Table S5. Primers and conditions for bacterial species specific qRT-PCR and results.
Table S6. Significant bacterial species determined by metagenomic shotgun sequencing.

ACKNOWLEDGEMENTS

I owe a great deal of gratitude to many for their direct and indirect scientific contributions to the data presented here, as well as countless others for their help shaping my professional and personal development without whom none of this would be possible.

First and foremost, I thank my thesis advisor and mentor Thomas Gajewski. Your guidance was helpful navigating graduate school, which can at times be an isolating and disparaging process. The confidence you inspired in me through our thoughtful discussions and the credibility with which you listened to my ideas early in my career was instrumental in my growth. You have a knack for encouraging optimism when I doubted a path forward. I am grateful for the way in which you helped shape my scientific thinking, how to approach problems, and how to present data and craft a compelling story. These skills are invaluable, and I am fortunate to have learned from one of the best.

To the rest of the Gajewski lab, your intelligence, diligence, and willingness to help has created an incredible environment to work in. To past members Stefani, Brendan, and Jay, I will forever be indebted to you for donating your time and energy to help train me. To my fellow graduate students, Kyle, Blake, Emily, and Alex, you make coming to lab fun. I think of you all as lifelong scientific colleagues and friends. To Vyara, thank you for the late nights, long meetings, and willingness to work together these past years. Your help has been instrumental in what we have been able to accomplish, and I am very thankful for our teamwork. To Shuyin and Andrea, thank you for keeping me smiling in lab. To the clinical fellows, Athalia, Sherin, and Jonathan, thank you for your expertise, and especially for your tremendous undertaking leading a COVID-19 project during a global pandemic. I will always be grateful for how our lab responded to help during crisis. To Yuanyuan for your important contributions in the Human Immune Monitoring

core. To Riyue Bao, thank you for your hard work and computational guidance as I forayed into unknown territory with my own data analysis.

I also extend a special thanks to members of the Alegre lab, in particular Kevin Lei, Christine McIntosh and Martin Sepulveda. Your thoughtful questions and generous help with microbiome related endeavors has always been appreciated.

To the Committee on Cancer Biology, including its faculty, students, and administrators, I thank you for providing a fertile training ground and inclusive environment. A special thanks to Kay Macleod, who I credit with a large part of my decision to attend the University of Chicago. Thank you, Kay, for your commitment to the program. To the other faculty in CCB, thank you for your time and effort spent instructing classes and ensuring a strong didactic foundation. To my fellow CCB classmates, thank you for your camaraderie and your steadfast help over the years together.

To the Committee on Immunology, I am thankful for the rigorous training environment you have established. I have benefitted greatly from the COI's institutional commitment to excellence and my inclusion in your community. My gratitude extends to the COI faculty and staff, from whom I have all learned a great deal from, and who have elevated my research pursuits.

To my thesis committee members, past and present, thank you for your critical insight. To my committee chair, Cathy Nagler, thank you for your generosity with ideas and resources. To Justin Kline, thank you for your pointed questions and thorough evaluation. To Marisa Alegre, thank you for your always discerning eye, and for your guidance navigating academia. To Jeff Hubbell, thank you for your kindness and added translational expertise.

A big thank you to the many University of Chicago core facilities whose often thankless work facilitates the execution of important biomedical research. Thank you to Dr. Pieter Faber,

Sandy Arun, and the University of Chicago Genomics Core. Thank you to Laura Johnston, David Leclerc, and the rest of your team for your above and beyond efforts to ensure the smooth operation of the Cytometry and Antibody Technology Core Facility.

Thank you to the University of Chicago Animal Resource Center. Animal research has become a cornerstone of impactful biomedical research, and I feel great responsibility in conducting this research in a meaningful and ethical manner. I am incredibly appreciative of all that you do to support the humane treatment of research animals and extend my thanks to the technicians and veterinarians in GCIS. A special thank you to Dr. Betty Theriault and her team that works in the Gnotobiotic Research Animal Facility. This project has required often unconventional techniques and approaches, and your willingness to offer input and adapt protocols to advance the science has been extremely appreciated.

Thank you to my funding sources, the University of Chicago Cancer T32 Training grant, and the National Cancer Institute for the Predoctoral to Postdoctoral Fellow Transition Award (F99/K00).

Prior to my study at the University of Chicago, are research mentors who I am obliged to for their training and for encouraging my scientific pursuit. Namely, thank you to my undergraduate mentor, Jing Ge, and PI, Bevin Engelward. Also, thanks to my very first research mentor, Kamila Naxerova, for your patience.

Lastly, I must acknowledge all those in my life outside the ivory tower that have had an important part in my success. Thank you to the close friends I've made during my time in grad school, for our conversations about science, grad school, life, and everything in between—especially to Ryan, my rock during it all. And thank you to my family, for your endless love and support throughout this journey. I love you all more than I will ever be able to express.

ABSTRACT

Immune checkpoint blockade has revolutionized cancer treatment but has only benefited a subset of patients. Among the variables that could contribute to interpatient heterogeneity is differential composition of the patients' microbiome, which has been shown to affect anti-tumor immunity and immunotherapy efficacy in preclinical mouse models. We began by investigating whether there is an association between response to anti-PD-1 therapy and the composition of the gut microbiome (Chapter 3). We analyzed baseline stool samples from metastatic melanoma patients before immunotherapy treatment through an integration of 16S ribosomal RNA gene sequencing, metagenomic shotgun sequencing, and quantitative polymerase chain reaction for selected bacteria. A significant association was observed between commensal microbial composition and clinical response. Reconstitution of germ-free mice with fecal material from responding patients could lead to improved tumor control, augmented T cell responses, and greater efficacy of anti-PD-L1 therapy. These results suggest that the commensal microbiome may have a mechanistic impact on anti-tumor immunity in human cancer patients. Next, we explored the cellular mechanisms responsible for variable responses to cancer immunotherapy using mice stably colonized by patient commensals (Chapter 4). We rigorously evaluated the tumor immune infiltrate in representative responder and non-responder models using single cell gene expression, flow cytometry and functional tests to identify the source of resistance to immune checkpoint blockade. We found that variable tumor control with anti-PD-L1 was $CD8^+$ T cell-dependent, and likely stemmed from distinct activation states of myeloid cells within the tumor microenvironment. Collectively, these results illustrate how the gut microbiome can impact the tumor microenvironment by tuning innate immunity and offer direction for future studies investigating the link between commensal bacteria and immunotherapy efficacy in patients.

Chapter 1: Introduction

1.1 The battle between cancer and the immune system

Immune evasion as a hallmark of cancer

As the second-leading cause of death worldwide, the term "cancer," is as menacing as it is ambiguous. In its most general definition, cancer is the unchecked growth of transformed cells. Underneath the umbrella that encompasses cancer are more than 30 organ subtypes, which can be further categorized by morphology and molecular characteristics. Despite the many different types of malignancies within the broader definition of cancer, there are certain shared principals which define cancer and are central to its initiation and growth. Weinburg and Hanahan succinctly describe these unifying features as the hallmarks of cancer (1). Among these key pillars which unite the diverse landscape of cancer is its capacity to avoid immune destruction.

Every individual's immune system undergoes a unique, and highly regulated education process in order to distinguish between self and non-self. This education serves as the foundation for our immune system to recognize and attack foreign entities, such as pathogens, while remaining passive, or tolerant, to our own cells in the many forms that they take. Cancer occupies territory between the ends of the spectrum "self" and "non-self," and has been described as "altered self" (2). Through the transformation process, cancer cells acquire genetic alterations which drive its uncontrolled proliferation. While the origin of cancer is "self," these mutations lead to novel proteins which our immune system has not been educated to ignore, thus marking cancer cells as a target for elimination. Therefore, as a central tenet to cancer progression, cancer cells must find a way to evade immune detection and destruction.

Tumor cells avoid eradication by the immune system via multiple mechanisms. Among the many mechanisms is the elimination of MHC class I, the surface molecule through which cells

present peptides which distinguish themselves as “self” or “non-self”. Deletion or downregulation of this molecule can render the cancer cell invisible to cytotoxic T cells which sense and eliminate foreign entities presented by unfamiliar peptide MHC-I complexes. To safeguard against such acquired advantages that cancer cells develop are natural killer (NK) cells, which seek out and destroy cells which lack MHC-I, a key signal of “self”. In this way, the immune system has multiple mechanisms by which to distinguish detrimental cells within the body. The cancer cell, however, with genomic instability and a growth advantage inherent to its genesis, can continually develop new means to evade immune detection. For example, to avoid NK cell detection, cancer cells can upregulate molecules which engage negative regulatory receptors on NK cells to impede their function (3).

In this evolving back and forth battle between cancer and the immune system, cancer cells which are readily recognized by the immune system are thought to be eliminated, while those that have circumvented identification persist and multiply. Through this course, cancer cells evolve and expand based on their proliferative advantage and avoiding immune detection. This process, termed “immunoediting” can result in cancer cells with low immunogenicity, through a combination of low to no expression of peptide MHC ligand, adhesion molecules, or co-stimulatory signals necessary to mount an effective immune response (4). Other means by which cancer cells avoid immune recognition include tumor-induced immune suppression. Factors expressed by the tumor cells can directly inhibit T cells or induce other suppressive cell types (described in greater detail below). Tumor cells can also produce factors which help create a physical barrier to prevent immune infiltration. Through these different methods, cancer has numerous means to outmaneuver the immune system.

The cancer immunity cycle

Regardless of the cancer subtype, the immune response to cancer follows a common pattern. This cancer-immunity cycle has been articulately summarized by Chen and Mellman (5). The cycle begins with the release of cancer cell antigens, likely due to cancer cell death. This facilitates the uptake and presentation of tumor-derived antigen by antigen presenting cells (APCs), particularly dendritic cells (DCs), in the tumor microenvironment. APCs then carry their tumor cargo to the tumor draining lymph node (tdLN) where they will prime and activate T cells capable of recognizing tumor antigens. $CD103^+$ DCs have been identified as the main cell type responsible for carrying tumor antigens from the tumor to the tdLN (6). After T cells have been primed within the lymph node, they will then traffic to and infiltrate the tumor. Once within the tumor, T cells will recognize cancer cells and exert their cytotoxic function to kill tumor cells. During this period, known as the effector phase, T cells receive additional positive signals from APCs which support their survival and cytotoxic function. Through this process, the innate and adaptive immune system cooperate to generate a strong and specific immune response. In the face of this anti-tumor immune response are numerous immune-inhibitory elements present in the tumor microenvironment which attempt to subvert anti-cancer immune control.

Role of negative mechanisms in the tumor microenvironment

One of the ways which anti-tumor immunity can be hindered is through an immune suppressive environment. Tumor cells can directly suppress immune responses through the cancer-cell intrinsic production of inhibitory factors, such as IL-10, TGF-β and Indoleamine 2, 3-dioxygenase 1 (IDO1), or via the activation and recruitment of other suppressive cells (7, 8). Immune cells in the tumor microenvironment can have both pro- and anti-tumor functions. Furthermore, certain immune cell types can have opposing roles depending on their activation

status and tumor context. For example, tumor-associated macrophages, or TAMs, have been both positively and negatively associated with tumor progression and outcome (9). This is in large part due to the plastic nature of macrophage differentiation states. Depending on the combination of environmental signals, macrophages can assume different states of polarization. While there have been many macrophage phenotypes described in various disease contexts, traditionally macrophage polarization is defined by the states "M1" and "M2" which occupy opposite ends of the macrophage spectrum. These states are related to the cytokines which induce the analogous Th1 and Th2 T cell states, respectively (10). Important to the cancer context, M1 TAMs are generally considered to have greater tumoricidal potential and generally be anti-tumor (11). In contrast, M2 macrophages, also called alternatively activated macrophages, tend to be associated with immune suppression, and produce immune inhibitory cytokines TGF-β and IL-10. M2 TAMs, therefore, are typically considered pro-tumor (11).

Neutrophils in the tumor microenvironment have been similarly described as having either pro- or anti-tumor function (12). Neutrophils are the most abundant circulating leukocytes in humans and are one of the first responders to tissue damage and inflammation (13). In the context of cancer, neutrophils have recently come under greater scrutiny in part due to observations that an elevated neutrophil to lymphocyte ratio is associated with more advanced disease in various types of cancer (14). Despite this general negative association, neutrophils are plastic, and can have either anti-tumor or tumor-promoting characteristics. Neutrophils can directly kill cancer cells by generating reactive oxygen species (ROS), as well as through antibody-dependent cell-mediated cytotoxicity (15, 16). In contrast, neutrophils can also receive external stimuli which can cause them to adopt immune-suppressive features. These immune-inhibitory neutrophils are called granulocytic myeloid-derived suppressor cells (G-MDSCs). G-MDSCs can suppress tumor

immunity by recruiting other immune suppressive cells (17) and are capable of directly suppressing T cell proliferation through the production of Arginase 1 (Arg1) and proteinase 3 (P3) (18, 19).

In addition to cancer cell-extrinsic modes of immune cell suppression, cancer cells can also directly dampen the anti-tumor immune response. One process is through the expression of ligands for immune-inhibitory receptors, including immune checkpoint molecules, which is expanded on below. Collectively, many negative signals, either originating from the tumor directly, or induced within the tumor microenvironment, act in concert to create a hostile environment that is unconducive to a robust anti-tumor immune T cell response. An immune system which is losing an on-going battle with cancer, however, can be reinvigorated if the relevant functional barriers are overcome. This approach of harnessing the power of the immune system to fight cancer is known as "cancer immunotherapy". Among the leading interventions developed are antibodies which target the aforementioned immune checkpoint molecules, referred to as immune checkpoint blockade (ICB).

1.2 Cancer immunotherapy: Successes and shortcomings

Introduction to immune checkpoint blockade

The primary strategy behind ICB is to interrupt immune inhibitory interactions on T cells that impair the anti-tumor response using antibodies specific for these receptors. During a typical immune response, such as against a pathogen, regulatory molecules known as immune checkpoints are induced following the initial pro-inflammatory signals to act as negative feedback to T cells. This process ultimately dampens the T cell response to keep adaptive immunity in a carefully regulated state. Within the tumor microenvironment, these immune-inhibitory signals are co-opted

to restrict T cell proliferation and function. The T cell inhibitory receptors that have been most comprehensively studied in cancer are CTLA-4 and PD-1.

CTLA-4 expression is tightly linked to T cell activation and increases following T cell receptor engagement (20, 21). CTLA-4 limits further T cell activation via competitive inhibition of CD28, a costimulatory molecule which interacts with CD80 and CD86 on APCs. In addition, CTLA-4 is highly expressed on $CD4^+$ T regulatory cells (Tregs). Tregs are essential for maintaining tolerance under homeostatic conditions, but in the tumor Tregs suppress the activity of anti-tumor cytotoxic T cells. Antibodies which target CTLA-4 can bind to and block CTLA-4, freeing CD28 to continue receiving positive co-stimulatory signals, and can additionally deplete Tregs via antibody-dependent depletion (22, 23).

PD-1 acts principally to diminish T cell activation within inflamed tissues, and its upregulation on T cells is associated with prolonged antigen stimulation and activation (24). Its ligands, PD-L1 and PD-L2, are expressed by many nonlymphoid tissues and immune cells, and are often upregulated within the tumor microenvironment (25). PD-L1 expression is typically induced in response to inflammatory cytokines such as IFN-γ, and so PD-1/PD-L1 regulation tends to occur in response to activated T cell function (26). Antibodies which target either the T cell receptor, PD-1, or its ligands function to block this immune-inhibitory interaction. This can block PD-L1/PD-L2 signals delivered by tumor cells, as well as by other APCs in the tumor microenvironment.

Clinical success of anti-PD-1 and anti-CTLA-4 antibody therapy

As a testament to the importance of these molecules, Dr. James Allison, and Dr. Tasuku Honjo were awarded the Nobel Prize in medicine in 2018 for their scientific contribution studying CTLA-4 and PD-1, respectively. Since their discovery, numerous antibodies which block the

activity of these receptors have been developed and tested clinically. Less than 10 years ago the first antibody targeting CTLA-4 was authorized for cancer treatment, followed quickly by antibodies against PD-1/PD-L1. The clinical results since their advent have been remarkable. Unlike anything observed with traditional chemotherapy or targeted agents, patients that received ICB experience durable responses, in some cases resulting in complete tumor shrinkage and leaving patients tumor-free (27). ICB has subsequently more than doubled the five-year survival rate for metastatic melanoma patients, extending the median overall survival to more than 60 months with the combination treatment of anti-CTLA-4 and anti-PD-1 (28). As proof of ICB's success, T cell-targeted immunomodulators are now used as a single agent or in combination as first or second lines of treatment in over 15 cancer types (29).

Despite the rapid adoption of cancer immunotherapy and its success, a majority of patients still fail to respond to treatment. In metastatic melanoma, which has reaped some of the greatest benefits from ICB, 42% of patients fail to achieve an objective response (28). Among other cancer indications, the response rate is even lower, or offers no tangible benefit at all (30). The capability of the immune system to recognize, attack, and eliminate tumors is undeniable, and the success of ICB only begins to scratch the surface of strategies which can untap immune potential. Key to devising the next generation of cancer immunotherapies will be a deep understanding of the biology which keep the anti-tumor immune response in check.

Tumor heterogeneity related to immune checkpoint blockade efficacy

The reasons underlying the limited success for ICB are varied, but is largely related to tumor heterogeneity, or the incredible diversity within and between tumors—particularly between individual patients. Tumor heterogeneity is responsible for not only the limited success of cancer immunotherapy but underlies many of the challenges associated with treating cancer generally. As

described, the cancer cells present within one tumor can vary genetically and phenotypically. While a select few mutations are essential for the initial oncogenesis and establishment of the tumor, additional mutations will confer further survival advantages. This molecular heterogeneity, as described earlier, is a key feature of cancer and enables its evolution to avoid immune detection. In addition to the intra-tumor heterogeneity, there is significant inter-tumor heterogeneity (31). This occurs both between tumor sites in a given patient, but more importantly between individual patients. In the latter case, heterogeneity additionally exists at the level of the host. This large degree of variability is a large part why one therapeutic approach is unlikely to be universally effective.

Within the tumor microenvironment lies a complex cellular milieu including cancer cells, immune cells, and stromal cells. The identity and role of the immune cells vary considerably across different tumor types, between different patients, and even within the same patient but across two cancerous lesions. Variability in the composition of the tumor microenvironment, including variable immune cell infiltration, has been linked with prognosis as well as response to therapy (32–34). For example, patients which have evidence of a strong $CD8^+$ T cell response tend to have better overall survival (32). More nuanced details regarding immune infiltration and outcome, however, are often cell type- and cancer type-specific (9, 34). These findings underscore the importance of understanding both the means of immune control and cancer immune escape in order to improve cancer treatment strategies.

One of the central concepts which has emerged related to the efficacy of ICB, is that the degree of tumor T cell infiltration is strongly associated with response (33, 35). This observation is consistent with expectations that tumors with an established immune cell infiltration, the function of which is kept in check by inhibitory mechanisms such as PD-L1, can be reinvigorated

with ICB resulting in cancer cell killing and tumor shrinkage. In contrast, in tumors that lack an existing immune presence, the addition of ICB offers little benefit. Therefore, it becomes essential to understand the factors which regulate the degree of spontaneous immune cell infiltration into tumor sites. There are many possible sources of variability which could lead to an immunologically non-inflamed, or "cold", tumor microenvironment. Each possible cause of immune exclusion represents an opportunity for future therapeutic interventions or companion treatments alongside ICB.

Factors which contribute to the composition of the tumor microenvironment can generally be categorized as either tumor cell-intrinsic or -extrinsic. Intrinsic to the cancer cells is the expression of neoantigens, which may induce varying degrees of immune response based on their immunogenicity (36). In addition, certain oncogenic signaling pathways in tumor cells have been clinically associated with T cell exclusion, and were experimentally shown to have negative consequences on anti-tumor immunity (37). Examples include activation of β-catenin and c-Myc, and loss of PTEN among others (38–40). Variables external to the tumor cells and likely to impact on the tumor microenvironment include germline genetic variants. Previous studies in cancer patients have found HLA class I genotype influences response to ICB (41). There have also been associations between ICB response and genetic risk variants which had previously been linked to autoimmunity (42).

Additionally, environmental factors, such as diet, exercise, and history of infection or vaccination have the potential to alter tumor immune infiltrate. Diet is known to be related to cancer initiation and development, and dietary patterns can affect immune function (43, 44). Preliminary data in patients treated with immunotherapy found that patients who consumed a high-fiber diet were nearly five times more likely to respond to ICB (45). Increased exercise through

voluntary running in a mouse model was shown to reduces tumor incidence and growth by increasing NK cell infiltration (46). Within this broad class of external environmental factors is the composition of the gut microbiome.

The term “gut microbiome” encompasses all the microbes which live within the intestine. The gut is a key site for immune regulation. Within this site, the immune system must be poised to recognize and respond to pathogenic invaders while simultaneously maintaining homeostasis in the presence of innocuous food antigens and commensal bacteria. This balance between immune surveillance and tolerance can rapidly change in response to shifts in the microbiota. These changes originating at the gut can then subsequently influence systemic immunity and affect extra-intestinal disorders (47). Therefore, the microbiome is key to setting the overall immune tone and can play an important role in the anti-tumor immune response. The contribution of the gut microbiota on anti-tumor immunity, and its ensuing effect on ICB efficacy, will be the focus of this thesis.

1.3 Immunity and the gut microbiome

Introduction to the gut microbiome

The human body is a complex ecosystem inhabited and influenced by an abundance of microorganisms including bacteria, yeast, fungi, protozoa, archaea, and viruses, all of which collectively constitute the commensal microbiota. The commensal microbiota and the human host have co-evolved in a mutualistic relationship, in which each benefits the fitness of the other and the two can be collectively viewed as a superorganism. Much recent research has focused on the bacterial component of the microbiota. On average, a healthy human body is comprised of approximately 30 trillion cells and is inhabited by approximately 39 trillion bacterial cells (48). The collection of genes within the commensal microbiota is defined as the commensal microbiome

and vastly outnumbers human genes. The microbiota is capable of synthesizing or transforming a wide variety of metabolites, including hormones, essential vitamins, and other bioactive compounds, which cannot be otherwise acquired by the host (49). These metabolites can modulate various biological functions, most notably the immune and nervous systems (50). Alterations in the normal microbiota have been reported to contribute to the development of many diseases (51–62). In the cancer context, some specific bacteria have been demonstrated to be involved in the process of carcinogenesis (62).

Next generation sequencing methods in microbiome studies

Culturing of bacterial strains has been central to classical microbiology and has enabled the study of individual pathogens and some commensal bacteria. For most commensal bacteria, culture methods had not been optimized for their in vitro isolation and study. With recent improvements in methodology, a large proportion of commensal bacteria is now considered culturable (63, 64). *Culturomics* is a strategy which incorporates multiple culture conditions, coupled with MALDI-TOF mass spectrometry and/or 16S ribosomal RNA (rRNA) or total genome sequencing for bacterial identification (65, 66). This high-throughput approach can enable isolation and identification of commensals for further manipulation and mechanistic studies.

The most common method for taxonomic characterization of complex bacterial communities is based on selective amplification and sequencing of part of the gene encoding the 16S rRNA, part of the small ribosomal subunit in prokaryotes. This is a ubiquitous 1.5 kb gene, containing conserved sequences and hypervariable regions (nine regions: V1-V9), the latter being useful for bacterial taxonomic classification, as originally described by Woese and colleagues (67). In the first step of this technique, a pair of universal primers targeting conserved sequences flanking a hypervariable region are used to generate an amplicon library, which is then sequenced.

To account for sequencing errors, amplicons which share sequence similarity above a certain threshold are grouped into operational taxonomic units (OTUs). A representative amplicon is selected from each OTU bin and assigned a taxonomic identity based on cross-referencing to pre-existing databases (68–70). All other amplicons in the OTU are also assigned the same identity. Thus, OTU binning can artificially decrease the observed diversity of a microbial community (71) and alternative methods for analysis have been proposed (72–74). Because bacterial identification is based on a portion of the 16S rRNA gene, species-level resolution is usually not feasible with this method and identification is typically limited to family or genus level (75). Another consideration in 16S analyses is that most bacteria contain multiple copies of the 16S rRNA gene, which can lead to inaccurate quantitation of bacterial cells (76). Additional bias can be introduced in the amplification step, depending on the choice of primers. Despite these limitations, the low cost and high-throughput potential of this technique make it the most commonly used for initial descriptive data.

Metagenomic shotgun sequencing generates short reads representing the whole genomic content within an environmental sample and is considered less biased than 16S rRNA gene amplicon sequencing, because it does not contain a PCR amplification step. However, this can result in contamination with human genomic DNA and requires higher sequence coverage to detect bacterial species of low abundance. This necessitates additional data storage, computing power, and more sophisticated analysis pipelines. Errors can also be introduced in the downstream analysis at the step of genome assembly or gene prediction (77). Various bioinformatic tools have been developed for metagenome assembly, and databases have been established for gene prediction, but there is no consensus on the best strategy (78). Compared to 16S rRNA gene amplicon sequencing, superior resolution down to species- and strain-level identity is feasible with

shotgun sequencing because multiple marker gene sequences are used for taxonomic annotation (75). This approach can also be used to characterize non-bacterial compartments of the commensal microbiota, including archaea, fungi, or viruses. Another advantage of shotgun sequencing is that it can be used for characterization of the functional capacity encoded by the microbiome using gene prediction tools and databases (78). By contrast, functional capacity can only be inferred indirectly from 16S rRNA amplicon sequencing data (79–81). Each of these sequencing methods has its limitations, but the two can be integrated to improve the accuracy of bacterial identification and quantitation (as described in Chapter 3).

Immune homeostasis and the gut microbiome

The role of the commensal microbiota in modulating host physiology becomes particularly evident when conventionally raised specific pathogen-free (SPF) mice are compared to germ-free (GF, axenic) mice. GF mice are defined as devoid of detectable microbiota during their life. The term gnotobiotic pertains to animals with known (defined) microbiota composition and encompasses GF, as well as ex-GF animals colonized with defined microbial communities. The commensal microbiota broadly impacts host physiology, and this has been mainly shown in studies with GF mice, which have inefficient energy extraction from the diet, abnormal fluid balance and electrolyte status, and disturbances in liver, lung, cardiovascular system, endocrine organ, nervous system, and immune system functions (82, 83).

The gut microbiome and systemic immunity

Systemic innate immune modulation is also influenced by the commensal microbiota, with multiple lines of evidence indicating stimulatory effects on myelopoiesis at the level of granulocyte-macrophage progenitors in the bone marrow and in the periphery, as well as on the

function of DCs, macrophages, and neutrophils (reviewed in (84)). In many cases, these systemic effects have been attributed to circulating bacteria-derived molecules (microbe- or pathogen-associated molecular patterns, MAMPs and PAMPs, respectively), such as lipopolysaccharide (LPS), peptidoglycan, or flagellin, which when recognized by pattern-recognition receptors (PRRs) on innate immune cells, can signal via a MyD88-dependent pathway to enhance systemic innate immune cell responsiveness (84). Bacterial metabolites, such as short-chain fatty acids (SCFA), the products of dietary fiber fermentation by the microbiota, have been implicated in stimulating DC generation in the bone marrow and their phagocytic capacity (85). Systemic adaptive immunity is also stimulated by the presence of commensal bacteria, particularly the proper development of distant (non-mucosal) lymphoid tissues, such as the spleen and peripheral lymph nodes. This is evidenced by the poorly developed B cell follicles and T cells zones in these organs in GF mice, leading to decreased IgG levels in the serum (86, 87). Commensal bacteria are also required for proper programming of the Th1/Th2 balance and in GF mice there is a bias towards Th2-type allergic responses, which can be corrected by colonization with commensal bacteria (88).

Specificity of microbiota-mediated immune programming

Different members of the commensal microbiota are not equivalent in their capacity to polarize T cell responses. For instance, in SPF mice the group of segmented filamentous bacteria (SFB), which colonize the mouse terminal ileum and adhere to the epithelial cells, are particularly potent inducers of Th17 cell differentiation (89). SFB are not found within the human microbiota, but further studies have shown that other bacteria derived from human fecal samples are also capable of adhering to the epithelial layer and inducing Th17 cells when transferred to mice (90–92). By contrast, Treg differentiation and function are strongly induced by *Bacteroides fragilis*

(93) and *Clostridium* clusters XIVa, IV, and XVIII (94, 95). Polysaccharide A (PSA) from the capsule of *B. fragilis* can polarize towards Th1-type responses (88). Higher Bacteroidetes/Firmicutes ratio resulting from high-fiber diet increased the levels of circulating SCFAs and alleviated Th2 cell-mediated allergic airway inflammation by reducing the capacity of lung-resident DCs to drive Th2-type responses (85). Monocolonization of GF mice with 52 different human commensal bacteria demonstrated that most of the species were capable of inducing alterations in the frequency and function of immune subsets within the intestinal lamina propria (LP), Peyer's patches, mesenteric lymph nodes (MLN), and spleen. Some more notable effects were alterations in cytokine production in the LP and in frequencies of Treg, pDC, $CD103^+$ dendritic cells (DCs), macrophages and mononuclear phagocytes (92). Notably, many species were able to translocate to the MLN and spleen (92). This is likely an artifact of the model, due to the poor intestinal barrier function in GF mice, or an artifact of their isolation and culture methods. Therefore, the mechanisms leading to the observed alterations in immune cell subset composition, especially those seen systemically, may not in all cases reflect the physiological state.

Mouse models to study the gut microbiome and immunity

SPF mice have been used to gain valuable insight in the impact of microbiota-host interactions on host physiology in health and disease. When it comes to clinical translatability, a question arises regarding the degree of similarity between the microbiomes of humans and laboratory mice. Although a direct comparison between datasets from different studies can be blurred by differences in analysis platforms and protocols, a general consensus exists that on a phylum through family level, the microbiomes of SPF mice and humans are similar with both species being predominantly colonized by Bacteroidetes and Firmicutes (96, 97). Comparison between datasets on a deeper taxonomic level is challenging because of limited representation of

microbial genes in the current databases causing difficulties with genus, species, and strain level annotation. A study comparing microbial metagenomes of humans and SPF mice of different genetic backgrounds and housed in different facilities showed that only 4% of microbial gene sequences were shared between humans and mice. Despite that discordance, functional annotation of the mouse and human microbiomes using the KEGG database revealed that 85% of the annotated gene orthologs were shared between mouse and human microbiomes (98). Therefore, the murine organism as a host appears to have similar functional requirements for the commensal microbiota, which makes it an appropriate recipient of human microbiota for studying its effects on host physiology. A high value of GF mice in microbiome research is their utility in generating purely human microbiota-associated mouse models for studying microbe-host interactions and demonstrating causal effects of the microbiota on the health/disease states of the host. Indeed, successful transfer of microbiota from humans to GF mice often imprints the human health phenotype onto the murine recipient. Importantly, transfer of human commensals to mouse recipients typically results in stable engraftment of some, but not all, human-associated microbes. This incomplete fidelity of transfer may result from loss of bacterial viability in the storage or transfer process, or due to host-incompatibility stemming from differences such as diet.

GF mice have many physiological defects, which can become a confounding factor in microbiome studies. Notably, due to compromised intestinal barrier function and immature immune system in GF mice, microbial colonization could result in systemic translocation and abnormal microbe-host interactions (92). A more physiologically relevant mouse colonization would be the acquisition of experimental microbiota from the mother at birth. Thus, the offspring from mice artificially colonized by gavage (or ex-GF mice) can be used for experimentation. It has been shown that the microbiota from artificially colonized or ex-GF mice bred in an isolator can

be vertically transmitted to generations F1 and F2 without significant drift between generations (99). The use of such offspring mice could also capture effects of microbiota-mediated epigenetic immune programming occurring in utero. In addition to proper guiding of immune system maturation, such natural colonization of offspring mice with a functionally complex microbiota could eliminate other confounding factors such as the metabolic and endocrine abnormalities characteristic of GF mice. Therefore, an important experimental tool is to generate gnotobiotic mouse colonies maintaining a stable and defined microbiota derived from individual human subjects, functionally recapitulating the complex SPF microbiota and normalizing mouse physiology (100). Towards this goal, it has been shown that a small number of culturable bacterial strains can cover most of the functional potential of the gut microbiome (101, 102). Individual strains of interest can then be introduced and their immunomodulatory roles can be studied in the context of more physiologically relevant conditions (102).

1.4 The role of the gut microbiome and anti-tumor immunity

Preclinical evidence that commensals impact tumor growth via immune-dependent mechanisms

Multiple preclinical studies support that gut microbes can profoundly influence the potency of immunotherapy and some chemotherapies with immunostimulatory functions (103–107). Pioneering work in this field found that in mice, intestinal microbiota was essential for optimal responses to CpG-oligonucleotide immunotherapy which activates innate immune cells through TLR9 (105). Similarly, the gut microbiota was found to shape the anti-cancer immune response in a mouse tumor model by stimulating generation of a specific subset of “pathogenic” Th17 (pTh17) cells and memory Th1 immune response after treatment with immune-stimulatory chemotherapy cyclophosphamide (106). Initial evidence for the contribution of specific microbes to ICB, including CTLA-4 and PD-1/PD-L1 blockade, was demonstrated in mouse models (103,

104). *B. fragilis* was reported to enhance anti-CTLA-4 efficacy via a proposed mechanism involving the activation of Th1 cells with cross-reactivity to bacterial antigens and tumor neoantigens (104). Oral administration of *Bifidobacterium* increased tumor infiltration and IFN-γ production by $CD8^+$ tumor-specific T cells and improved both basal tumor control and anti-PD-L1 efficacy via a proposed mechanism involving increased activation of splenic and intratumoral DCs (103). These animal studies established the importance of the microbiome in cancer ICB therapy and inspired clinical pursuits to assess the microbiome's impact on anti-CTLA-4 and anti-PD-1/PD-L1-based therapies in patients.

Mechanisms by which the gut microbiome might impact on anti-tumor immunity

When it comes to exploring the possible mechanisms of microbiota-mediated modulation of anti-tumor immunity, two general questions arise. First, what is the nature of the messenger, which delivers a signal from the gastrointestinal tract to the tumor and/or tdLN? Such a messenger would be able to enter the circulation in order to access the distant tumor site and can be classified as either microbiota- or host-derived cell (live microbes or host immune cells) or molecule (MAMP/PAMP, microbial metabolite, or host cytokine). The second question is what is the nature of the immune effect that the messenger confers within the tumor? An immunosuppressive effect could be achieved by augmenting regulatory functions (Tregs, MDSCs, tumor-associated macrophages) or by directly inhibiting anti-tumor immunity; an immunostimulatory effect could be achieved by alleviating regulatory functions or by stimulating anti-tumor T cell responses (via antigenicity, adjuvanticity or bystander activation). The exact mechanisms of microbiota-mediated effects on tumor growth and efficacy of immunotherapy are only beginning to be understood.

Live bacteria or MAMPs/PAMPs as messengers

Commensal bacteria have been identified in extra-gastrointestinal tissues typically considered to be sterile. Notably, Geller et al. identified bacteria within the tumor microenvironment (TME) in human pancreatic ductal adenocarcinoma (108). In this study, viable bacteria were hypothesized to gain access to the cancerous lesions via a retrograde migration from the duodenum towards the pancreatic duct and were shown to decrease gemcitabine chemotherapy efficacy by metabolizing the active form of the drug. One comprehensive study analyzed over 1500 tumors and adjacent normal tissue across seven different cancer types and found that each tumor type has a distinct microbiome composition (109). Furthermore, intratumor microbial composition among metastatic melanoma patients was correlated with response to immunotherapy (109). In terms of impact on immune function, it was experimentally shown that bacterial translocation into the MLN and spleen generated a Th1 memory response specific to the translocated species (106). In the scenario of bacterial translocation, live bacteria gaining access to spleen, lymph nodes, or tumor may initiate a strong immune response by providing both foreign antigens and adjuvants (MAMPs/PAMPs). Consequently, tumor cell killing may ensue due to T cell cross-reactivity or bystander activation within the TME. Thus, commensals might bolster anti-tumor immunity through both augmented *antigenicity* as well as *adjuvanticity*, as described below.

Augmented antigenicity due to cross-reactivity to bacteria and tumor antigens

Some data suggest a mechanistic role for T cell epitopes shared between bacteria and tumor cells (104, 110, 111). Under this proposed model, cross-reactive T cells primed against bacterial antigens might exert anti-tumor effects either by providing help ($CD4^+$ T cells) or through direct killing ($CD8^+$ T cells). In a preclinical study, adoptive transfer of *B. fragilis*-reactive $CD4^+$ T cells conferred enhanced tumor control and restored anti-CTLA-4 efficacy in GF mice (104). Peripheral

immune cells isolated from patients receiving ICB treatment and assayed for in vitro T cell IFN-γ production following stimulation with certain bacteria showed an association with progression-free survival (PFS), whereas non-specific T cell activation with polyclonal activators demonstrated no relation to ICB response (110). Further supporting this notion, Balachandran et al. found intra-tumoral and circulating T cell clones with specificity to both neoantigens and predicted cross-reactivity with microbial epitopes (111).

Adjuvanticity of MAMPs/PAMPs

Microbiota-derived MAMPs or PAMPs can traverse the mucosal barrier and enter the circulation. For instance, serum from healthy individuals was demonstrated to contain stimuli capable of activating a range of TLR and NOD receptors (112). In the cancer context, bacterial LPS aberrantly entering the circulation following total body irradiation augmented the activity of adoptive T cell therapy in mouse models (107). Additionally, nucleic acids from bacteria have also been shown to act as natural adjuvants (113). In particular, the unmethylated CpG dinucleotides enriched in prokaryotes are potent activators via TLR9. These pro-inflammatory microbial products can trigger at least partial activation of innate immune cells such as DCs. Such conditioned APCs might possess enhanced capacity to prime anti-tumor T cells. Evidence for heightened DC activation stemming from distinct microbiome compositions was illustrated in Sivan et al. which showed that splenic DCs isolated from mice colonized with *Bifidobacterium* sp. showed superior priming of naïve $CD8^+$ T cells ex vivo (103). Enrichment in *Faecalibacterium* genus in patients with metastatic melanoma associated with responsiveness to ICB therapy was also associated with increase in antigen processing and presentation markers in the tumor (114).

Microbial metabolites as messengers

Gut bacteria produce various bioactive molecules as byproducts of their metabolism. These metabolites can exhibit diverse effects on the host, including modulating the immune system (115). SCFAs are one of the most extensively characterized classes of microbial metabolites known to shape host immunity (116). Through anaerobic fermentation, bacteria break down complex carbohydrates into SCFAs such as acetate, butyrate, and propionate. These metabolites are the primary energy source consumed by intestinal epithelial cells (117) and can also affect cytokine production (118), macrophage and DC function (85, 119), and B cell class switching (120). SCFAs can additionally act to inhibit histone deacetylases, facilitating Treg differentiation (121). By mimicking human signaling molecules, SCFAs can also act as ligands for G-protein coupled receptors (122). Other bacterial metabolites relevant to host immunity include retinoic acid and co-metabolites, such as polyamines and aryl hydrocarbon receptor ligands (123). These small molecules can impact immunity by acting as signaling molecules, epigenetic regulators, and metabolic switches and may ultimately shape anti-tumor immunity.

Given the predicted importance of bacterial metabolic contribution to host immunity and immunotherapy efficacy, there is significant interest in identifying both the specific bacteria exerting immune modulatory effects, as well as the functional and metabolic characteristics of these bacteria. To address this question, metagenomic and metatranscriptomic sequencing approaches coupled with metabolomic analysis of patient serum and stool samples will be critical for a more complete characterization of the biosynthetic pathways present within a given microbiome. Insights into metabolic contributions of the microbiome in the context of immunotherapy also may lead to new candidate therapeutic strategies, either through provision of desired metabolites as drugs, or via genetic manipulation of selected commensals for clinical administration.

Host cytokines as messengers

Another potential mechanism by which gut bacteria could modulate systemic immune responses is through local induction of soluble immunomodulatory factors that then disseminate systemically. Circulating cytokines may shift the activation threshold of key immune subsets within the TME or tdLN, thus leading to augmented adaptive immune responses in the context of immunotherapy. Candidate mechanisms include increased production of type I interferons, IL-12 and TNF-α, or decreased production of immune suppressive cytokines such as IL-10 and TGF-β. As an example, segmented filamentous bacteria can induce secretion of IL-22 from type 3 innate lymphoid cells in mice, causing production of serum amyloid A in the terminal ileum which, in turn, acts on the LP DCs to drive Th17 polarization (89, 124). In cancer models, oral administration of *Akkermansia muciniphila* improved the efficacy of PD-1 blockade in an IL-12–dependent manner in mice (110).

Innate immune cells play a key role in the gut-tumor immune axis

A recurring theme in many of the described mechanistic studies in mice is that innate immune cells, often DCs, represent the central cell type affected by perturbations within the commensal community (103–106, 125, 126). DCs are key microbial sensors that bridge innate to adaptive immunity and are also critical for molding T cell responses within the TME. Microbial signals might only need to function locally in the LP and MLN to drive DC function and the subsequent delivery of the immunomodulatory effect to the TME might be carried out by the DCs themselves or downstream by T cells. Various innate immune cells have been shown capable of exiting the intestinal LP and translocating to the spleen and peripheral lymph nodes under steady state (127).

Different mechanisms of microbial sensing by DCs might be in play in the context of a damaged versus intact intestinal barrier. Compromised barrier integrity could allow for translocation of live bacteria or microbial products into the circulation. These could then be recognized by PRRs on innate immune cells, such as DCs, and affect downstream innate and adaptive immunity. Such potential mechanisms may contribute to microbiota-mediated modulation of anti-tumor immunity in situations of gut inflammation, such as with total body irradiation, chemotherapy agents that cause mucositis, or with anti-CTLA-4 treatment where 11% of patients experience colitis and 34% develop diarrhea (128). However, anti-PD-1 therapy shows only 2% incidence of colitis (128), suggesting that additional mechanisms by which commensals shape host immunity likely exist. In the context of an intact barrier, mucosal DCs constantly sample bacterial-derived antigens via various mechanisms. For instance, a subset of DCs in the LP are reported to be capable of extending dendrites between epithelial cells to sample the lumen (129). DCs may also acquire proteins via goblet cell channels (130) or microfold cells (M cells) (131). Bacterial antigen-loaded DCs could induce immune tolerance to commensal bacteria, or they could prime bacterial antigen-reactive T cells, which in some instances might be capable of cross-reacting with tumor antigens (104, 110, 111) or in other cases might provide bystander help during anti-tumor responses. In this respect, understanding the mechanisms driving tolerogenicity vs. immunogenicity might provide insight into the mechanisms of microbiota impact on anti-tumor immunity.

Discovery opportunities in the gut microbiome and anti-tumor immunity

Despite a growing body of evidence supporting the importance of the gut microbiome and its impact on anti-tumor immunity, these observations raise key questions regarding its relative importance, as well as for the potential for translation to the clinic. Primarily, can the gut

microbiome affect immune responses in cancer patients, and if so, to what extent? Furthermore, if the microbiome can improve the response to ICB, what are the biological mechanisms involved? More precisely, what are the important microbial sources, immune cell types, and cellular sensors impacting anti-tumor immune responses via the gut microbiota? Lastly, if the impact of the microbiome holds true in cancer patients, does this represent a viable therapeutic strategy?

Given the complexity of the commensal-host interaction, the diversity of the microbiome, and inter-individual variability, it is likely that multiple mechanisms contribute to the impact of the microbiota on immunotherapy efficacy. Furthermore, the relative contribution of the microbiome will need to be integrated along with other dimensions affecting the potency of immunotherapy, including germline genetic determinants and tumor cell-intrinsic oncogenic alterations (38, 40, 132). Determining the relative contribution of all these factors and the most translatable aspects to human health will require careful experimental design in cancer patients to test hypotheses stemming from murine experiments.

Chapter 2: Materials and Methods

2.1 Patient fecal sample collection

Stool samples were collected from 42 metastatic melanoma patients prior to immunotherapy initiation. Eligible patients were provided an EasySampler Collection Kit (ALPCO) to collect stool sample at home. The stool samples were brought to the lab within 24 hours after collection. DNA was immediately isolated from 250 mg of stool and the rest of the sample was aliquoted and stored at -80°C.

2.2 Microbial DNA isolation

Patient stool samples were handled under BSL2 laminar flow hood using sterile technique. The technician wore gloves, gown, face mask and hair net to prevent contamination of the samples. Isolation of microbial DNA from patient and mouse fecal samples was performed using QIAamp PowerFecal DNA Kit and QIAmp DNA Stool Mini Kit, respectively (Qiagen, Germantown, MD), including a bead-beating step. DNA concentration was measured using a Nanodrop-nd1000 and the DNA was stored at -80°C.

2.3 16S rRNA gene amplicon library preparation and sequencing

16S rRNA gene amplicon library preparation and sequencing were performed at the Argonne National Laboratory. Briefly, PCR amplicon libraries targeting the 16S rRNA encoding gene were produced using a barcoded primer set adapted for the Illumina HiSeq2000 and MiSeq (133). DNA sequence data were then generated using Illumina paired-end sequencing at the Environmental Sample Preparation and Sequencing Facility (ESPSF) at Argonne National Laboratory. Specifically, the V4 region of the 16S rRNA gene (515F-806R) was PCR-amplified with region-specific primers that include sequencer adapter sequences used in the Illumina

flowcell (133, 134). The forward amplification primer also contains a twelve-base barcode sequence that supports pooling of up to 2,167 different samples in each lane. Each 25 μL PCR reaction contained 9.5 μL of MO BIO PCR Water (Certified DNA-Free), 12.5 μL of QuantaBio's AccuStart II PCR ToughMix (2x concentration, 1x final), 1 μL Golay barcode tagged Forward Primer (5 μM concentration, 200 pM final), 1 μL Reverse Primer (5 μM concentration, 200 pM final), and 1 μL of template DNA. The conditions for PCR were as follows: 94 °C for 3 minutes to denature the DNA, with 35 cycles at 94 °C for 45 s, 50 °C for 60 s, and 72 °C for 90 s; with a final extension of 10 min at 72 °C to ensure complete amplification. Amplicons were then quantified using PicoGreen (Invitrogen) and a plate reader (Infinite®200 PRO, Tecan). Once quantified, volumes of each of the products were pooled into a single tube so that each amplicon was represented in equimolar amounts. This pool was then cleaned up using AMPure XP Beads (Beckman Coulter) and quantified using a fluorometer (Qubit, Invitrogen). The pool was diluted down to 2 nM, denatured, and further diluted to a final concentration of 6.75 pM with a 10% PhiX spike for sequencing on the Illumina MiSeq. Amplicons were sequenced on a 151bp x 12bp x 151bp MiSeq run using previously described sequencing primers and procedures (133). The average sequencing depth for the patient samples was 51,029, ranging from 28,040 to 68,928 reads; the average sequencing depth for mouse samples was 158,728, ranging from 54,632 to 327,216 reads per sample.

2.4 Microbial 16S rRNA gene amplicon analysis

Qiime v1, Chapter 3

The microbial 16S rRNA gene amplicon sequencing data from human and mouse fecal collections were processed separately with Quantitative Insights Into Microbial Ecology (QIIME) (version 1.91) (135) using similar protocols as previously described (103). In brief, raw reads were

trimmed to remove low quality bases and paired-end 3' overlapping mates were merged using SeqPrep (https://github.com/jstjohn/SeqPrep). The open reference OTU picking protocol was used at 97% sequence identity against the Greengenes database (08/2013 release) (136). PyNAST was used to align sequences (137) and uclust consensus taxonomy assigner was used for taxonomic assignment (138). Data were rarefied to an even depth of 13,190 reads for the human microbial cohort and 22,560 reads for the mouse microbial cohort, respectively. OTUs occurring in less than 10% of the samples were removed per comparison in each cohort. Permutation tests (also known as, non-parametric t-tests in QIIME v1.9 manual) using Monte Carlo simulation were performed to identify differences in bacterial taxa occurrence between fecal communities of responders (R) and non-responders (NR) from human samples, and between slow and fast tumor growth groups from human microbiota-colonized mice. The tools and parameters used in each analysis step are described as follows: 1) The FastQ files were demultiplexed based on unique sample barcodes usingsplit_libraries_fastq.py and paired-end reads were merged based on overlapping 3' end mates using join_paired_ends.py (SeqPrep method with low quality base trimming and adaptor clipping turned on by default). 2) Reads were clustered into OTUs based on 97% sequence similarity and searched against reference database followed by de novo assembly of clustered sequences using pick_open_reference_otus.py, with option "enable_rev_strand_match" set to TRUE and requiring at least 2 sequences per OTU for singleton removal. The OTU abundance table was generated and phylogenetic tree was reconstructed. 3) All samples were rarefied to the same sequencing depth using single_rarefaction.py based on the least number of reads mapped per sample. 4) Alpha (e.g., Shannon index) and beta diversity metrics were collected using core_diversity_analyses.py and compared between NR and R groups using compare_alpha_diversity.py (option "nonparametric" test with Monte Carlo permutations) and compare_categories.py (ANOSIM and PERMANOVA

methods with weighted UniFrac distance), respectively, with 999 permutations and FDR correction for multiple comparisons. 5) OTUs were filtered for those present in at least 10% of the samples using filter_otus_from_otu_table.py, leaving 2,181 OTUs in the human 16S dataset and 3,235 OTUs in the mouse 16S dataset for statistical comparison of group differences. 6) OTUs differentially abundant between NR and R groups were identified by permutation test implemented in group_significance.py with option "nonparametric_t_test" and 1000 permutations and filtered by a statistical significance level of 0.05 for subsequent analysis. Analysis of the mouse 16S dataset revealed 519 OTUs differentially abundant between the fast and slow tumor growth groups at FDR-adjusted $P < 0.05$. Among these, 298 OTUs were assigned with known reference IDs and 221 with new reference ID. The new reference OTU IDs are not comparable between different cohorts, hence we focused on the OTUs with known reference IDs. Out of 298 OTUs, 207 OTUs were matched with human donors and used for generation of the heatmap depicted in Figure 3.11B. In addition, binary Bray–Curtis dissimilarity index was computed for each donor-mouse sample pair based on presence/absence of matched OTUs. For each pair, OTUs of relative abundance > 0.0001 in the donor or the mouse sample was included for the calculation.

Qiime v2, Chapter 4

For 16S analysis presented in Chapter 4, QIIME version 2 (2018.2.0) was used (139). Samples were demultiplexed and first 12 bases trimmed based on lower sequence quality, followed by denoising with DADA2 (via q2-dada2) (74). All amplicon sequence variants (ASVs) were aligned with mafft (140) (via q2-alignment) and used to construct a phylogeny with fasttree2 (141) (via q2-phylogeny). Alpha-diversity metrics (observed features and Faith's Phylogenetic Diversity (142), beta diversity metrics (unweighted UniFrac (143) and weighted UniFrac (144), Jaccard distance, and Bray-Curtis dissimilarity), and Principal Coordinate Analysis (PCoA) were estimated using q2-diversity after samples were rarefied (subsampled without replacement) to

17,288 sequences per sample. Taxonomy was assigned to ASVs using the q2-feature-classifier (145) classify-sklearn naïve Bayes taxonomy classifier against the Silva 119 99% OTUs (515-806 region, seven-level taxonomy) reference sequences (70). Statistical tests were completed in R using Wilcoxon-Mann-Whitney test (non-parametric) a raw p-values adjusted for multiple testing using Benjamini-Hochberg FDR correction (146).

2.5 BLASTN methodology

To investigate the identity of the OTUs differentially abundant between responders and non-responder patients, the assembled 16S rRNA gene amplicon sequences were characterized by a BLAST search against NCBI bacterial nucleotide sequence database (the search results were last updated on 10/04/2017). Using the blastn command line tool and the "megablast" program selection method, the top hits with ≥98% identity to the query sequence were returned from the nucleotide collection database restricted to bacteria and excluding environmental or uncultured sample sequences. Results are shown in table S3. For some OTUs there were no hits with ≥98% identity and the top 10 hits are listed regardless of the percent identity value.

2.6 Metagenomic shotgun sequencing

Metagenomic shotgun sequencing was performed at the Marine Biological Laboratory affiliated with the University of Chicago. Briefly, the quantity of the DNA sample was measured using Picogreen (Invitrogen). DNA was then sheared using a Covaris and the libraries were constructed with the Nugen Ovation Rapid DR Multiplex System (PCR-free). The aimed insert size is between 400-600 bp. Amplified libraries were visualized on an Agilent DNA1000 chip or Caliper HiSens Bioanalyzer assay, pooled at equimolar concentrations and size selected using a Sage PippinPrep 2% cassette. The library pool was quantified using a Kapa Biosystems qPCR library quantification protocol, then sequenced on the Illumina NextSeq in a 2x150 paired-end

sequencing run using dedicated read indexing. The samples were demultiplexed with bcl2fastq.An average of 80.4 million reads were generated per sample, ranging from 38.9 to 156.7 million reads.

2.7 Microbial shotgun metagenomics analysis

The microbial shotgun metagenome sequencing data from human fecal collections were taxonomically profiled using Metagenomic Phylogenetic Analysis (MetaPhlAn 2) (147). Species-level taxonomic relative abundances were inferred for all samples following protocols detailed elsewhere (148). In brief, host contamination in the metagenomic reads was identified using KneadData version 0.61 (http://huttenhower.sph.harvard.edu/kneaddata) with human (GRCh37) reference databases (example command: kneaddata -i fq1 -i fq2 -db kneaddataDB -o out --output-prefix sample -t threads -q phred33 --trimmomatic trimmomaticPath --max-memory 2048m --trimmomatic-options 'LEADING:20 TRAILING:20 AVGQUAL:30 SLIDINGWINDOW:4:20 MINLEN:70 TOPHRED33' --run-trf). The high-quality reads were then mapped against a catalog of ~1 million clade-specific marker sequences identified from ~17,000 reference genomes currently spanning bacteria, archaea, eukaryotes and virus phylogenies to assign reads to microbial clades (example command: metaphlan2.py in1,in2 --bowtie2out out.bowtie2.bz2 --nproc threads --input_type fastq > out.txt). The relative abundance of each taxonomic unit in each sample was estimated by normalizing read counts assigned to each clade by the nucleotide length of its markers and by the sum of all weighted read counts in this clade including all subclades (example command: metaphlan2.py out.bowtie2.bz2 --nproc threads --input_type bowtie2out -t rel_ab > out.rel_ab.txt). To compare species identified from 16S and shotgun sequencing, the profiled bacterial species were then compared to the taxonomy of OTUs generated from 16S sequencing at family level, and the statistical dependence between the relative abundance of 16S OTUs and each

matched shotgun species was determined using Spearman's rank correlation tests, followed by filtering for those with positive correlation and at $P < 0.05$.

2.8 qRT-PCR validation of metagenomic and 16S rRNA gene sequencing of fecal samples

The abundance of some of the bacterial species identified with the metagenomic and 16S rRNA gene amplicon sequencing approaches were further measured by qPCR using previously validated subgroup- or species-specific primers and probes (149–161) and SYBR Green or TaqMan PCR master mix (Applied Biosystems). The primers and probes were synthesized by Integrated DNA Technologies (Coralville, IA) and Life Technologies, respectively. qPCR was performed on StepOnePlus Real-Time PCR System (Applied Biosystems, Foster City, CA) and analyzed with StepOnePlus Software. The primer concentrations were as previously described (Table S5). The cycling conditions for the TaqMan-based reactions were 50°C for 2 min, 95°C for 10 min, 40 cycles of 95° for 15 secs, 60-65°C for 1 min, with varying annealing temperatures depending on the primer pair. The cycling conditions for the SYBR Green-based reactions were 95°C for 10 min, 40 cycles of 95° for 15 sec, 60-75°C for 10-40 sec, 72°C for 20-50 sec, with varying annealing temperatures and times depending on the primer pair. Fluorescence signal was detected at the end of each cycling stage. For some reactions, fluorescence detection was done during an additional 15 sec step at a higher temperature to minimize signal from primer dimers and minor non-target products (150). Melt curve analysis was performed to confirm amplification specificity. The results were expressed as relative abundance normalized to the total bacterial load. Specifically, to calculate the total bacterial load, qPCR was performed using previously described universal bacterial primers (162). A standard curve was generated using the PCR blunt vector (Invitrogen) containing a single copy of the 16S rRNA gene derived from a member of the Porphyromonadaceae family (163) and the total 16S rRNA gene copies per ng DNA was

calculated for each sample. Relative abundance for each species was expressed as 2^{-Ct} normalized to the number of total 16S rRNA gene copies per ng DNA in each sample and multiplied by a constant ($7.3x10^{19}$) to bring all values larger than 1. A summation qPCR score was computed per individual sample taking into consideration the abundance of 10 validated qPCR targets (*Enterococcus faecium, Collinsella aerofaciens, Bifidobacterium adolescentis, Klebsiella pneumoniae, Veillonella sp., Parabacteroides merdae, Lactobacillus sp., Bifidobacterium longum, Ruminococcus obeum* and *Roseburia intestinalis*). First, data transformation was applied on the relative abundance to bring signal close to Gaussian distribution. The relative abundance of each species was log10 transformed and scaled by dividing the value by their root mean square across samples. The abundance of *Ruminococcus obeum* and *Roseburia intestinalis* (more abundant in non-responders) were multiplied by (-1). The sum of the transformed abundance of the 10 qPCR results was calculated to generate the score and compared between groups of interest using two-sided Student's t-test.

2.9 RNAseq of tumor samples and data analysis

RNA was isolated from tumor samples using the QIAGEN AllPrep DNA/RNA FFPE kit (Qiagen, Hilden, Germany) according to the manufacturer's instructions. The quality of RNA was measured on Agilent 2100 Bioanalyzer (Agilent Technologies, Santa Clara, USA). cDNA was reverse transcribed from RNA and used for library preparation following dUTP strand-specific protocol by the University of Chicago Genomics Core Facility. Ribosomal RNA was removed using the Ribo-Zero rRNA Removal Kit (Human) (Illumina, San Diego, USA). Sequence reads were generated on an Illumina HiSeq 4000 instrument at the Functional Genomics Facility. An average of 133.3 million 2x100bp paired-end (PE) reads were generated for each sample, ranging from 93.2 to 208.0 million reads. The quality of raw reads was assessed by FastQC (164) (v0.11.5).

Reads were aligned to human reference transcriptome with Gencode gene annotation (v26, GRCh38) by Kallisto (165) (v0.43.1) with the strand-specific mode, which implements kmer-based pseudoalignment algorithm for accurate quantification of transcripts from RNAseq data and is robust to errors in the reads. Transcript abundance was quantified at transcript level specifying strand-specific protocol, summarized into gene level using tximport (166) (v1.4.0), normalized by trimmed mean of M values (TMM) method, and log2-transformed for further analysis. Selected transcripts (PD-L1 and PD-1) were compared between responders and non-responders. A gene signature score was calculated for each sample using xCell (167). The raw values for "Macrophages M1" and "Macrophages M2" were used to calculate a gene signature ratio and were defined utilizing 188 and 159 genes, respectively.

2.10 Animals and tumor model

Specific pathogen-free (SPF) C57BL/6 mice were obtained from Taconic Biosciences (Hudson, NY). SPF mice were fed Teklad irradiated 2918 diet (Envigo), or in some cases autoclaved 5K67 diet (Lab Diet, St. Louis, MO), and housed in the University of Chicago SPF animal facility. Germ-free (GF) C57BL/6 mice were initially purchased from Taconic biosciences, then bred and housed in flexible-film isolators in the University of Chicago Gnotobiotic Research Animal Facility and fed autoclaved 5K67 diet. Some GF mice were gifted by Dr. Eugene Chang at the University of Chicago. For all experiments, 6–8-week-old mice were used. The C57BL/6-derived melanoma cell line B16.F10.SIY (henceforth referred to as B16.SIY) was generated as described (168). The MC38 cell line was a gift from Dr. Yang-Xin Fu (UT Southwestern). Tumor and other cell lines were maintained in DMEM (Fisher #11140076) plus 10% FBS, 1% penicillin/streptomycin (Fisher #15140122) and 1% non-essential amino acids (Fisher #11140050), henceforth referred to as "complete media". Mice were injected subcutaneously with

1×10^6 B16.SIY or MC38 tumor cells. Tumor size was measured three times per week until the endpoint and tumor volume determined by length x width^2 x 0.5 (Chapter 3) or length x width x height (Chapter 4). Microbiota composition of the colonized mice was assessed with 16S rRNA gene amplicon sequencing of DNA extracted from fecal samples collected 4 weeks after colonization. Taconic SPF mice were used as a control. The experimental animal procedures were approved by the University of Chicago Animal Care and Use Committee.

2.11 Fecal matter transfer and antibiotics

For tumor growth experiments, some GF mice were colonized with fecal microbiota from either patient samples or from mice, by oral gavage. Briefly, 200 mg of human stool was thawed and suspended in 3 ml of PBS or mouse fecal pellets were collected fresh and suspended in 0.4 ml of PBS per pellet. After settling of the particulate material, each mouse was gavaged with 10 ml/kg body weight (approximately 200 μl per mouse) of the fecal supernatant. At the time of gavage, mice were transferred to Biological Containment Unit (BCU rack) to minimize microbial cross-contamination. Two weeks after gavage, mice were injected subcutaneously with tumor cell lines (described in 2.10). For antibiotics treatments, used either alone or in combination with fecal matter transfer (FMT), mice received 2 mg ampicillin (Gold Biotechnology), 2 mg metronidazole (Sigma), 2 mg neomycin (Gold Biotechnology), and 1 mg vancomycin hydrochloride (Gold Biotechnology) by oral gavage in 200 μL sterile water twice daily for five days.

2.12 Antibody treatment

For immunotherapy experiments, mice were injected intraperitoneally on days 7, 10, 13, and 16 after tumor inoculation with 100 μg of anti-PD-L1 monoclonal antibody (BioXCell, 10F.9G2). For $CD8^+$ T cell depletion experiments, mice were injected intraperitoneally with 200

μg of anti-CD8β monoclonal antibody (BioXCell, Lyt 3.2) weekly starting one day before tumor inoculation.

2.13 Tissue processing and immune cell isolation

Tumors, lymph nodes, and spleens were dissected and digested for 30 min at 36°C while shaking at 200 RPM in RPMI plus 2% FBS, 200 units/mL Deoxyribonuclease I from bovine pancreas (Sigma-Aldrich, DN25), 1 mg/mL Hyaluronidase (Sigma Aldrich, H6254), and 1 mg/mL Collagenase Type IV (Sigma-Aldrich C5138). The digested tissues were passed through a 70 μm cell strainer and washed with 15 mL (lymph nodes and spleen) or 50 mL (tumors) PBS. Lymph node and spleen suspensions were then prepared for staining by flow cytometry or other applications. Tumor cell isolates were washed a second time with 50 mL of PBS and resuspended in 7 mL PBS. Immune cells from tumors were further enriched by layering 3 mL Ficoll-Hypaque beneath the cell suspension and centrifuged at 400*g* for 30 minutes without breaks. The buffy layer was isolated and washed with PBS before proceeding to staining or other downstream analysis.

2.14 Flow cytometry of tumor immune infiltrates

For immune profiling in Chapter 3, cells were labeled with a PE-MHC class I pentamer (Proimmune) consisting of murine H-2K^b complexed to SIYRYYGL (SIY) peptide or to an irrelevant SIINFEKL peptide. Tumor cell suspensions were subsequently stained with anti-CD3-AlexaFluor700 (Ebioscience, 17A2), anti-CD8α-Pacific Blue (Biolegend, 53-6.7), anti-CD4-BrilliantViolet711 (Biolegend, RM4-5), anti-CD44-FITC (BD, IM7), anti-FOXP3-APC (Ebioscience, FJK-16a) and Fixable Viability Dye-eFluor780 (Ebioscience). The cells were then washed and fixed in 1% paraformaldehyde and analyzed on LSRFortessa flow cytometer with FACSDiva software (BD). Data analysis was performed using FlowJo software (Tree Star).

For immune profiling of tumor infiltrates described in Chapter 4, cells were prepared for flow cytometry by washing twice with FACs Buffer (10% FBS, 1 mM EDTA in PBS). Cells were stained for 30 min at room temperature with the PE-MHC class I SIY pentamer and purified CD16/32 (to block non-specific Fcγ R III/II binding) in FACs Buffer followed by staining with remaining surface antibodies for an additional 30 minutes at room temperature in FACs Buffer plus Brilliant Stain Buffer Plus (BD Biosciences). Cells were then fixed and permeabilized for 30 minutes at room temperature (eBioscience™ Foxp3 / Transcription Factor Staining Buffer Set) and washed with 1X Permeabilization Buffer (eBioscience). Intracellular antibodies were prepared in Permeabilization buffer and cells were stained overnight at 4^{o}C. The following day, cells were washed three times in Permeabilization buffer and resuspended in FACs buffer for flow cytometry. Samples were run on the Cytek™ Aurora with SpectroFlo® Software. Data analysis was performed using FlowJo software (Tree Star).

Table 1. Table of flow cytometry antibodies used for profiling immune infiltrates

Marker	Clone	Fluorophore	Vendor
CD103	2E7	BV421	Biolegend
CD11b	M1/70	BV570	Biolegend
CD11c	N418	AF 647	Biolegend
CD16/32	93	NA	Biolegend
CD19	6D5	BV510	Biolegend
CD206	C068C2	BV605	Biolegend
CD3	17A2	AF700	Biolegend
CD4	GK1.5	Spark NIR 685	Biolegend
CD44	IM7	FITC	Biolegend
CD45	30-F11	AF532	Invitrogen
CD80	16-10A1	PE/Dazzle 594	Biolegend
CD86	PO3	BUV 496	BD Biosciences
CD8a	53-6.7	BUV395	BD Biosciences
F4/80	BM8	PerCP/Cy5.5	Biolegend
Foxp3	FJK-16a	APC	Biolegend
I-A/I-E	M5/114.15.2	Pacific Blue	Biolegend
Ki67	B56	BV711	BD Biosciences
LAG-3	C9B7W	PerCP eFluor710	eBiosciences
Ly6C	HK1.4	BV785	Biolegend
Ly6G	1A8	BUV 661	BD Biosciences
NK1.1	PK136	APC Cy7	Biolegend
PD-1	RMP1-30	PE-Cy7	Biolegend
PDCA-1	927	BV650	Biolegend
Viability	Zombie NIR™ Fixable Viability kit		Biolegend

2.15 IFN-γ ELISPOT

ELISPOT was carried out using anti-IFN-γ capture/detection antibody pair from BD Biosciences. ELISPOT plates (Millipore, MAIP S4510) were coated with capture antibody (Cat No. 51-2525KD) overnight at 4^{o}C and then blocked with DMEM + 10% FBS for 2 hours at room temperature. Splenocytes were enumerated using flow cytometry, plated at 10^6 cells per well and stimulated overnight at 37^{o}C with 160 nM SIY peptide, an irrelevant OVA peptide as negative control, or 500 ng/ml ionomycin plus 50 ng/ml PMA as positive control. The following day, IFN-γ spots were detected with biotinylated detection antibody (Cat No. 51-1818KZ), followed by streptavidin-HRP and AEC substrate kit (all from BD Biosciences). The spot number and size

were quantified using an Immunospot Series 3 Analyzer and ImmunoSpot software (Cellular Technology).

2.16 In vivo intestinal permeability assay

To assess gut permeability in vivo, an assay using FITC-labelled dextran was performed as previously described (169). Mice were removed from access to food or water for 4 hours, and then received by oral gavage 60 mg per 100g body weight of freshly prepared FITC-dextran (either MW 4,000 or 20,000, Sigma-Aldrich, 46944) diluted to 60 mg per mL in sterile PBS. Blood was collected 3.5 hours post gavage by cardiac puncture, and serum isolated by centrifugation at 1,500*g* for 10 minutes. To quantify blood FITC-dextran levels, 50 µL of serum was transferred (in duplicate) to a black, flat-bottom 96-well plate and read with emission and excitation wavelengths of 520 nm and 490 nm, respectively (Victor X3 Multilabel Plate Reader). FITC-dextran concentration was calculated using a standard curve generated by a serial dilution of FITC–dextran.

2.17 Bacterial culture of immune organs to assess bacterial translocation

Mice were injected subcutaneously with B16.SIY and euthanized 14 days later. The outside of each mouse was thoroughly sprayed with the disinfection agent Clidox®-S, and mice dissected in a laminar flow hood using sterilely prepared instruments. Tumor and spleen were immediately transferred into an anaerobic chamber and manually dissociated in 2 ml sterile PBS and passed through a 70 µM filter. From the total tissue cell suspension, 100 µl was added to 10 ml of brain-heart infusion broth and cultured anaerobically or aerobically for 6 days. Optical density measurements were taken at the beginning and end of culture to measure bacterial growth.

2.18 Single cell RNA sequencing analysis

Immune cells isolated from day 14 B16.SIY tumors were stained with Fixable Viability Dye-eFluor780 (eBioscience) and CD45 AF488 (clone 30-F11, Biolegend). The CD45 live cells were sorted using an AriaII automated cell sorter. For each sample 10,000 cells were targeted and encapsulated using the 10x Chromium 3' v2 chemistry kit following the manufacturer's protocol. Libraries were then prepared according to manufacturer's instructions. Samples were sequenced to an average depth of 540 million reads on a HiSEQ4000 with 100 base paired end reads at the University of Chicago Genomics Core.

After library demultiplexing, gene libraries were aligned to the mm10 reference transcriptome (version 3.0.0) and count matrices were generated using the Cell Ranger (version 3.0.2). The resulting 'filtered-feature' matrix output was used for downstream analysis conducted in R using primarily the Seurat (v3) package (170–172). Cells which passed quality control metrics (total gene count between 500 and 7000, UMI greater than 500, and percent mitochondrial DNA less than 2%) were retained for analysis. All samples were integrated using "SCTransform" and then clustered using "RunPCA" "FindNeighbors" and "RunUMAP" using the first 50 principal components. Optimal resolution was determined using "clustree" (173) and clusters defined using "FindClusters" with the resolution set to 0.75. For differential gene expression analysis, transcript expression was normalized using "NormalizeData" using the method "LogNormalize". Genes which best distinguished cluster identity were found using "FindAllMarkers" and used to annotate clusters. To calculate differentially expressed genes within the same cluster across conditions the function "FindMarkers" was used with the MAST test method used (174). The calculation of the IFNAR gene signature score was determined by the summation of normalized gene expression of Mx1, Ifi44, Ly6e, and Oas3 and the IFNAR-signaling genes identified in Ourthiague et al., Oas2, Axl, Tap1, Rtp4, Isg20, Il15ra, Trex1, Cmpk2, Lilrb4, Ifit3, Mx2 and Ifit2 (175).

2.19 Mouse serum isolation and cytokine analysis

We collected blood from mice at tumor endpoint by cardiac puncture, and isolated serum by allowing blood to clot at room temperature for approximately 15 minutes, centrifuging at 1500*g* for 10 min, and collecting resulting serum which was then stored at -80^{o}C for downstream applications. To assess serum levels of cytokines and chemokines (GM-CSF, IFN-γ, IL-1α, IL-1β, IL-2, IL-4, IL-5, IL-6, IL-7, IL-10, IL-12p70, IL-13, LIX, IL-17α, KC, MCP-1, MIP-2, TNF-α) we used MILLIPLEX MAP Mouse High Sensitivity T Cell Premixed Panel according to manufacturer's directions (Millipore Sigma, Cat No. MHSTCMAG-70KPMX).

2.20 Dendritic cell stimulation and T cell proliferation in vitro

DCs were purified from the spleen of naturally colonized A and B mice using the MACs Pan Dendritic Cell Isolation Kit (Miltenyi, Cat No. 130-100-875). $CD8^{+}$ T cells were isolated from 2C TCR transgenic mice using the CD8 T cell isolation kit (Miltenyi, Cat No. 130-095-236) and labeled with CellTrace™ Violet according to manufacturer's instructions (Invitrogen, C34557). DCs and T cells were plated at ratio of 1:2 with 12,500 DCs and 25,00 T cells each in a 96-well round bottom plate with varying concentrations of SIY peptide and incubated at 37^{o}C for three days. On the third day, GolgiPlug (BD, 555029) and GolgiStop (BD, 554724) were added to DC T cell co-culture according to manufacturer's protocols for 5 hours after which cells were stained and prepared for flow cytometry using the protocol described in 2.14 and the following antibodies.

Table 2. Table of flow cytometry antibodies used for in vitro DC stimulation of 2C T cells

Marker	Fluorophore	Clone	Vendor
CD3	AF700	17A2	Biolegend
CD8a	PE	53-6.7	Biolegend
PD-1	APC	RMP1-30	Biolegend
IFNy	PE-Cy7	XMG1.2	eBioscience
TNFa	Alexa Fluor 488	MP6-XT22	eBioscience
Viability	ef780 Fixable Viability Dye		eBioscience

2.21 CellTrace violet (CTV)-labeled TCR transgenic T cell adoptive transfer

$CD8^+$ T cells were isolated from the spleen and lymph nodes of naïve $CD90.1^+$ 2C TCR transgenic mice using the MACs CD8 T cell isolation kit (Miltenyi, Cat No. 130-095-236). Isolated T cells were labeled with CellTrace™ Violet according to manufacturer's instructions (Invitrogen, C34557) and 1 x 10^6 T cells injected retro-orbitally into mice bearing day 7 B16.SIY tumors. Three days post-adoptive T cell transfer, tumor draining lymph nodes was harvested and restimulated ex-vivo with SIY peptide for five hours at 36ºC. One hour into peptide stimulation GolgiPlug (BD, 555029) and GolgiStop (BD, 554724) were added to cells for the remaining four hours. Following the re-stimulation cells were washed and stained according to the cell staining protocol for flow cytometry described in 2.14 using the following antibodies.

Table 3. Table of flow cytometry antibodies used for 2C adoptive T cell transfer

Marker	Fluorophore	Clone	Vendor
CD90.2	PerCP-eFluor 710	30-H12	Biolegend
CD4	BV605	RM4-5	Biolegend
CD8a	BV711	53-6.7	Biolegend
CD45	PE	30-F11	Biolegend
CD90.1	AF700	OX-7	Biolegend
IFNy	APC	XMG1.2	eBioscience
TNFa	Alexa Fluor 488	MP6-XT22	eBioscience
Viability	ef780 Fixable Viability Dye		eBioscience

2.22 Ex vivo stimulation of myeloid-enriched splenocytes

Spleen from endpoint B16.SIY tumor bearing animals were harvested and processed as described in 2.13. Red blood cells from spleen cell suspensions were lysed using Gey's solution (4.15g NH_4Cl plus 0.5g $KHCO_3$ in 500 mL water and filter sterilized). In the proceeding steps splenocytes were washed and incubated in MACs buffer (0.5% BSA plus 2mM EDTA in 1X PBS). Post RBC lysis splenocytes were washed and incubated with biotin labeled anti-NK1.1 (clone PK136, Biolegend), anti-CD3 (clone 145-2C11, Biolegend) and anti-CD19 (clone 6D5,

Biolegend) antibodies for 10 min on ice. Cells were washed and incubated with anti-Biotin MicroBeads (Miltenyi) for 10 minutes on ice. After incubation cells were washed and resuspended in 1 mL of buffer and passed through a MACs magnetic column (LS column, Miltenyi) and negatively selected cells in the flow through collected. The sample was divided according to the number of conditions tested, and a small fraction (approximately $1/50^{th}$) was reserved to check for purity by flow cytometry. Fewer than 5% of remaining cells were B, T or NK cells. The panel used to check isolation purity and compare remaining immune populations is below (representative data shown in Figure 4.17D).

Table 4. Table of flow cytometry antibodies used to assess immune cells post lymphocyte negative selection.

Marker	Clone	Fluorophore	Vendor
Ly6C	HK1.4	PerCP Cy5.5	eBioscience
CD8a	53-6.7	BV605	Biolegend
CD3	145-2C11	Pacific Blue	eBioscience
CD19	6D5	BV510	Biolegend
CD11b	M1/70	APC	Biolegend
CD11c	N418	BV711	Biolegend
NK1.1	PK136	PE	Biolegend
F4/80	BM8	FITC	Biolegend
I-A/I-E	M5/114.15.2	AF700	eBioscience
CD45	30-F11	PE Cy7	Biolegend
Viability	ef780 Fixable Viability Dye		eBioscience

Cells were resuspended in complete media, transferred to Eppendorf tubes and stimulated with varying concentrations of DMXAA (Cayman Chemical) for 2 hours at 36^{o}C. Following stimulation cells were immediately lysed (Qiagen RLT Lysis Buffer) and frozen at -80^{o}C.

2.23 In vitro stimulation of macrophage cell line

A mouse macrophage cell line was used to evaluate the effect of LPS pre-treatment on subsequent IFN-β production with DMXAA. Immortalized WT macrophages were developed as described in Roberson and Walker (176) and were obtained from Dr. K. Fitzgerald (University of

Massachusetts). Macrophages were passaged in complete media. One million macrophages were plated in 6-well tissue culture treated dishes with varying concentrations of LPS (from *E. coli* serotype O111:B4, Cell Signaling #14011) or complete media. The following day (21 hours later), the cells were washed with room temperature PBS and stimulated with 50 µg/mL DMXAA (Cayman Chemical) for 2 hours at 36^{o}C. Following stimulation, cells were washed with PBS and lysed directly with 350 µL of Qiagen RLT Lysis Buffer, scraped from the plate, transferred to Eppendorf tubes, and frozen at -80^{o}C.

2.24 RNA isolation and quantitative real-time PCR

Procedure used for ex vivo and in vitro stimulation with DMXAA to quantify IFN-β transcription. All steps followed manufacturer's recommended protocol unless otherwise noted. RNA was isolated from cells using the Qiagen RNeasy Micro Kit according to manufacturer's protocol. RNA concentration was quantified by nanodrop and 1.5 µg total RNA was treated with DNase I (Sigma #4716728001) according to the manufacturer's protocol. cDNA was synthesized using high-capacity reverse transcriptase (Fisher # 4368814), resuspended to a final volume of 200 µL and 5 µL used for qRT-PCR reactions in a final volume of 25 µL per reaction. Quantification of mRNA was conducted using the Taqman gene expression master mix (Fisher # 4369514) on a StepOne Plus real-time PCR system (Applied Biosystems # 4376600). Roche's Universal Probe Set was used in conjunction with a mRNA specific forward and reverse primers noted below.

Table 5. Mouse qRT-PCR primers

Target	Roche Probe	Name	Sequence
Gapdh	#9	GAPDH-F	agcttgtcatcaacgggaag
		GAPDH-R	tttgatgttagtggggtctcg
Ifnb	#108	IFNb-F	ggaaagattgacgtgggaga
		IFNb-R	cctttgcaccctccagtaat

2.25 Statistical analysis

Tumor growth curves were analyzed using two-way ANOVA with Tukey's multiple comparisons post-test using GraphPad PRISM. For other comparisons between two groups, including evaluating significance in immune profiling or quantitative PCRs, unpaired, two-tailed Student's t-test, or Wilcoxon-Mann-Whitney test (non-parametric) was used as indicated in the figure legends. Microbial composition comparisons were performed using permutation tests implemented in QIIME (option "nonparametric_t_test"). For multiple comparisons, p-value was adjusted using Benjamini-Hochberg FDR correction (146). Spearman's rank correlation coefficient ρ was used for measuring statistical dependence between relative abundance of bacteria produced by different platforms (Chapter 3). $P<0.05$ was considered statistically significant and denoted as follows: *$P < 0.05$, **$P < 0.01$, ***$P < 0.001$, ****$P < 0.0001$. Statistical analysis was performed using GraphPad PRISM and R.

Chapter 3: The commensal microbiome is associated with anti-PD-1 efficacy in metastatic melanoma patients and influences tumor growth in a preclinical cancer model

3.1 Introduction

The therapeutic efficacy of immunotherapies targeting the PD-1/PD-L1 interaction is favored in patients who show evidence of a T cell–inflamed tumor microenvironment at baseline (33, 35). Therefore, host and tumor factors that regulate the magnitude of endogenous immune priming and T cell infiltration into the tumor microenvironment are being sought as an opportunity to further expand therapeutic efficacy (177). Preclinical studies have indicated that the composition of the commensal microbiome could exert a major influence; mice with favorable microbiota showed far greater therapeutic activity of anti–PD-L1 treatment than did mice with an unfavorable microbiome, and this benefit could be transferred by cohousing or fecal transplant (103). These observations prompted an analogous analysis of the human microbiome with respect to therapeutic efficacy of anti–PD-1 in cancer patients.

3.2 The composition of the gut microbiome is associated with patient response to immunotherapy

To evaluate whether commensal bacterial composition might be associated with clinical efficacy of PD-1 blockade immunotherapy, stool samples were collected from 42 patients before treatment as part of a multidimensional biomarker analysis in metastatic melanoma. The majority of patients received an anti–PD-1 regimen; four patients received anti–CTLA-4 treatment, but the downstream data conclusions did not change with the removal of these subjects, so they were retained in the analysis. Clinical response rate was determined in a blinded manner from biomarker results by using Response Evaluation Criteria In Solid Tumors (RECIST) version 1.1. There were 16 responders (from here on, referred to as R) and 26 nonresponders (NR), yielding a response

rate of 38%, which is in line with published clinical data of anti–PD-1 therapy in metastatic melanoma patients (178, 179). No major differences in patient characteristics were observed in R versus NR, except a borderline difference in prior (but not current) smoking history (table S1).

To determine whether the composition of the commensal microbiota is associated with clinical response, we integrated three methods for DNA sequence–based bacterial identification (Figure 3.1A). First, using 16S ribosomal RNA (rRNA) gene amplicon sequencing, we identified

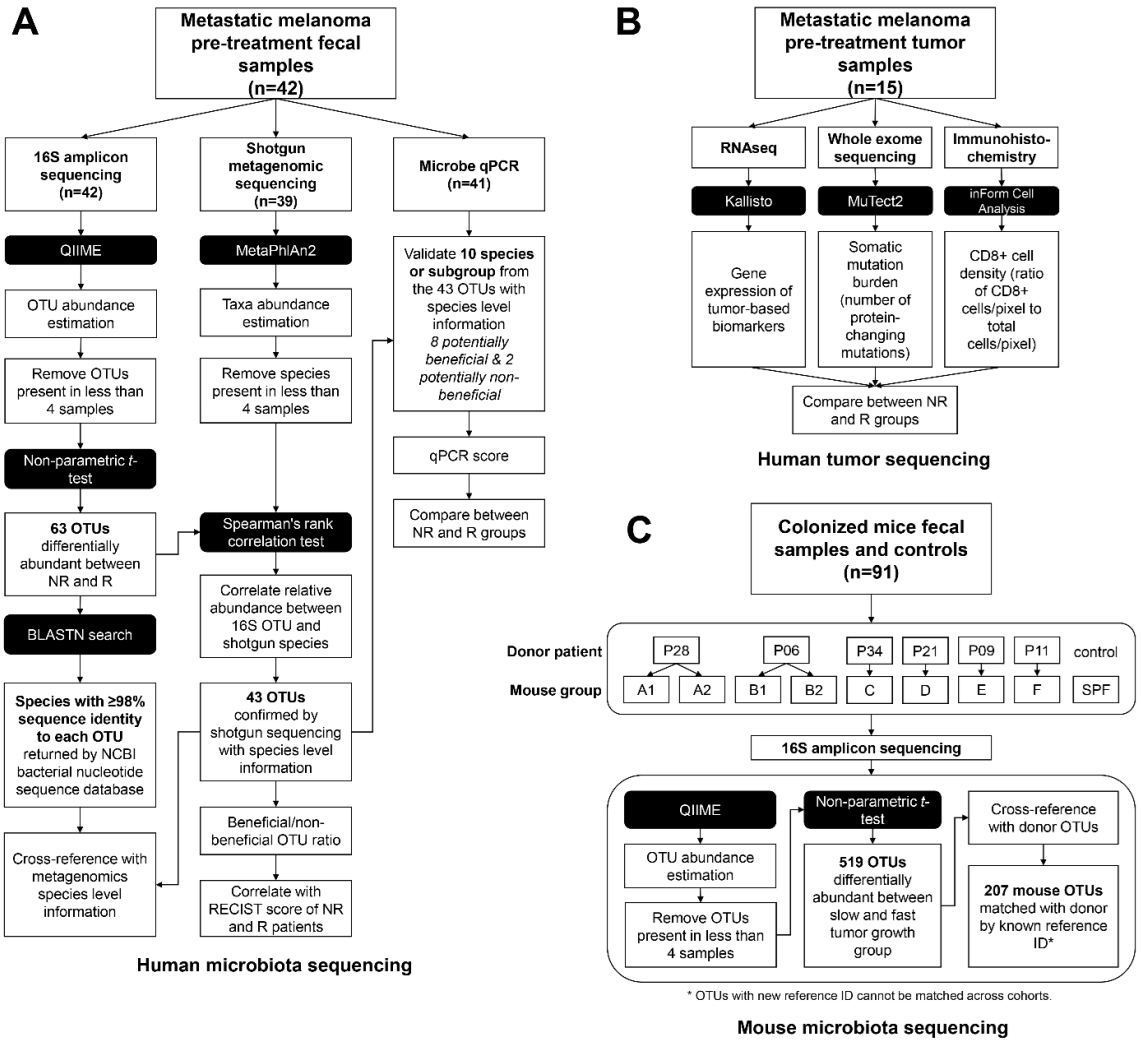

Figure 3.1 Analysis pipeline for microbial identification.
Workflow schematic indicating (A) the integration of methods for microbial identification, (B) analyses of tumor-associated biomarkers, and (C) 16S sequencing-based identification of bacteria in patient stool samples with a potential role in modulating anti-tumor immunity in a mouse melanoma model.

operational taxonomic units (OTUs) with taxonomic assignment present at different abundance in R versus NR (table S2). We used a Basic Local Alignment Search Tool (BLAST) search of the 16S sequences against the National Center for Biotechnology Information (NCBI) database to reveal potential species-level identities (table S3). Further level of confidence in species identification was gained by matching the OTUs from the 16S data set to species-level identities revealed through metagenomic shotgun sequencing (table S4). We used species-specific quantitative polymerase chain reaction (PCR) for those candidate species having previously validated primers (table S5). Compared with the 16S analysis, the metagenomic sequencing yielded a smaller number of species differentially represented in R versus NR, which overlapped with the 16S results (table S6). Treating these assays as a screen for maximizing the number of candidate species, we used the 16S sequencing method as a starting point in our analysis.

After removing OTUs present in less than 10% of the samples, the 16S sequencing revealed 62 OTUs of different abundance in R versus NR [$P < 0.05$, unadjusted, permutation test with Quantitative Insights Into Microbial Ecology (QIIME)] (table S2). Hierarchical clustering of samples based on relative abundance of these OTUs revealed that most patients were accurately grouped according to clinical response (Figure 3.2). Clustering of patients within each clinical group is depicted in Figure 3.3A. Thirty-nine OTUs were more abundant in R, and 23 were more abundant in NR. One *Bifidobacteriaceae* OTU was significantly more abundant in R, and a second *Bifidobacteriaceae* OTU (559527) had borderline significance ($P = 0.058$, unadjusted) and was included in the analyses (total = 63 OTUs). This observation recapitulates previous findings that associated *Bifidobacteriaceae* family members with improved immune-mediated tumor control and efficacy of anti–PD-L1 therapy in mice (103). A principal component analysis (PCA) of the 63 OTUs revealed separation of R from NR (Figure 3.3B).

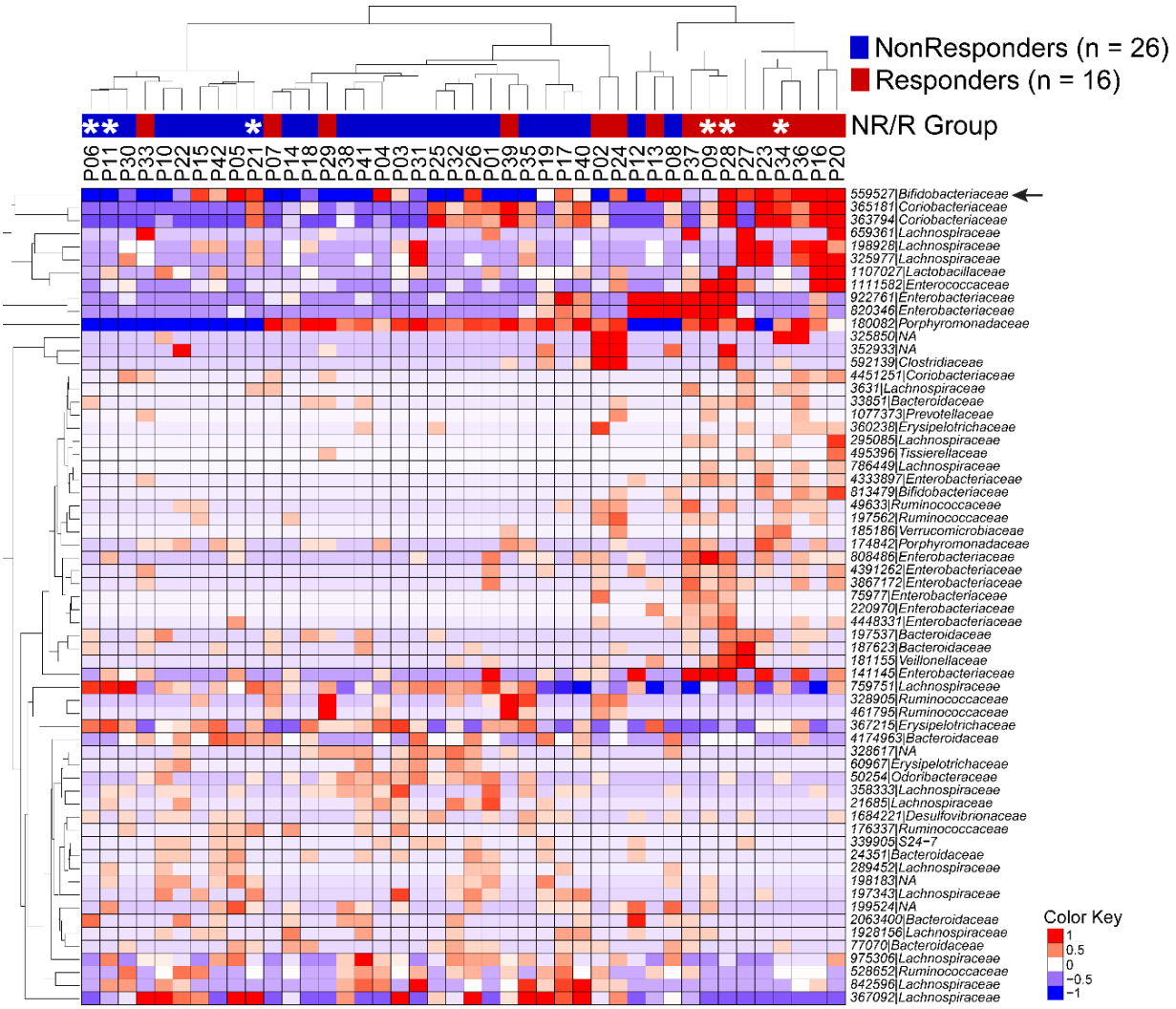

Figure 3.2 Segregation of responder and non-responder samples based on relative abundance data for the 63 differentially abundant OTUs.

Segregation of responder and non-responder samples based on relative abundance data for the 63 differentially abundant OTUs determined with 16S sequencing using unadjusted, non-parametric t test. (62 OTUs were significantly different with $P<0.05$; 1 OTU, Bifidobacteriaceae OTU 559527 indicated with arrow, approached significance with $P<0.058$). Columns depict individual patients clustered using unsupervised hierarchical clustering with Euclidean distance. Asterisks indicate samples used in further in-vivo experiments. Annotation bar above the heatmap indicates clinical response to immunotherapy. The ID of de-novo assembled OTUs (new clean-up reference OTUs picked by QIIME) were abbreviated to show only the unique identifier digits, and the full OTU IDs are provided in table S4.

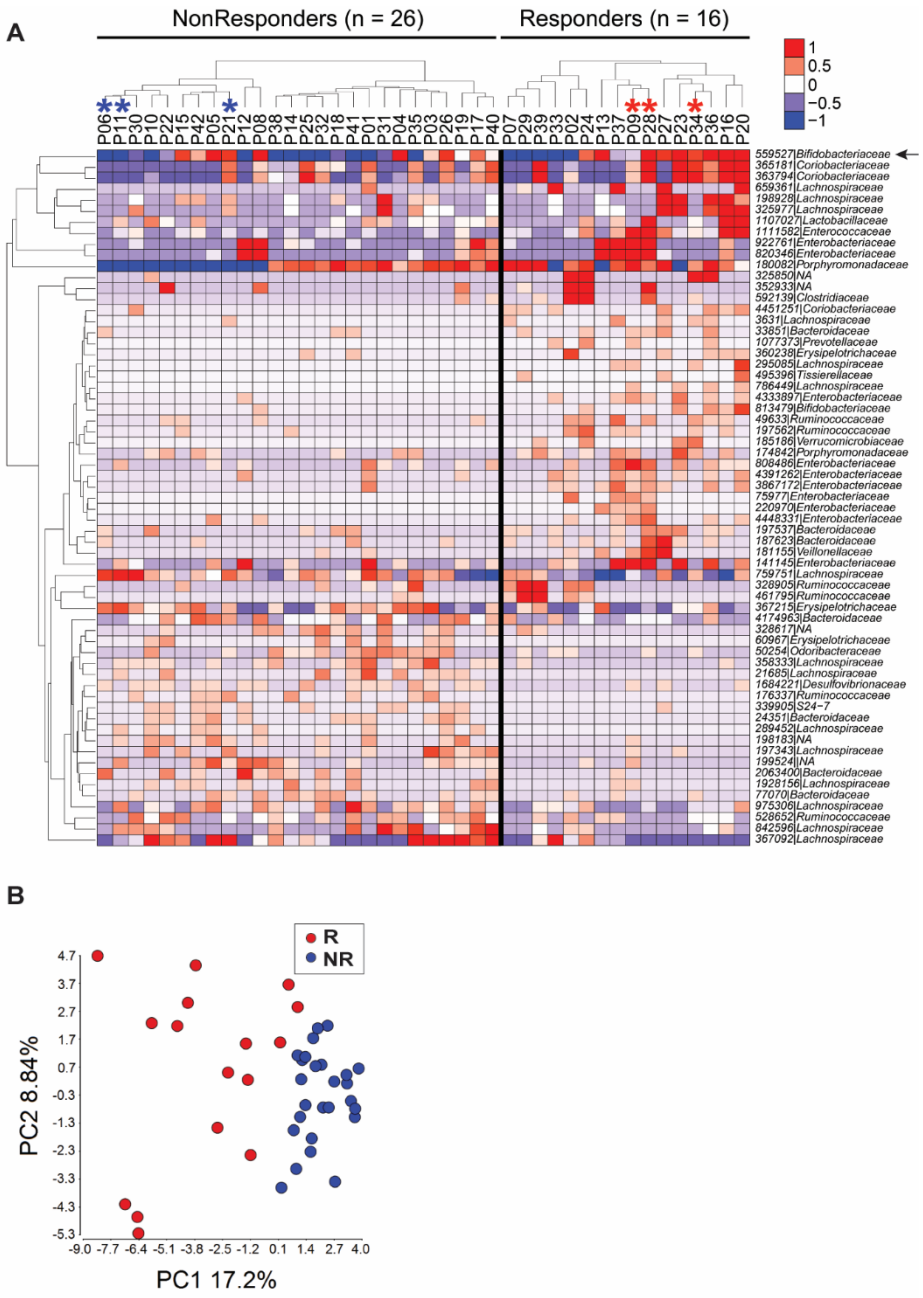

Figure 3.3 Distinct commensal microbial communities in anti–PD-1 responding patients and nonresponding patients as assessed with 16S rRNA gene amplicon sequencing.

(**A**) Relative abundance of differentially abundant taxa in responders versus nonresponders; 62 OTUs were identified as different with $P < 0.05$ (unadjusted, permutation test). An additional OTU 559527 (arrow) identified as *Bifidobacteriaceae* approached significance ($P = 0.058$). Hierarchical clustering of the samples was performed within each clinical group. Individual samples are organized in columns, labeled with patient identification number. Asterisks indicate samples used in further in vivo experiments. The ID of de novo assembled OTUs (new clean-up reference OTUs picked with QIIME) were abbreviated to show only the individual identifier digits, and the full OTU IDs are provided in table S4. (**B**) PCA of relative abundance of the 63 OTUs shown in 3.3A.

3.3 Specific bacterial species are found enriched among the microbiome of responding and non-responding patients.

A BLAST search of the 63 OTUs against the NCBI database of bacterial sequences returned for most OTUs multiple species with ≥98% identity (table S3). To gain more accurate species-level characterization, the same samples were subjected to metagenomic shotgun sequencing (available for 39 of the 42 samples). Illumina paired-end reads were assigned to microbial clades and analyzed for closest matches to the 63 OTUs identified with 16S sequencing. Potential species matches were identified for 43 of the original 63 OTUs (table S4). Species-specific quantitative PCR assays were performed as an additional approach to assess the identity of species, for which sufficiently validated quantitative PCR primers were available (table S5). Thus, integration of the three methods led to the selection of 10 species differentially enriched in R versus NR. Eight of these were more abundant in R—*Enterococcus faecium*, *Collinsella aerofaciens*, *Bifidobacterium adolescentis*, *Klebsiella pneumoniae*, *Veillonella parvula*, *Parabacteroides merdae*, *Lactobacillus* sp., and *Bifidobacterium longum*—whereas two were more abundant in NR: *Ruminococcus obeum* and *Roseburia intestinalis*. As an example, the integrative analysis for *B. longum* (OTU 559627) is depicted in Figure 3.4A-C. Similar correlation analyses for the remaining nine species are depicted in Figures. 3.5 and 3.6. Quantitative PCR results for these 10 species were integrated into a summation quantitative PCR score for each patient, which was significantly higher in responders ($P = 0.004$) (Figure 3.4D).

This list of species is likely an underestimate of the total number of entities showing differential abundance in R versus NR because of the stringency of this composite analysis. For example, *Akkermansia muciniphila* OTU (185186), in line with the study of anti–PD-1 efficacy in epithelial cancers by Routy *et al*. (110), was detected by means of 16S sequencing in four patients, and all were responders, but statistical analysis of the entire cohort is limited by the number of

samples above the detection threshold. As an alternative way to represent the aggregate data toward development of a candidate predictive biomarker, the total numbers of potentially "beneficial" and "nonbeneficial" OTUs were scored for each patient (Figure 3.7), and a ratio was calculated. When plotted against the absolute change in tumor size as assessed with RECIST, a clean correlation was observed so that patients with a ratio over 1.5 all showed clinical response (Figure 3.4E). These results suggest that the commensal microbiota composition might be useful as a biomarker to predict response to checkpoint blockade therapy, which motivated comparison with other candidate predictive biomarkers. Archived pretreatment tumor specimens that passed quality control were available for 15 patients (5 R, 10 NR). Microbial composition remained significantly different in R versus NR for this subset ($P < 0.01$) (Figure 3.8 A-B). Exome sequencing followed by enumeration of nonsynonymous somatic mutations showed a trend of higher frequency in R, as did levels of PD-L1 and PD-1 mRNA (Figure 3.8C-E) and enumeration of baseline $CD8^+$ T cells by means of immunohistochemistry (Figure 3.8F). Although these trends not reaching statistical significance level of 0.05 were likely limited by sample size, the microbiota parameters still markedly separated responders and nonresponders.

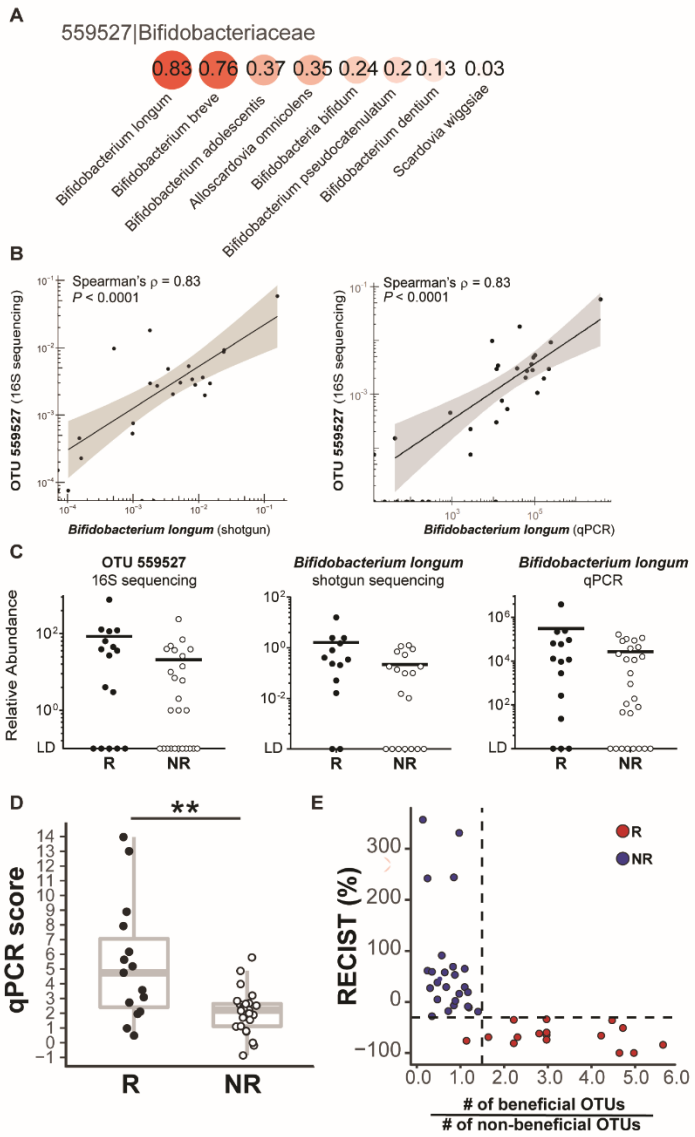

Figure 3.4 Identification of commensal bacterial species associated with patient clinical response to anti–PD-1 therapy.

(**A**) Spearman's correlation coefficients between the relative abundances of *Bifidobacteriaceae* OTU 559527 from the 16S data set and species-level identities suggested by shotgun sequencing. The species profiled with shotgun sequencing were compared with the taxonomy of OTUs generated from 16S sequencing at the family level. (**B**) Spearman's correlation between abundance of OTU 559527 from the 16S data set and *B. longum* identified by means of metagenomics shotgun sequencing analysis (left) and quantitative PCR (right). Shaded band indicates 95% confidence interval (CI) of the values fitted by linear regression. (**C**) Relative abundance in responders (R) versus nonresponders (NR) of OTU 559527 (16S sequencing; left), *B. longum* (shotgun sequencing; middle), and *B. longum* (quantitative PCR; right). LD, limit of detection. (**D**) Quantitative PCR score representing aggregate data for the relative abundances of 10 species correlated to OTUs with differential abundance in R versus NR. Wilcoxon-Mann-Whitney test (nonparametric) was used to compare quantitative PCR score between R and NR groups. (**E**) Ratio of beneficial to nonbeneficial OTU numbers for each patient versus the patient's RECIST aggregate tumor measurement change. Dashed lines label RECIST% = –30 and ratio = 1.5. Only the 43 16S OTUs confirmed with shotgun metagenomic sequencing were included.

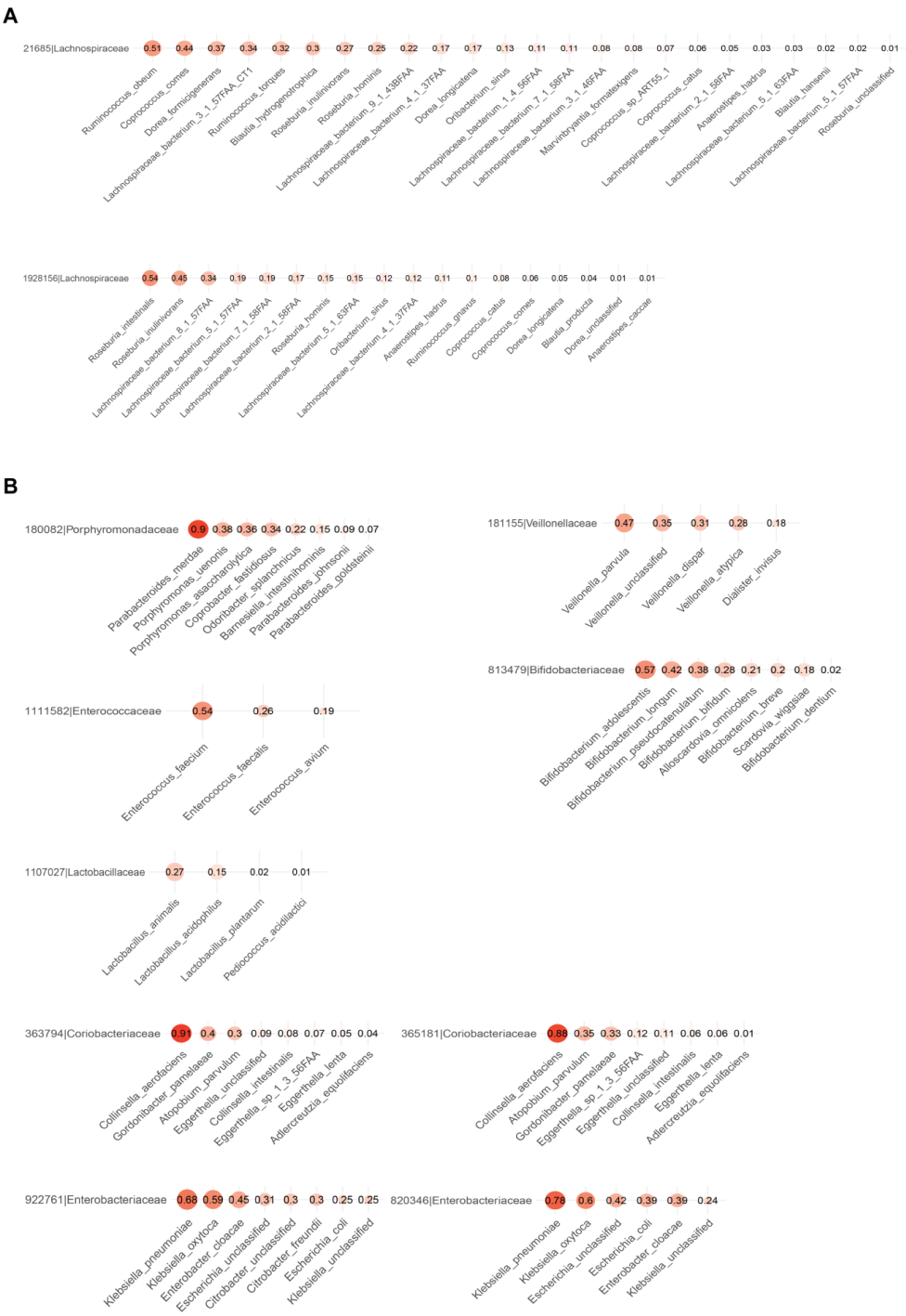

Figure 3.5 Ranked species-level identities of 16S OTUs predicted with shotgun sequencing. OTUs picked by 16S sequencing analysis were first matched to species identified by shotgun sequencing at the family level. Then, pairwise tie-corrected Spearman's correlation was computed for each matching pair and the species matched to each OTU were ranked based on the correlation coefficient ρ value. A complete list of the 63 OTU-to-species matching between the 16S and shotgun sequencing datasets is included in table S4.

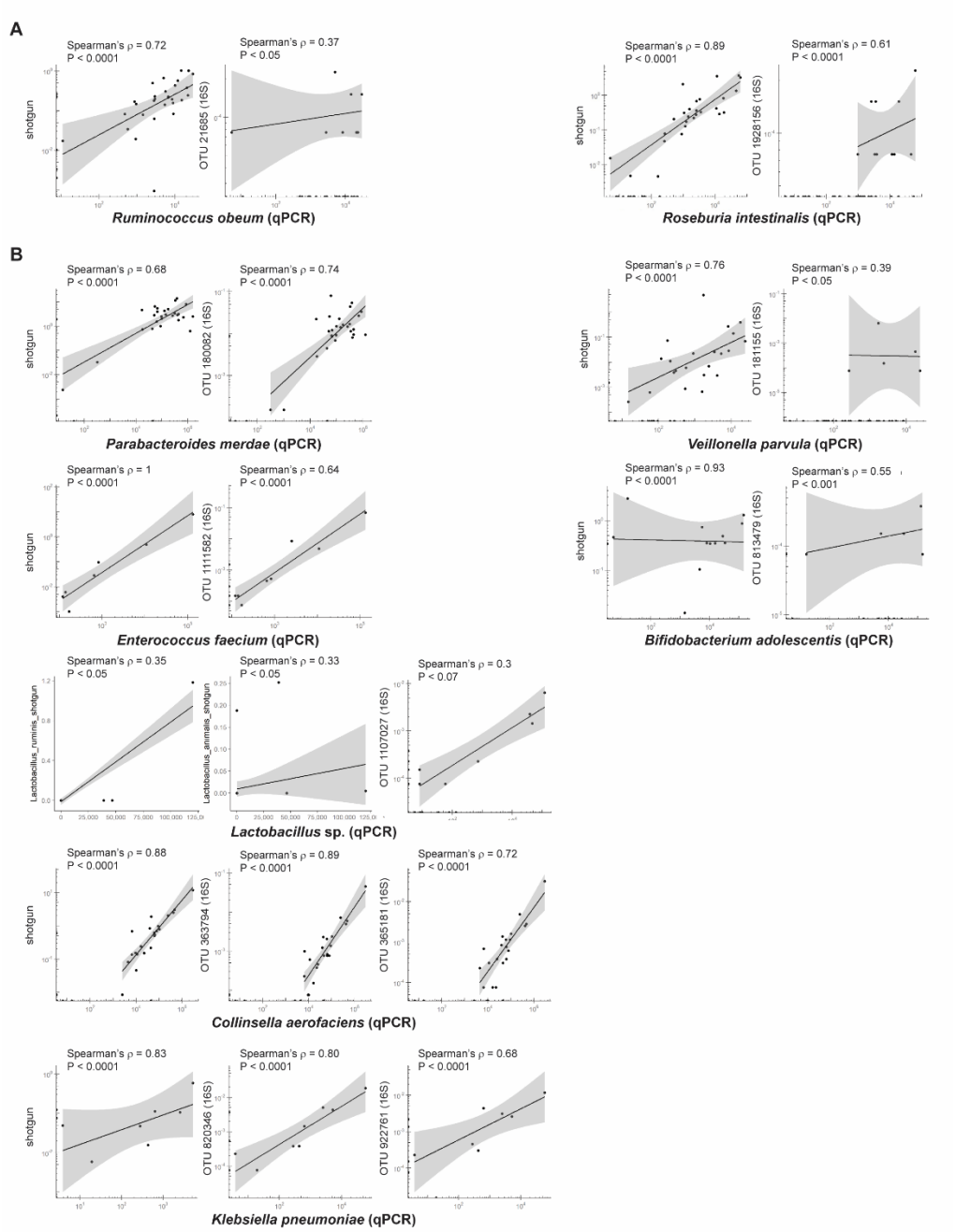

Figure 3.6 Use of species-specific qPCR for additional confirmation of the OTU-to-species matches determined by 16S and shotgun sequencing data comparisons.

OTUs and their best-match species as measured with 16S and shotgun sequencing, respectively, were correlated by Spearman's test against the relative abundance of the corresponding species measured with qPCR. Depicted are correlations for OTUs (and their best-match species), which are more abundant in non-responders (A) or in responders (B) and are used for computation of the qPCR score. Of note, OTU 1107027 (identified as *Lactobacillus ruminis* with 16S sequencing analysis) was best matched to *Lactobacillus animalis* (from the shogun sequencing data set) with P<0.1 (table S4) and was included in the qPCR score because a primer set with a broader Lactobacillus sp. specificity was used (table S5).

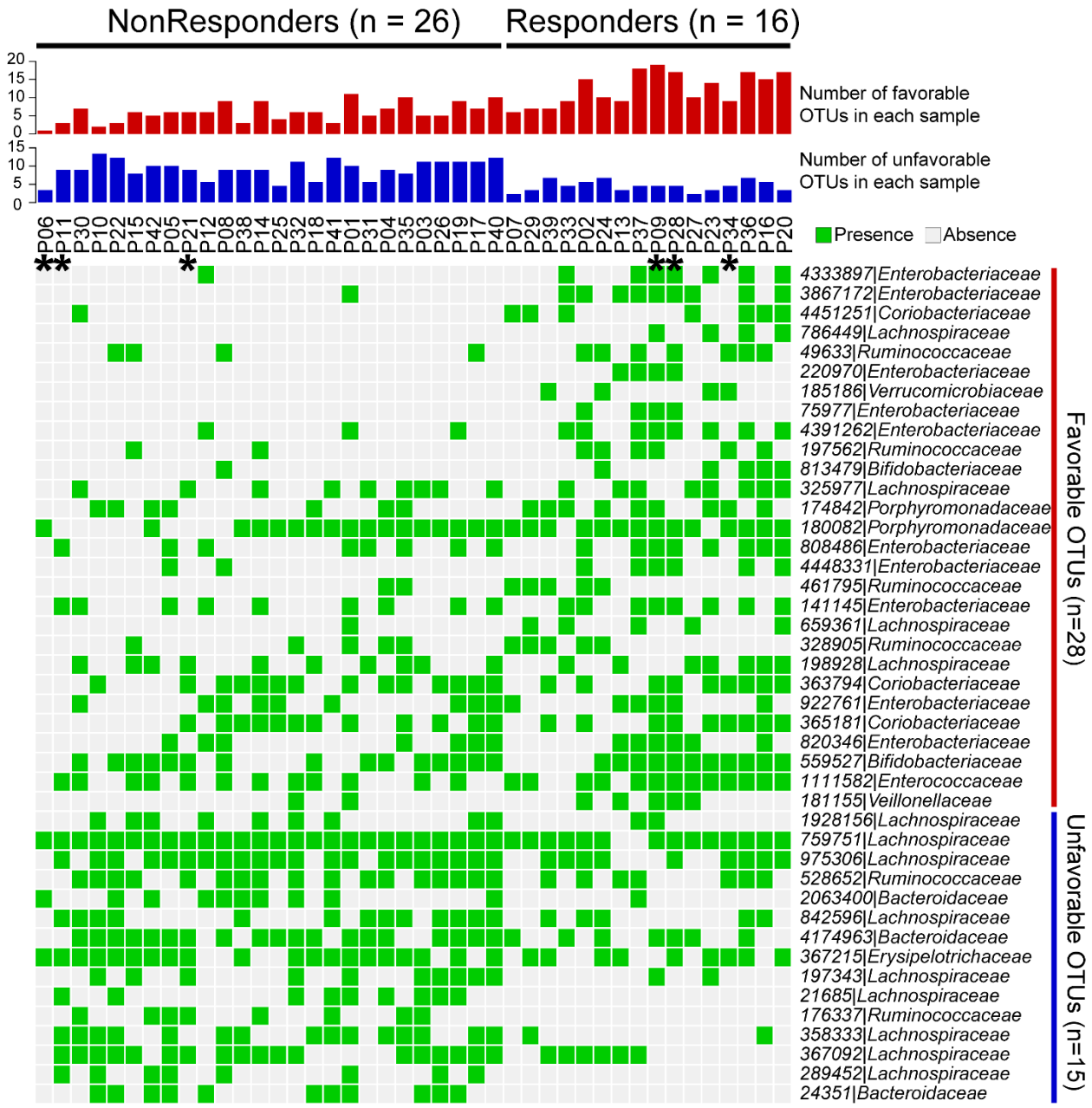

Figure 3.7 Visual representation of the presence/absence-based ratio of favorable/unfavorable OTUs.

The bar graphs represent the total number of favorable OTUs (more abundant in responders; depicted in red) and unfavorable OTUs (more abundant in non-responders; depicted in blue) in each patient. The grid map represents presence (green) or absence (white) of favorable and unfavorable OTUs in each patient sample. Columns depict individual patients grouped based on clinical response to immunotherapy in the same order as in Figure 1A. Rows indicate the 43 OTUs from 16S sequencing that were confirmed by shotgun sequencing (table S4). Asterisks indicate samples used in further in-vivo experiments. The ID of de novo assembled OTUs (new clean-up reference OTUs picked by QIIME) were abbreviated to show only the unique identifier digits, and the full OTU IDs are provided in table S4.

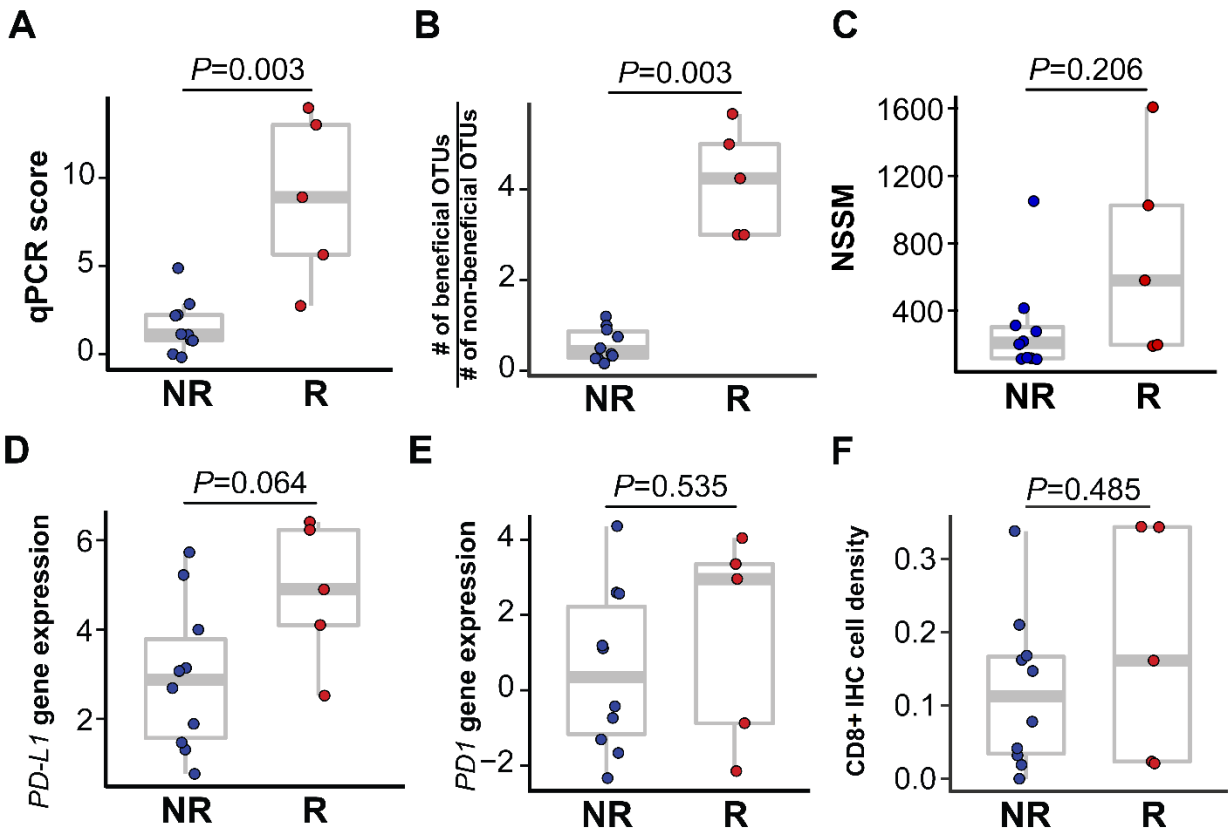

Figure 3.8 The qPCR score and the beneficial/non-beneficial OTU ratio as candidate predictors of clinical response to immunotherapy.
The qPCR score (A) and the ratio of beneficial-to-non-beneficial OTUs (B) were more distinct between non-responders (NR) and responders (R), compared to the non-synonymous somatic mutational (NSSM) load (C), expression levels of PD-L1 (D) and PD-1 (E), as determined by whole transcriptome sequencing of tumor samples, and intra-tumoral $CD8^+$ T cell infiltration (F) as determined with immunohistochemistry of tumor samples. This analysis was limited to subset of 5 responders and 10 non-responders from the original 42 patient cohort, whose samples passed quality control for RNA sequencing. Wilcoxon-Mann-Whitney test (non-parametric) was used for comparing qPCR score, OTU ratio, and NSSM between NR and R groups, which does not assume data follow normal distribution. Student's t-test was used for the rest of the markers.

3.4 Human commensal communities modulate anti-tumor immunity in a mouse melanoma model.

The strong correlation between commensal bacteria and clinical response to immunotherapy suggested a potential causal effect, in light of data demonstrating an immune-potentiating impact of the microbiome in mouse tumor models (103, 105, 180). To investigate the capability of human commensal microbes to potentiate anti-tumor T cell responses, we used germ-

free (GF) mice as recipients. We had previously reported that spontaneous immune-mediated tumor control in Taconic mice could be improved by means of fecal microbiota transfer from mice obtained from a different vendor, the Jackson Laboratories (103). In setting up the current model, we found that B16.SIY melanoma tumor growth in GF mice was similar to that in specific pathogen–free (SPF) mice (both from Taconic), and colonization of GF mice with feces from Taconic SPF mice did not affect this baseline growth rate (Figure 3.9).

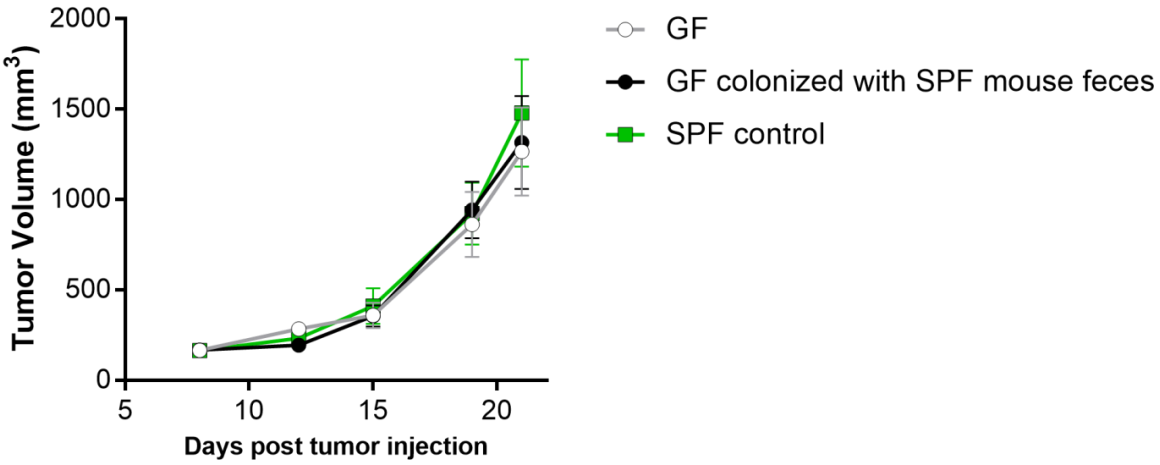

Figure 3.9 Germ-free mice and Taconic SPF mice show similar tumor growth rates.
Standard specific pathogen-free (SPF) mice were purchased from Taconic. Germ-free (GF) mice, originally purchased from Taconic, were bred in the University of Chicago gnotobiotic facility. The GF mice were divided into two groups and housed in two separate isolators in the same room. One group (black line; n=11) was colonized by oral gavage with fecal material from the SPF mice. The other group remained GF (grey line; n=10). Standard Taconic SPF mice (green line; n=5) were housed in ventilated cages in a standard barrier facility. All mice were maintained on the same diet. Two weeks later, the mice were injected with B16.SIY melanoma and tumor growth was measured.

These results suggest a reduced spontaneous immune-mediated tumor control inherent to GF mice, which makes them suitable recipients for human-derived microbiota, with an opportunity to detect improved anti-tumor immunity depending on microbial composition. Fecal material was transferred from three R and three NR into cohorts of GF mice (Figures 3.3A, 3.2, 3.7, 3.10),

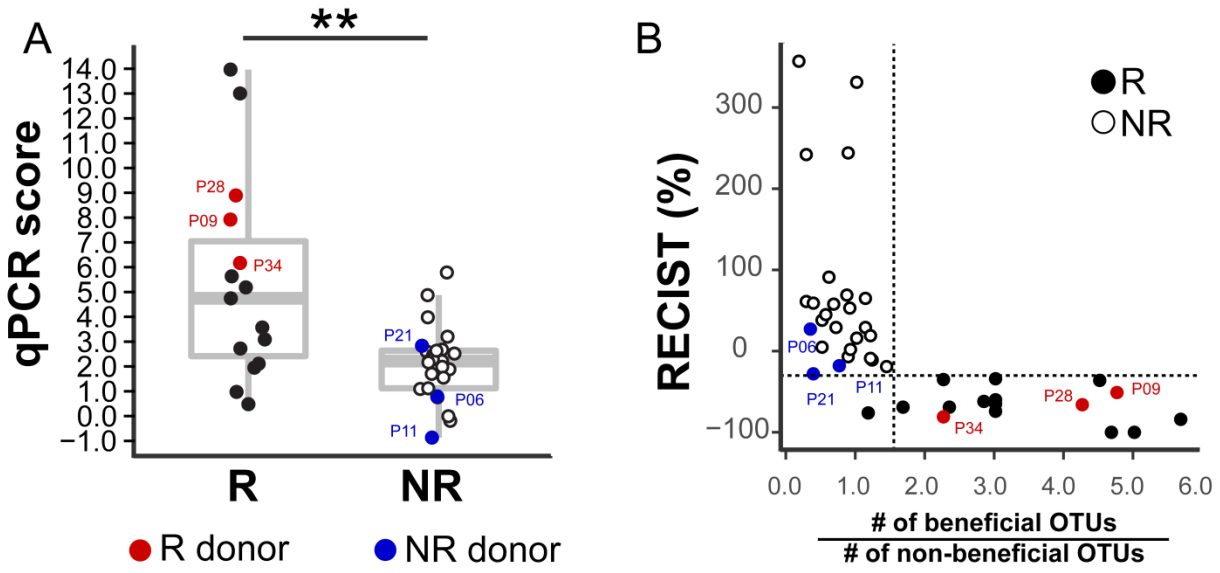

Figure 3.10 Commensal bacterial species associated with patient clinical response to anti–PD-1 therapy.
Donor samples used in mouse colonization experiments are representative of the responder and non-responder patient groups with respect to qPCR score (A) and ratio of beneficial to non-beneficial OTUs (B) as in Figure 2. Wilcoxon-Mann-Whitney test (non-parametric) was used to compare qPCR score between R and NR groups same as in Figure 3.4D.

followed by implantation of B16.SIY melanoma cells 2 weeks later. The human microbiota–colonized mouse groups segregated into two phenotypes with respect to tumor growth rate: (i) a faster growing group and (ii) a slower growing group (Figure 3.11A). Two of three mouse cohorts reconstituted with R fecal material had slower baseline tumor growth, and two of the three cohorts reconstituted from NR showed faster baseline tumor growth. Thus, the ability of the human microbiota to support improved tumor control in mice usually, but not always, paralleled the clinical response to anti–PD-1 seen in the donor patient. Achieving slower tumor growth with fecal transplant alone is similar to previous mouse studies, in which transfer of feces from Jackson into Taconic mice was sufficient for a partial therapeutic effect owing to a more favorable microbiome (103).

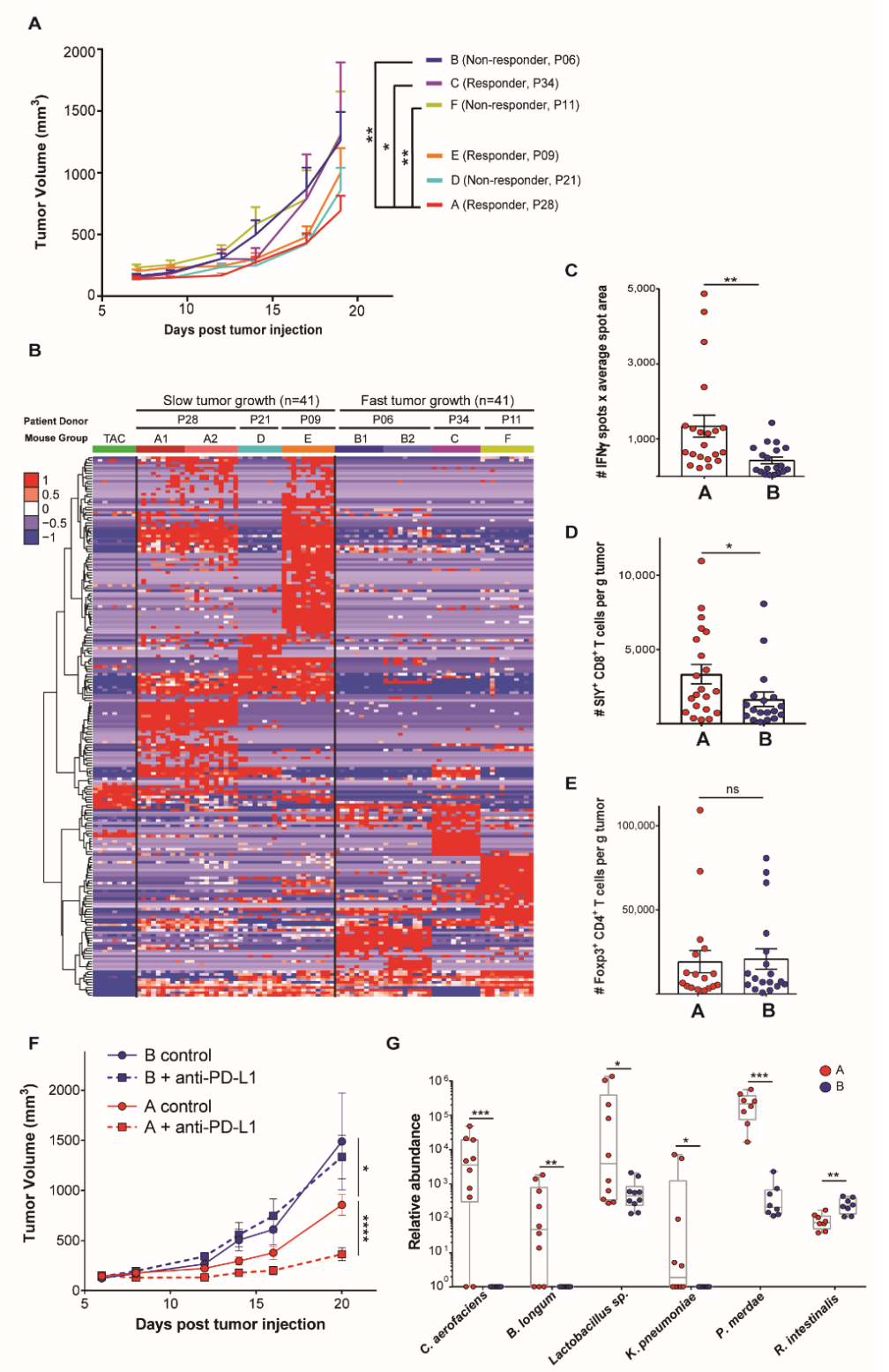

Figure 3.11 Human commensal communities modulate anti-tumor immunity in a mouse melanoma model.

GF mice were gavaged with fecal material from three responder (P28, P34, and P09) and three nonresponder (P06, P21, and P11) patient donors. (**A**) B16.SIY melanoma was injected

Figure 3.11 (continued)
subcutaneously 2 weeks after gavage; tumor growth data are from one (groups C, D, E, and F) or two experiments (groups A and B) with 7 to 11 mice per group per experiment. Error bars represent mean + SEM. (**B**) Relative abundance of 207 OTUs from patient donors that colonized in mice and were differentially abundant between slow- and fast-tumor-growth groups. Columns depict individual mice arranged in groups A through F. Groups A1, B1, A2, and B2 are from two independent duplicate experiments. Rows indicate individual OTUs with exact reference ID match between human and mouse 16S rRNA data sets. (**C**) In groups A and B, ex vivo activation of splenocytes by SIY peptide was measured with IFN-γ ELISPOT 3 weeks after tumor injection. (**D** and **E**) Tumor-infiltrating SIY-specific $CD8^+$ T cells (D) and $FoxP3^+$ regulatory T cells (E) were enumerated with flow cytometry. (**F**) Efficacy of anti–PD-L1 therapy was determined in groups A and B. Data are from one experiment with 7 or 8 mice per group. (**G**) Relative abundance in mouse groups A and B of key species validated for quantitative PCR scoring. Six out of the 10 species are shown that gave positive PCR signals. The remaining four species were absent from these particular recipient groups. Tumor growth curves were analyzed with two-way analysis of variance by Tukey's multiple comparisons post-test; flow cytometry and quantitative PCR data were analyzed by Wilcoxon-Mann-Whitney test (nonparametric).

Composition of bacterial taxa that successfully reconstituted mice and fidelity to the original human donor were assessed with 16S rRNA gene amplicon sequencing. Groups C and D, which did not show the same pattern of tumor control as the therapeutic outcome in the original human donors, showed a large degree of difference of microbiota composition from the original human donors (Figure 3.12). In agreement, a binary Bray-Curtis dissimilarity index for each donor/recipient pair was highest, at 0.7, for cohorts C and D versus 0.5 to 0.6 for the rest of the groups. We conclude that whereas reconstitution of GF mice with human fecal material often recapitulates the microbial composition and the phenotype of the human donor, in some cases there is a high degree of drift so that some bacteria expand and others contract to a degree that is sufficient to change phenotype. Nonetheless, for the reconstituted GF mice that do recapitulate the clinical outcome of the original donor, this model system may be useful for the ultimate isolation of specific bacteria that regulate anti-tumor immunity in vivo.

We focused on mouse groups A and B for further mechanistic studies. There was a high level of consistency between repeated experiments, both with respect to tumor growth rate and

microbial colonization (Fig. 3.11B, group A1 versus A2 and B1 versus B2 comparisons). To determine whether the difference in tumor control could be attributed to host immunity, interferon-γ (IFN-γ) enzyme-linked immunosorbent spot (ELISPOT) of ex vivo SIY-stimulated splenocytes was performed and indicated an increased frequency of activated T cells from R microbiota-reconstituted mice 3 weeks after inoculation with B16.SIY melanoma cells (Figure 3.11C). Analysis of the tumor microenvironment also showed a significantly greater number of SIY-specific $CD8^+$ T cells, but not of $FoxP3^+CD4^+$ regulatory T cells, in these mice (Figure. 3.11D-E), which is consistent with increased priming of tumor antigen–specific $CD8^+$ T cells. Anti–PD-L1 was markedly efficacious in mice colonized with R microbiota yet completely ineffective in NR-derived mice (Figure 3.11F), demonstrating a profound impact of the commensal microbiota on immunotherapy efficacy in vivo. Interrogation of fecal DNA from these mice by means of quantitative PCR recapitulated the results from our analysis of patients. Of the PCR reactions validated in patients, six were observed in reconstituted mice, with the same pattern of enrichment as was seen in patients (Figure 3.11G).

3.5 Significance of findings and comparison to other studies

Together, our data suggest that the composition of the commensal microbiota in patients is associated with therapeutic efficacy of anti–PD-1 monoclonal antibody (mAb). Although *B. longum* was one commensal identified in the current study that had also been found in mouse models to be associated with improved immune-mediated tumor control (103), it seems likely that multiple specific bacteria may contribute to improved anti-tumor immunity in patients. In addition to the panel of bacteria overrepresented in responders, several OTUs were overrepresented in nonresponders, and prior work in mice has indicated that some commensals have the potential to be immune-inhibitory—for example, through the induction of $FoxP3^+$ regulatory T cells (93, 94).

In addition, our current cohort suggested that a ratio of “beneficial” OTUs to “nonbeneficial” OTUs was the strongest predictor of clinical response. This may indicate that a higher frequency of beneficial bacteria, together with a lower frequency of bacteria with negative impact, may combine for the most favorable clinical outcome.

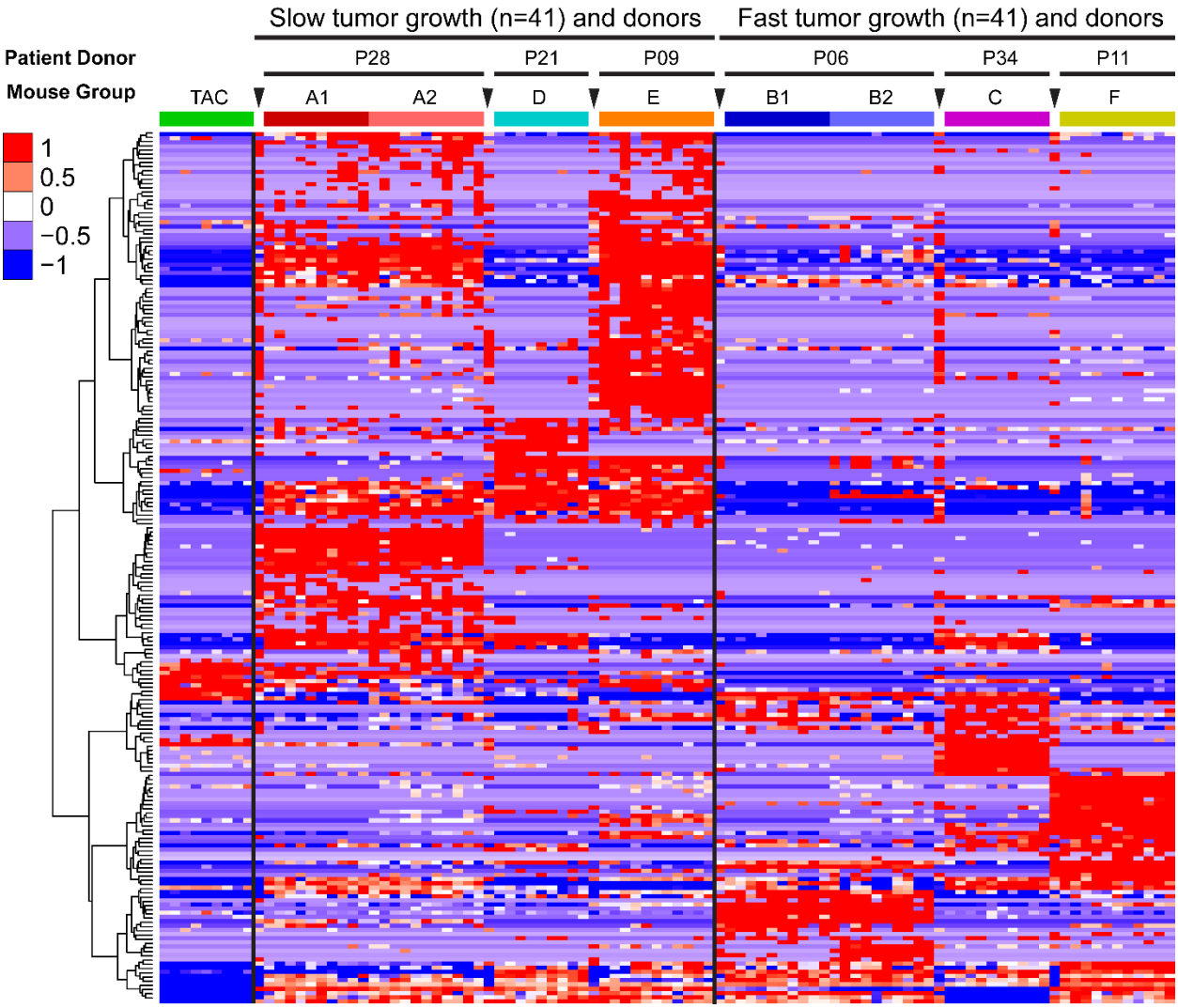

Figure 3.12 Shared OTUs between colonized mice and donor patient samples.
Relative abundance of 207 OTUs from patient donors that colonized in mice and were differentially abundant between slow and fast tumor growth groups. Columns depict individual mice arranged in groups A through F, with donor patient sample column indicated by arrowhead, and donor ID shown above each mouse group. Rows indicate individual OTUs with exact reference ID match between human and mouse 16S rRNA data sets.

Several of the bacterial species that were identified in the current study to be differentially abundant in responding versus nonresponding patients have been examined previously for mechanistic impact on host immune responses in GF mice in vivo (92). Monocolonization with several species found to be at increased frequency in our responders—including *E. faecium, C. aerofaciens, B. adolescentis,* and *P. merdae*—were reported to result in a decreased frequency of peripherally derived colonic regulatory T cells as compared with that of other bacterial species. An increased frequency of the Batf3-lineage dendritic cells (DCs) and greater T helper cell 1 (Th1) responses were also found with bacteria currently identified to be more abundant in responders (92). Decreased regulatory T cells, increased Batf3 DCs, and augmented Th1responses would all be expected to improve immune-mediated tumor control. Although care should be taken extrapolating these results in the setting of a complex microbiota, the data suggest that patient responder–associated bacteria may have a distinct effect on innate and adaptive immunity both locally and systemically.

Two additional studies have identified an association of the commensal microbiome with anti–PD-1 mAb efficacy in different solid cancers (110, 114). Our approaches differ in the method of segregation of patients between R and NR groups and in some methods of analysis. Therefore, direct comparison of the differentially enriched commensal microbiota in R and NR patients across publications should be addressed with caution. Nonetheless, there is agreement with respect to a mechanistic impact of the microbiome on efficacy of anti–PD-1 immunotherapy because fecal transfer from R versus NR patients to GF mice was also able to recapitulate the patient phenotype.

In addition to the microbiome, it is apparent that additional tumor and host factors can affect the efficacy of anti-tumor immunity and cancer immunotherapy. Tumor-intrinsic activation of the Wnt/β-catenin pathway (38) and deletion or mutation of *Pten* (40) have been shown to lead

to deficient T cell infiltration into the tumor microenvironment and resistance to checkpoint blockade immunotherapy. Germline polymorphisms in immune regulatory genes also have the potential to influence the magnitude of spontaneous anti-tumor T cell responses (181). Our results described here open the avenue for integrating commensal microbial composition, along with tumor genomics and germline genetics, into a multiparameter model with which to maximize the ability of predicting which patients are likely to respond to immunotherapies such as anti–PD-1.

Chapter 4: The gut microbiome modulates innate immunity, impacting cancer immunotherapy in mice

4.1 Responsiveness to PD-L1 blockade is inherited in offspring mice via the commensal microbiota

Based on the data presented in Chapter 3 which support the connection between the gut microbiome and immunotherapy efficacy in patients, we sought to establish a robust model to study the influence of the microbiota on anti-tumor immunity and elucidate the mechanism of this effect. Given our initial evidence with mice reconstituted with stool from responder A (Patient 28) and compared to non-responder B (Patient 06), we decided to use this representative R and NR pair to pursue a more detailed understanding of immunological mechanisms. Due to the physiological defects present in germ-free (GF) mice, we first wanted to establish whether the differences we observed were an artificial effect of colonization as adults. This acute transfer of bacteria into mice that completely lacked a microbiome could lead to bacterial translocation to typically sterile organs such as the mesenteric lymph nodes and spleen due to compromised barrier function seen in germ-free mice. It also could lead to sudden re-shaping of host immune homeostasis. Therefore, to establish a model of more "naturally" colonized mice which acquire microbes from birth and follow a normal course of immunological development, we bred mice which had been colonized as adults with patient stool samples (referred to as Ex-GF) (Figure 4.1A). The F1 generation, established from the Ex-GF founders, was then bred to establish an F2 generation. Subsequently, we established a colony of naturally colonized offspring in a sterile isolator to maintain microbial diversity without outside contamination, and fecal material from these mice was used to colonized germ-free mice as necessary to compare to their naturally colonized counterparts. These multiple generations were then used to evaluate the stability and heritability of the microbiome and its effects on anti-tumor immunity.

We observed a similar pattern of B16.SIY tumor growth with anti-PD-L1 therapy in the A and B models when comparing the Ex-GF and naturally colonized F1 and F2 generations, with the A mice, colonized by the R, growing more slowly than the B mice colonized by the NR (Figure 4.1B). These data support that the effect of the gut microbiome on tumor growth is not an artifact of acute bacterial colonization in adult mice and demonstrates that responsiveness to anti-PD-L1 therapy can be inherited in offspring mice via the commensal microbiota.

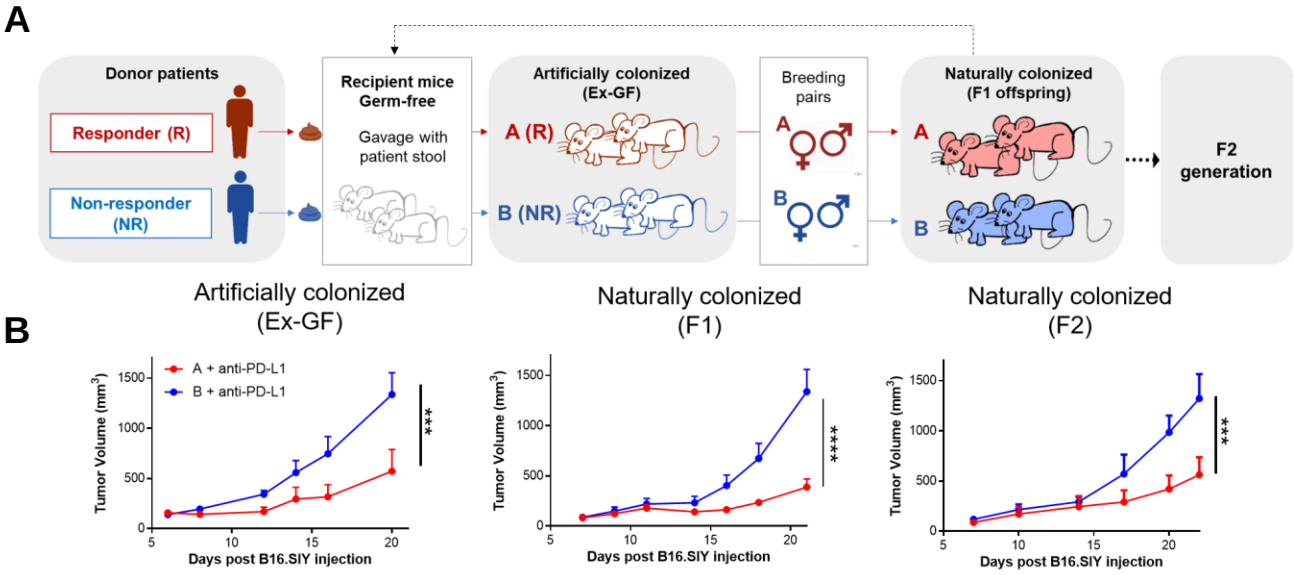

Figure 4.1 Responsiveness to PD-1/PD-L1 blockade is inherited in offspring mice via the commensal microbiota.
(A) Experimental approach to establish a colony of naturally colonized microbiota avatar mice from an original patient sample. (B) Similar R/NR growth kinetics using B16.SIY with anti-PD-L1 in Ex-GF and naturally colonized mice from the F1 and F2 generation.

Given the conservation of the tumor growth phenotype over multiple generations, we performed 16S rRNA gene amplicon sequencing on fecal samples in to assess whether the composition of the gut microbiome was similarly preserved. Based on the beta diversity of the samples, we found that the original Ex-GF mouse samples and subsequent naturally colonized mice clustered together with the original patient donor sample from which they were derived from (Figure 4.2A). Additionally, no global shifts in bacterial diversity were apparent via the different

modes of colonization. When comparing bacterial alpha diversity, or microbial richness, we found that the original R patient sample had higher diversity compared to the NR sample, and that difference in bacterial diversity was preserved in the avatar mice (Figure 4.2B). Comparing the relative abundance of taxa identified in all samples, 235 taxa were identified as differentially present between A and B mice (Figure 4.2C). These results demonstrate that these microbiota models are both experimentally robust and microbially distinct, offering the potential for novel discoveries into the mechanistic connection between the gut microbiome and anti-tumor immune response.

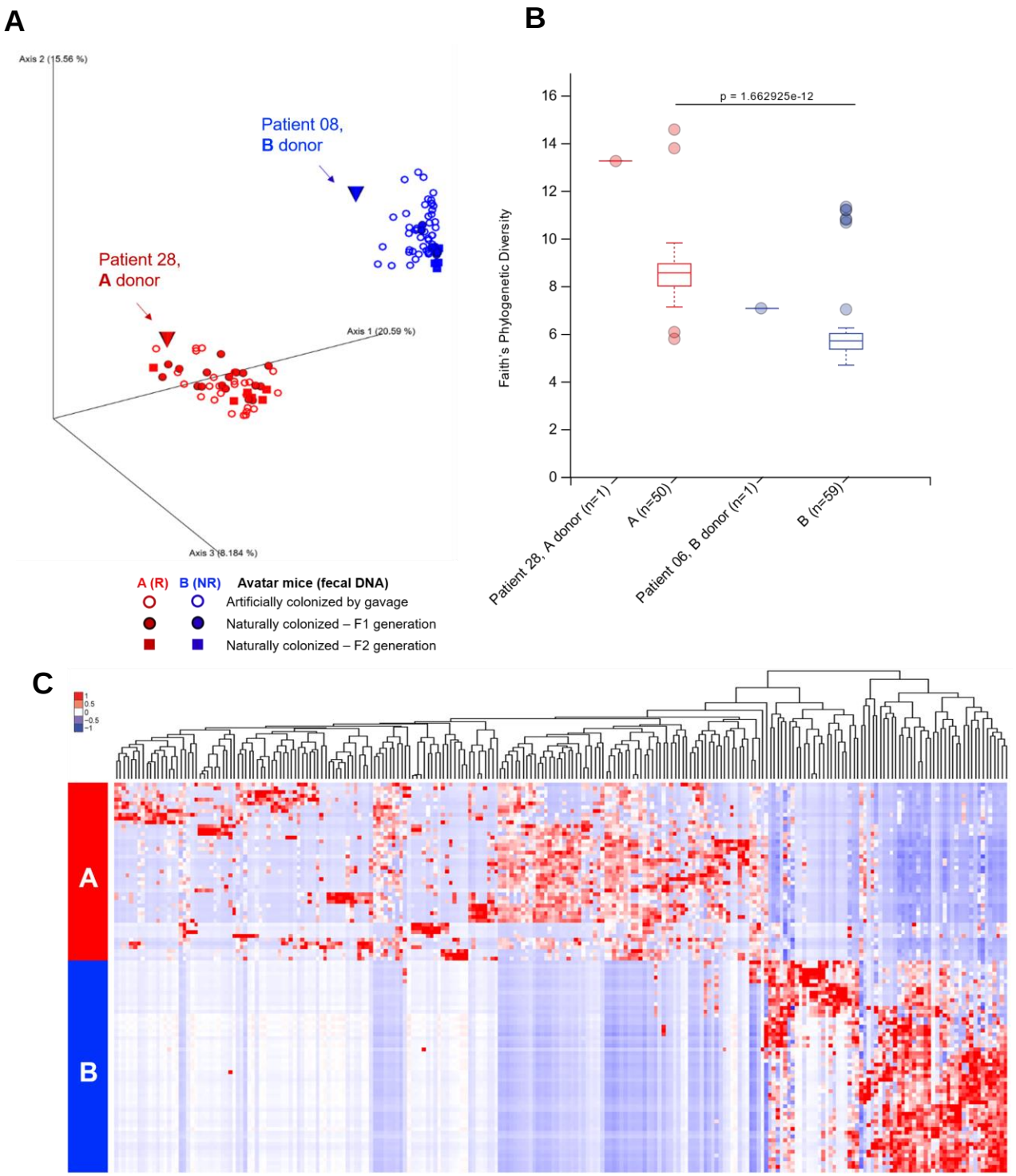

Figure 4.2 A stable and distinct gut microbiome is established between R and NR avatar mice with variable bacterial diversity and taxa.
(A) Bray Curtis PCoA plot representing microbial diversity of 16S rRNA sequencing from stool samples distinguishes A and B mice based on patient donor, but not mode of colonization. (B) Microbial richness is greater in original R patient sample compared to NR patient and difference in diversity is preserved in avatar mice. (C) Unsupervised hierarchical clustering of OTUs which differ between Mice A and Mice B show distinct taxa present in each model.

To determine whether either of these reconstituted mouse colonies showed evidence for bacterial translocation, we assessed intestinal barrier function in non-tumor bearing mice. We found comparable levels of intestinal integrity by measuring circulating levels of FITC dextran 3.5 hours after oral administration (Figure 4.3A-B). Additionally, we cultured cell suspensions isolated from the spleen and tumor to assess whether intestinally derived bacteria could be detected in those normally sterile organs. Germ-free mice were used as a negative control, and mice which received a 400-gray dose of total body irradiation, which had previously been shown to lead to bacterial translocation (107), were used as a positive control. In fact, there was no detectable systemic bacterial translocation or intra-tumoral bacteria in either model of naturally colonized mice 14 days after tumor transplantation (Figure 4.3C). These data collectively suggest that the two models develop barrier function equivalently and appear to lack detectable bacterial translocation. This observation is of particular importance within the tumor microenvironment, thus eliminating intra-tumoral bacteria as a possible explanation accounting for differences in anti-PD-L1 efficacy observed between the models A and B.

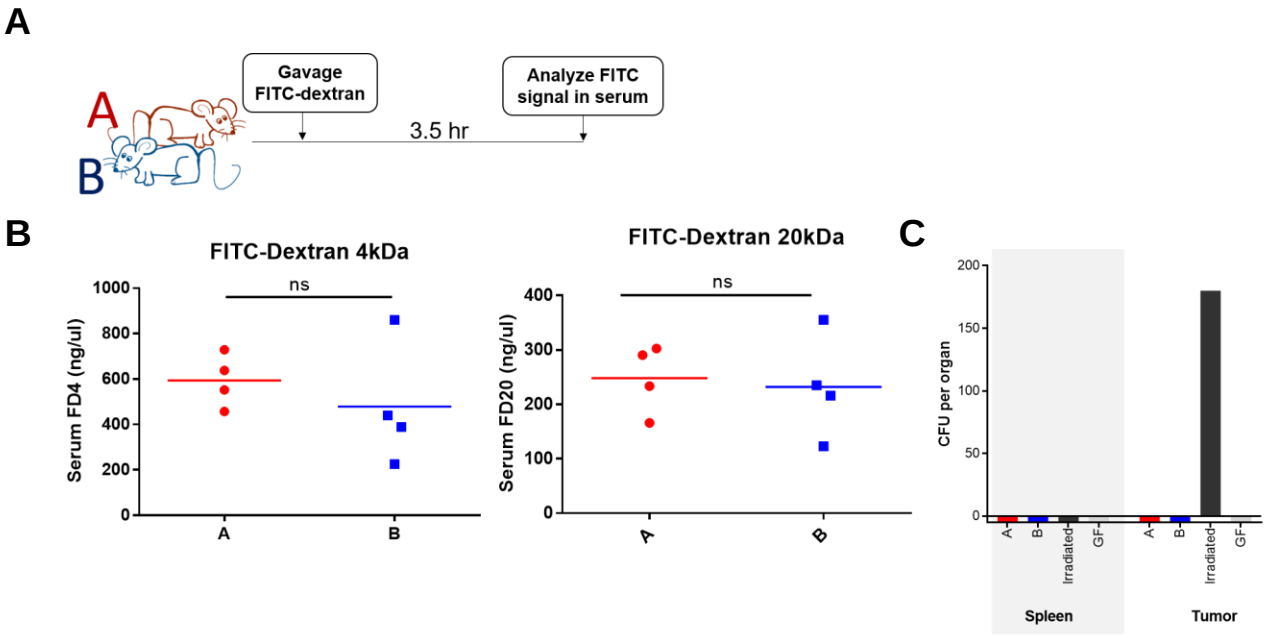

Figure 4.3 Equivalent barrier function and absence of bacterial translocation in naturally colonized microbiota avatar mice.
(A) Overview of experimental set up for Figure 4.3B. (B) No difference in intestinal barrier integrity or leakiness determined by circulating levels of FITC dextran of two different sizes in the serum of naturally colonized, non-tumor bearing mice. (C) There is no detectable systemic bacterial translocation or intra-tumoral bacteria in either model of naturally colonized mice 14 days after tumor transplantation. Colony-forming units calculated per organ using anaerobic culture conditions.

4.2 Differential tumor control between R and NR microbiota avatar with anti-PD-L1 is immune-dependent.

Given that the differences in tumor growth observed between models A and B become more pronounced upon the addition of immune-activating anti-PD-L1 therapy, with B mice unresponsive to treatment while A mice control tumors better, we expected that these differences were reliant on the immune system. To test whether the differences in tumor growth between A and B were immune-dependent, we used antibodies to deplete $CD8^+$ T cells. We found that in the absence of $CD8^+$ T cells, tumors in A and B grew with equivalent kinetics (Figure 4.4). These findings underscore that the difference between A and B is immune-dependent and requires the

adaptive immune response, specifically CD8$^+$ T cells. Thus, the mechanism explaining improved tumor control in A mice is likely connected to improved anti-tumor T cell responses.

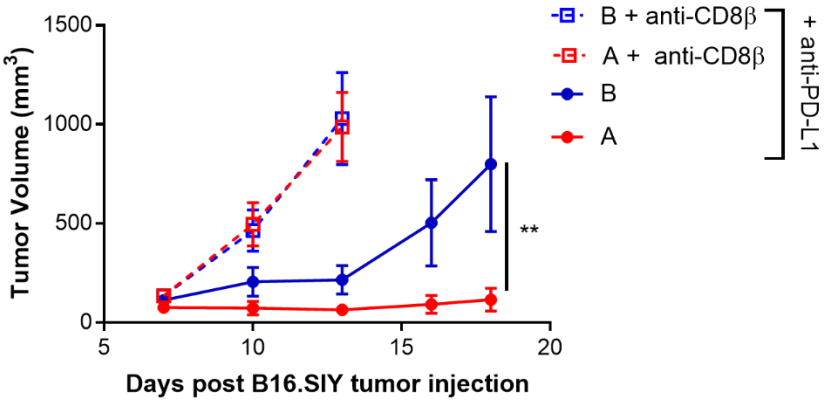

Figure 4.4 CD8$^+$ T cells are required for tumor growth differences between R and NR. Tumor growth kinetics of B16.SIY in ex-GF A and B mice treated with anti-PD-L1 and CD8β depleting antibodies administered weekly starting one day prior to tumor transplantation.

4.3 A combination of immune-potentiating and immune-inhibiting bacteria are likely modulating anti-PD-L1 efficacy

Having established that the difference in anti-PD-L1 efficacy between the two models was immune-dependent, we next investigated the directionality of the effect of the microbiome on anti-tumor immunity. More precisely, we wanted to test whether poor responsiveness to anti-PD-L1 therapy in B mice versus A mice is due to insufficient presence of immune-potentiating bacteria versus over-abundance of immune-inhibitory bacteria. To test the pro- and anti-tumor effects of the microbes present in these two microbiota models, we used a combination of antibiotics to deplete the abundance and diversity of the microbiome, in addition to fecal matter transfer (FMT) between models (Figure 4.5A). Through these various intervention strategies, numerous bacteria in A and B were depleted and transferred (Figure 4.5B). We found that administration of A microbiota to B mice via FMT improved tumor control, supporting that beneficial microbes present in A mice could confer benefit to these previously non-responding mice (Figure 4.5C). The beneficial effect of the A FMT to B mice become more pronounced with broad-spectrum oral

antibiotics prior to FMT administration, eliminating more of the native B microbiota and allowing for the establishment of more bacteria from A mice, which likely offered greater efficacy over FMT without pre-treatment with antibiotics (Figure 4.5C). In contrast, administration of B FMT significantly impaired tumor control in A mice, suggesting that when administered concurrently with anti-PD-L1, detrimental bacteria present in B could overcome the beneficial effects of the microbiota initially established in A mice (Figure 4.5D). Similarly, pre-conditioning with antibiotics before B FMT in A mice further worsened tumor control, with equivalent tumor growth kinetics to B mice (Figure 4.5D). Antibiotics alone also caused a moderate increase in tumor growth in A mice, supporting the notion that beneficial microbes are being depleted (Figure 4.5E). In contrary, treatment of B mice with antibiotics alone improved tumor control, theoretically by reducing numbers of detrimental bacteria (Figure 4.5F).

These data have important implications for the multiple mechanisms by which the microbiota can affect the anti-tumor immune response in these two models. The gut microbiome can both potentiate tumor control, as in the A model, or impair anti-tumor responses, as observed in B mice. The fact that reciprocal FMT can either potentiate or impair immune-mediated tumor control, depending on the nature of the donor and recipient, argues that the ratio of beneficial to inhibitory bacteria may be critical for therapeutic efficacy. Studying the bacteria in A mice which are transferred upon FMT and confer improved tumor control in B mice, as well as the reverse (bacteria from B mice which worsen tumor control in A mice) will help narrow in on a subset of potentially immune-modulating bacteria (Figure 4.5B). In addition, these data are important when considered in light of the somewhat conflicting data regarding the use of antibiotics and bacterial diversity as it relates to immunotherapy efficacy in cancer patients (182).

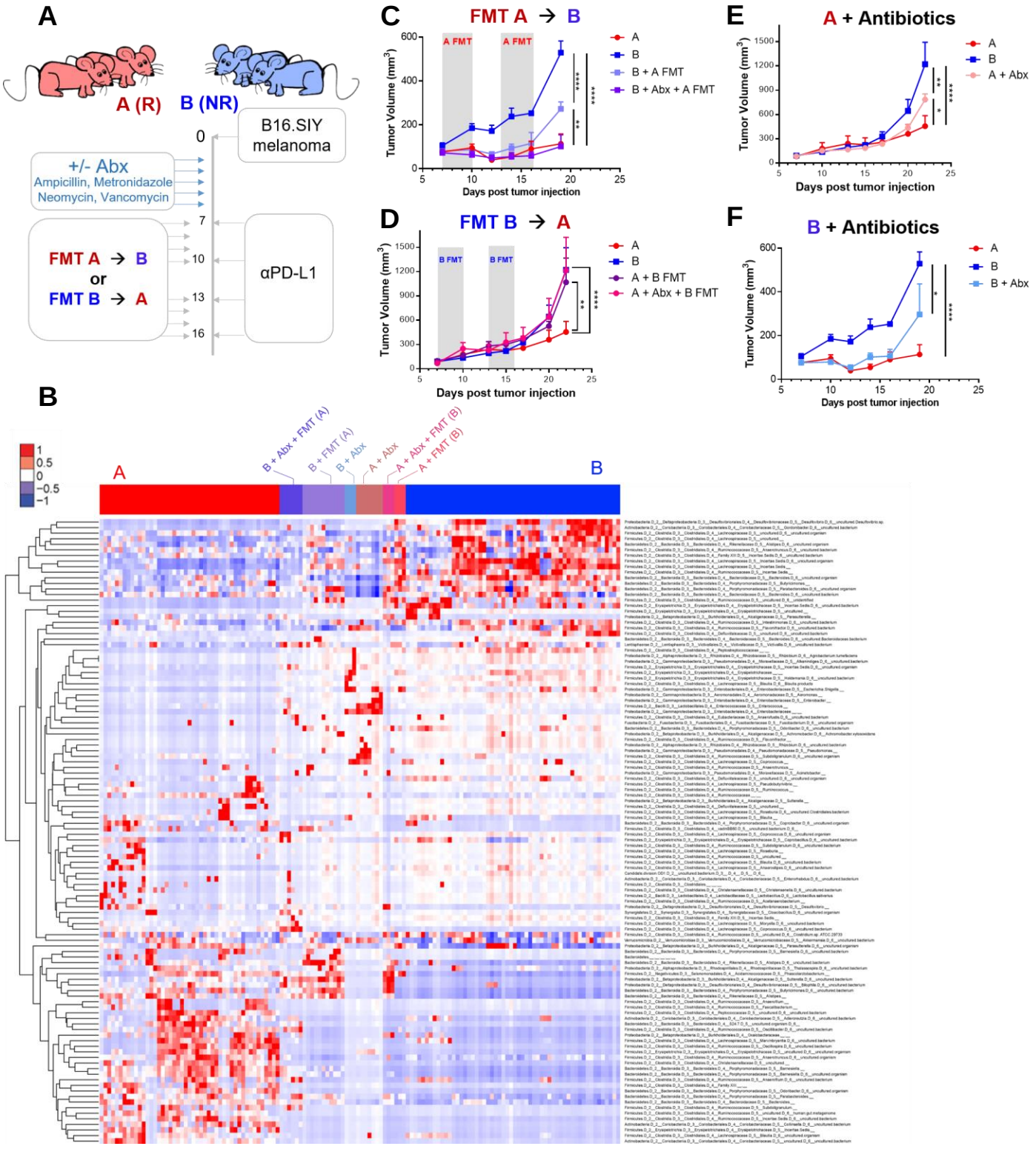

Figure 4.5 Manipulation of the gut microbiome through antibiotics or FMT suggests both the presence of detrimental taxa in NR avatar and beneficial taxa in R avatar.

Figure 4.5 (continued)
(A) Overview of experimental approach to test the effect of modulating the gut microbiome. (B) Relative abundance of 112 taxa assigned using the Silva classifier and differentially present in A and B mice across the different treatment conditions. (C-F) Tumor growth kinetics in naturally colonized mice using different intervention strategies with the B16.SIY tumor cell line.

4.4 Distinct gene expression patterns across immune infiltrate in R v NR microbiota avatar mice

Having established that the difference between model A and model B is immune-dependent and is likely influenced by the contribution of both immune-potentiating and immune-inhibitory microbes, we next assessed the impact of these two microbiotas on the detailed composition of the anti-tumor immune response. Given the multiplicity of effects that the microbiome can theoretically have on immune responses, including an impact on multiple different cell types, we employed an unbiased approach to study the changes in the identity and gene expression of the immune infiltrate in tumors from A and B mice using single cell RNA sequencing (scRNAseq) (Figure 4.6A-B). Briefly, we isolated $CD45^+$ immune cells from tumors 14 days post-transplantation in A and B mice with or without anti-PD-L1 treatment and processed the samples for single cell gene expression profiling. The following results include these four conditions from two independent experiments for 8 samples total.

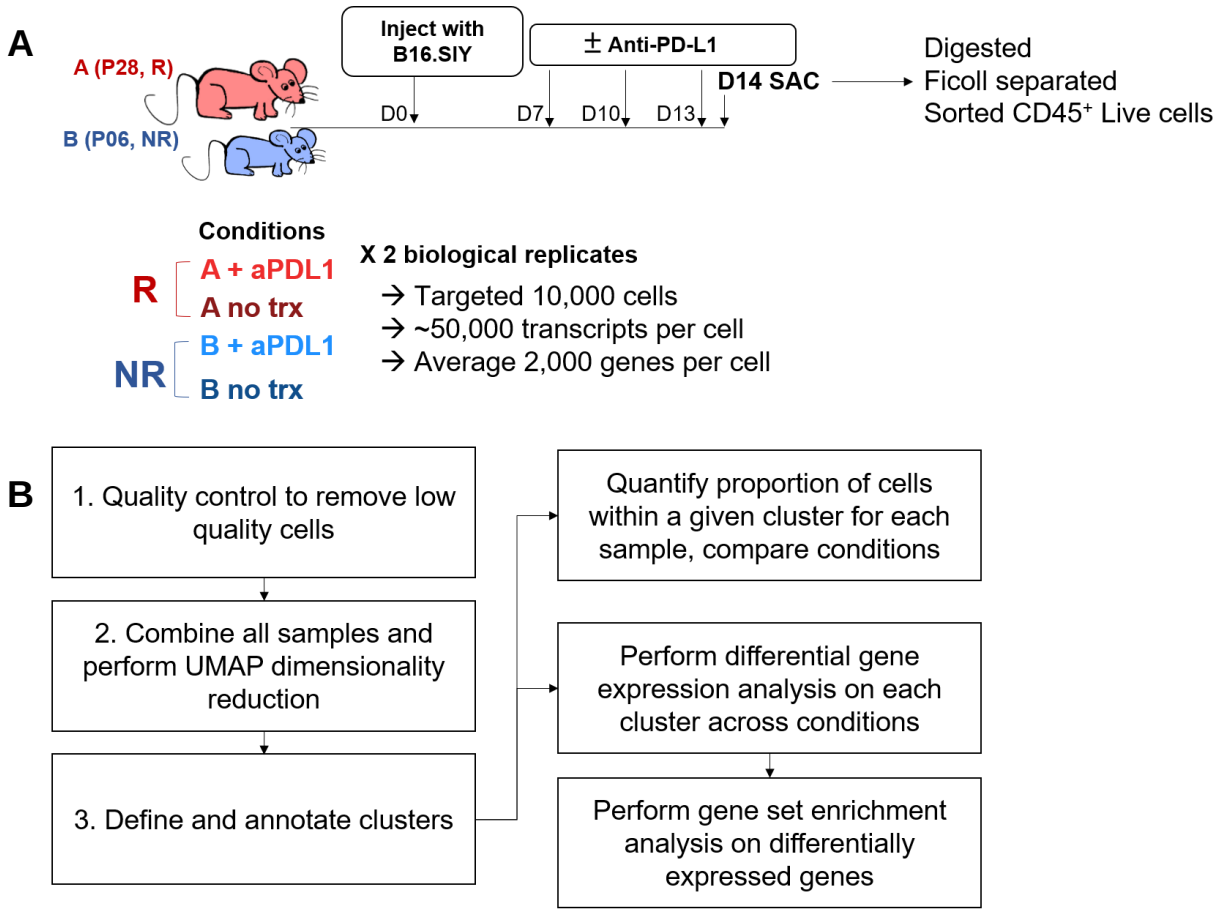

Figure 4.6 Unbiased approach to identify differences in immune infiltrates R and NR microbiota models using single cell RNA sequencing.
(A) Experimental setup to obtain tumor-infiltrating immune cells for 3' single cell RNA sequencing. (B) Overview of data analysis pipeline.

Using an unbiased analysis, we identified 32 stable cell clusters which were manually annotated based on gene expression (Figure 4.7A-B). One cluster (cluster 28) consisted of contaminating tumor cells (0.2%) and four others (2, 15, 19 and 27) were marked as low quality including suspected dead or dying cells (based on low read counts and high mitochondrial gene expression) as well as putative doublets (based on an unexpected pattern of both myeloid and lymphoid gene expression). Of the remaining 27 clusters, a distinction between lymphoid and myeloid lineage was evident across UMAP dimension 1. The group of lymphoid clusters consists

of NK cells (cluster 0, expressing Klrb1c or NK1.1) and T cells (clusters 7, 8, 13, 17 and 25 expressing CD3) including various $CD8^+$ T cell subsets as well as $CD4^+$ $Foxp3^+$ Tregs. A separate cluster marked by CD19 expression distinguished B cells (clusters 21 and 31). Among the non-lymphoid cells, the myeloid cluster consisted of cells marked by the neutrophil-specific marker S100a9 (clusters 11 and 22). A group of multiple clusters expressed macrophage-associated F4/80 (Adgre1) and could be distinguished by variable MHC-II expression among other markers, likely representing a continuum of monocytes and macrophages. Because of the ambiguous definition, these cells are collectively termed "Myeloid populations" and further categorized into two groups: "MHC-II high" (clusters 1, 4, 5 and 12) and "MHC-II low" (clusters 3, 6, 14 and 26). Two additional clusters (clusters 24 and 29) expressed low levels of F4/80 but were distinct from the previously described myeloid cell clusters via UMAP dimension 2 (clusters 24 and 29). These cells expressed high levels of genes characteristic of basophils and mast cells including Mcpt8 and Gata2. The remaining clusters included five DC populations. Two of the five clusters expressed CD11b (Itgam) and were either $CD301b^+$ (cluster 18) or $CD209^+$ (cluster 9). The remaining three DC clusters included plasmacytoid DCs based on expression of Siglec-h (cluster 20), and $CD103^+$ DCs based on CD103 (clusters 25 and 30), as well as the recently described $CCR7^+$ mregDCs (cluster 16) (183).

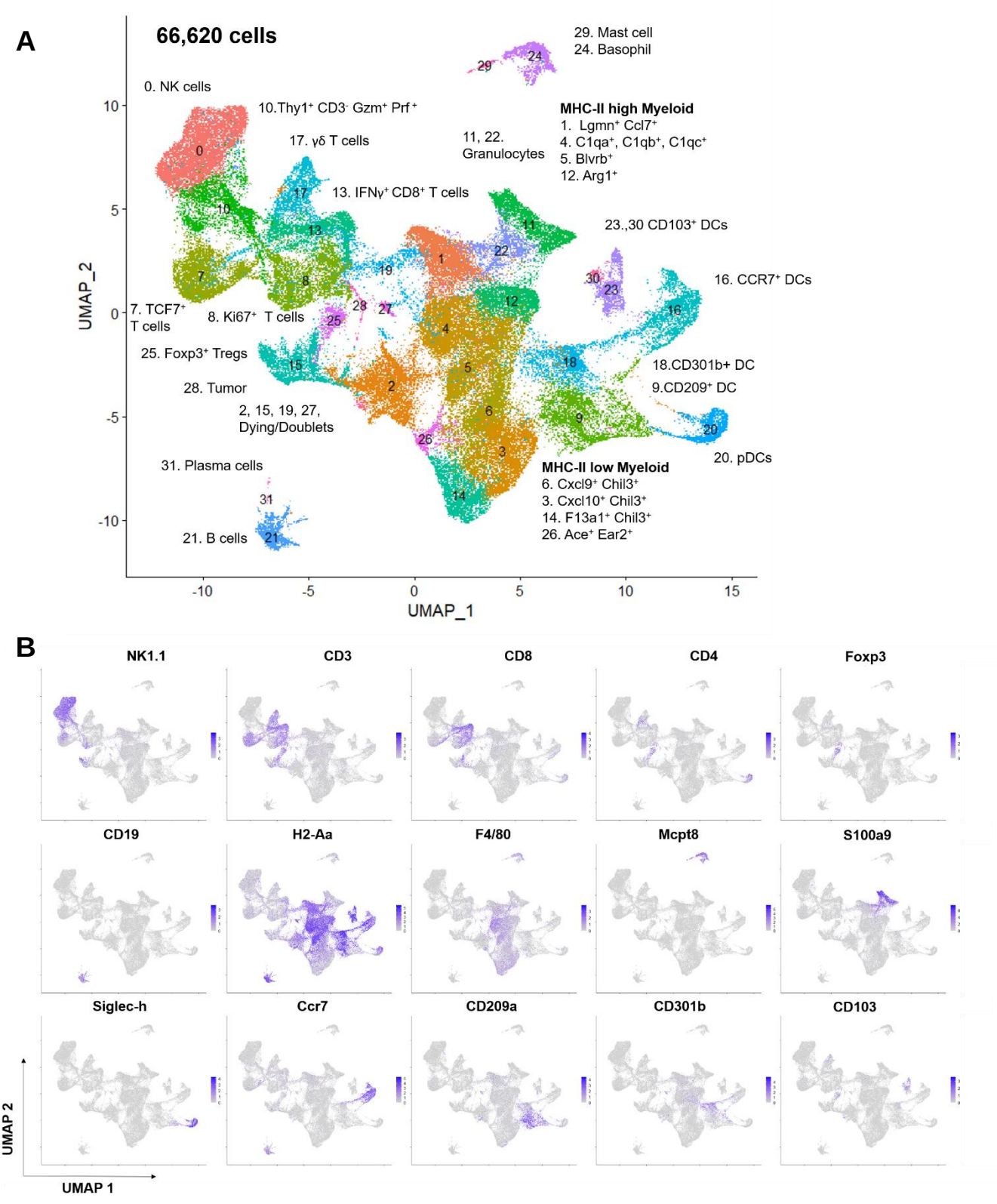

Figure 4.7 Identification of tumor-infiltrating immune cell populations by scRNAseq.
(A) UMAP reduction of tumor-infiltrating immune cells from all samples based on unsupervised clustering of scRNAseq. (B) Log transformed, normalized gene expression for indicated transcripts used to annotate clusters.

Once clusters had been annotated based on their gene expression patterns, we next evaluated whether the different commensal microbiota resulted in altered immune populations within the tumor. We observed no major expansion or contraction of any cluster across the four conditions (Figure 4.8A). When clusters were grouped by their cell type, only the proportion of MHC-II^{high} myeloid cells was significantly different between A and B in the absence of immunotherapy, with a greater proportion present in A mice compared to B, and a similar but non-significant trend was observed in mice which treated with ani-PD-L1 (Figure 4.8B).

We next asked whether gene expression was altered within the same cell types across the microbiota models. We performed differential expression analysis and found across all clusters a greater number of differentially expressed genes (DEGs) present when comparing the models A and B without treatment (DEGs = 3,055) compared to A and B treated with anti-PD-L1 (DEGs = 629) (Figure 4.8C). We speculate that this may be due to the strong effect of anti-PD-L1 therapy on gene expression, masking the effect of the microbiota at the time point assessed which was one day after the third dose of anti-PD-L1. MHC-II^{high} myeloid cells displayed the greatest number of DEGs in both comparisons with and without treatment, making up 35.6% and 26.8% of the total DEGs, respectively. Among the non-treated comparison, the largest number of differentially expressed genes within a single cluster was the IFN-γ^+ CD8$^+$ T cell cluster, comprising 16% of all DEGs. In the comparison between anti-PD-L1 treated conditions, the single cluster with the greatest number of differentially expressed genes was one of two granulocyte clusters, which collectively accounted for 29.3% of all DEGs. Given that these three populations—IFN-γ^+ CD8$^+$ T cells, MHC-II^{high} myeloid cells, and granulocytes—had the greatest number of differences in gene expression, further analysis on the DEGs was performed to understand the impact of the microbiome on these cell types.

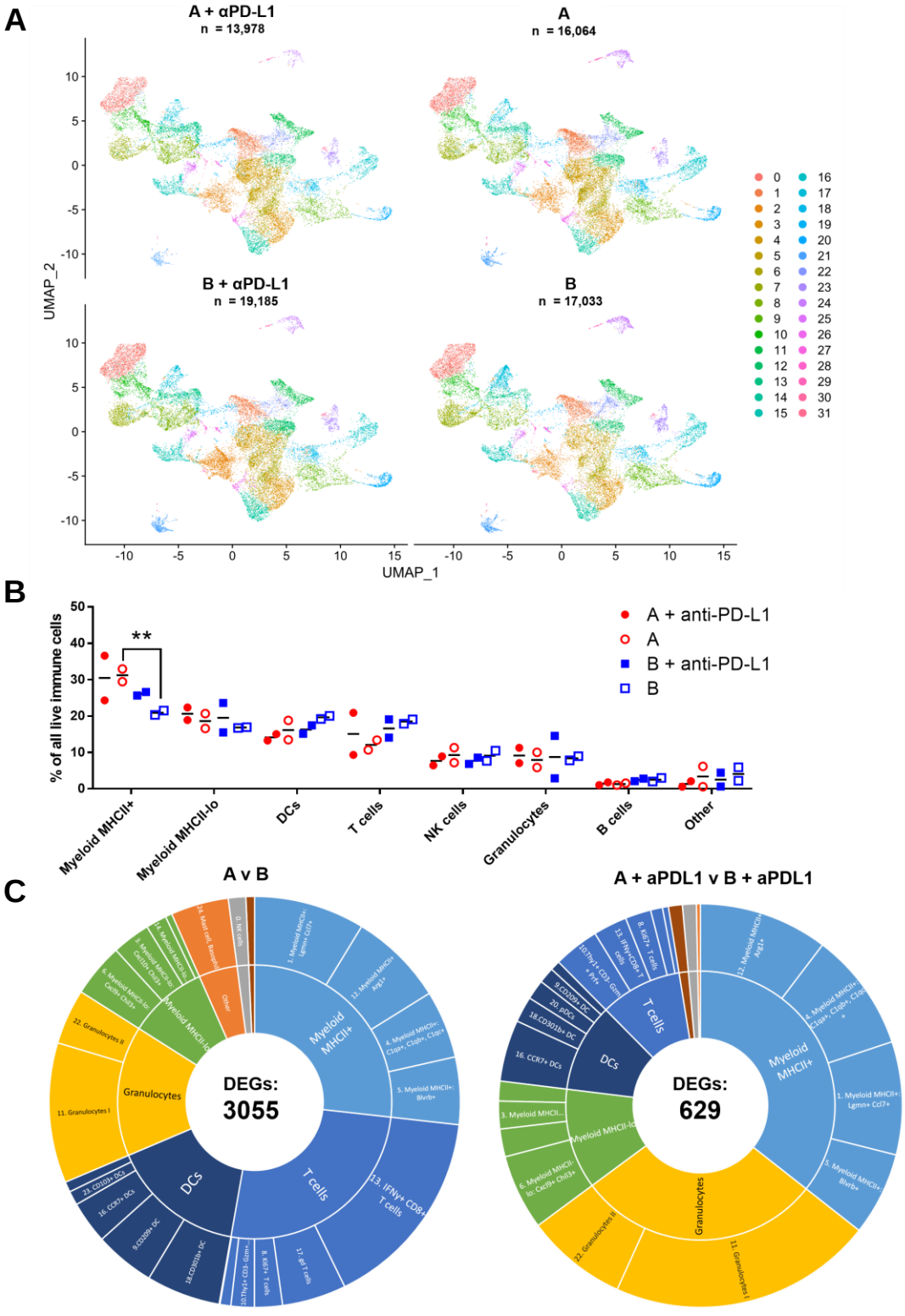

Figure 4.8 Distinct gene expression patterns across intra-tumoral immune cells in R v NR microbiota avatar mice.

Figure 4.8 (continued)
(A) UMAP projection of the four conditions including both biological replicates show no major shifts among clusters. (B) Percent of cells within major immune cell subtypes for each sample. Significant comparisons determined by two-way ANOVA corrected for multiple comparisons. (C) Differentially expressed genes across conditions where the percent of differentially expressed genes within a given cluster or cell type is represented by the proportion of the circle.

4.5 Tumor-infiltrating CD8$^+$ T cells are more activated in R mice compared to NR

We had previously observed a greater proportion of tumor-antigen specific CD8$^+$ T cells in A mice compared to B mice (Figure 3.11) and so many DEGs within the IFN-γ$^+$ CD8$^+$ T cell population was consistent with our expectations for an improved CD8$^+$ T cell response in A mice. Additionally, we had established that CD8$^+$ T cells were required for B16.SIY tumor growth differences between models A and B through depletion experiments. The IFN-γ$^+$ CD8$^+$ T cell cluster is likely the main T cell cluster responsible for anti-tumor control within the tumor microenvironment, given its high expression of IFN-γ compared to the other T cell clusters as well as the functional importance of IFN-γ for immune-mediated tumor rejection. Analysis of the DEGs within this cluster identified multiple markers associated with T cell activation and function increased in A mice compared to B (Figure 4.9A-B). CD8$^+$ T cells in B mice expressed very low levels of LAG-3, 4-1BB, PD-1 and TIM-3, indicating a reduced proportion of T cells showing evidence for activation. With the addition of anti-PD-L1 Ab treatment in B mice, T cells expressed slightly higher levels of these markers as expected, but still at levels lower than A mice. Similarly, the expression level for cytotoxic molecules perforin and granzyme was very low in B mice compared to A mice. These data support that A mice have a quantitatively superior anti-tumor CD8$^+$ T cell response based on gene expression.

To confirm the more activated CD8$^+$ T cell response we found in A mice via single cell RNA sequencing, we analyzed tumor-infiltrating T cells at endpoint by flow cytometry. Compared to B mice, A mice had increased frequency of CD44^{hi} PD-1$^+$ CD8$^+$ T cells within the tumor

consistent with increased activation (Figure 4.9C). We also found a higher percent and greater accumulation of tumor-antigen specific CD8$^+$ T cells using the MHC class I SIY peptide pentamer (Figure 4.9D-E). These data support that in A mice, tumor-infiltrating T cells have a more activated phenotype which is modulated either indirectly or directly by the gut microbiome.

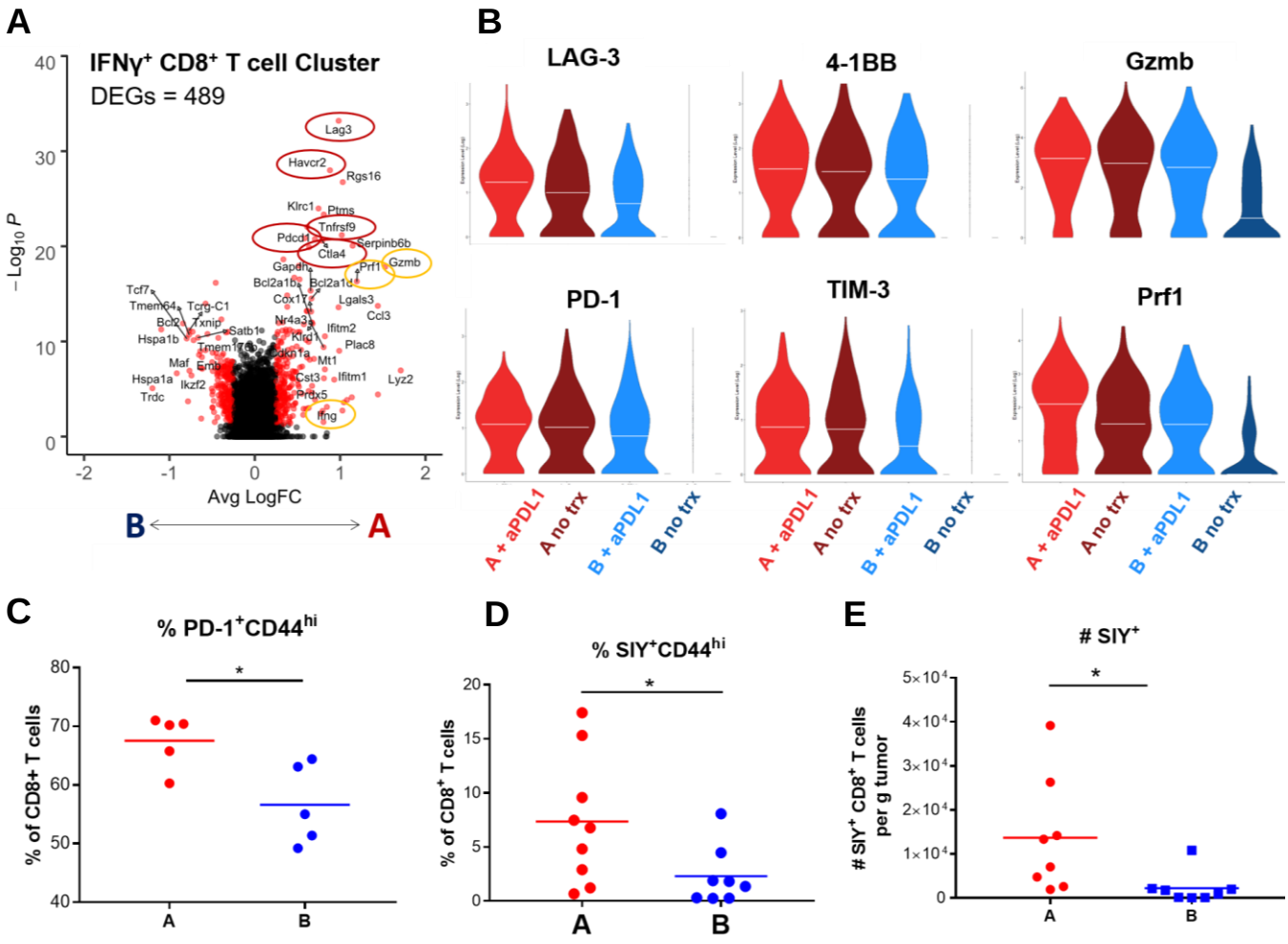

Figure 4.9 More activated CD8$^+$ phenotype T cell response in R mice compared to NR.
(A) Volcano plot of differentially expressed genes between models A and B within the IFN-γ$^+$ CD8$^+$ T cell cluster. (B) Violin plot of selected markers of T cell activation and exhaustion. (C-E) Flow cytometry at endpoint in B16.SIY tumors treated with anti-PD-L1. (C) Increased expression of CD8$^+$ T cell activation markers CD44 and PD-1 in A. (D-E) Increased accumulation of tumor antigen specific CD8$^+$ T cells using MHC-I/SIY pentamer in A mice compared to B by percent (D) and total number per gram tumor (E).

4.6 The gut microbiome influences the polarization of tumor-associated macrophages in the tumor microenvironment

The MHC-II^{high} myeloid cells were the only cell type which differed by percentage between A and B (Figure 4.8B) and also included the greatest number of DEGs (Figure 4.8C) across both the treated and untreated conditions. Inspection of the most significant DEGs across all MHC-II^{high} myeloid cell clusters revealed many genes associated with M2, or pro-tumor, macrophages that were more highly expressed in B mice compared to A which expressed higher levels of genes associated with M1, or anti-tumor, macrophages (Figure 4.10A). These patterns of M1 and M2 gene expression were consistent across all four clusters of the MHC-II^{+} myeloid cell types (Figure 4.10B).

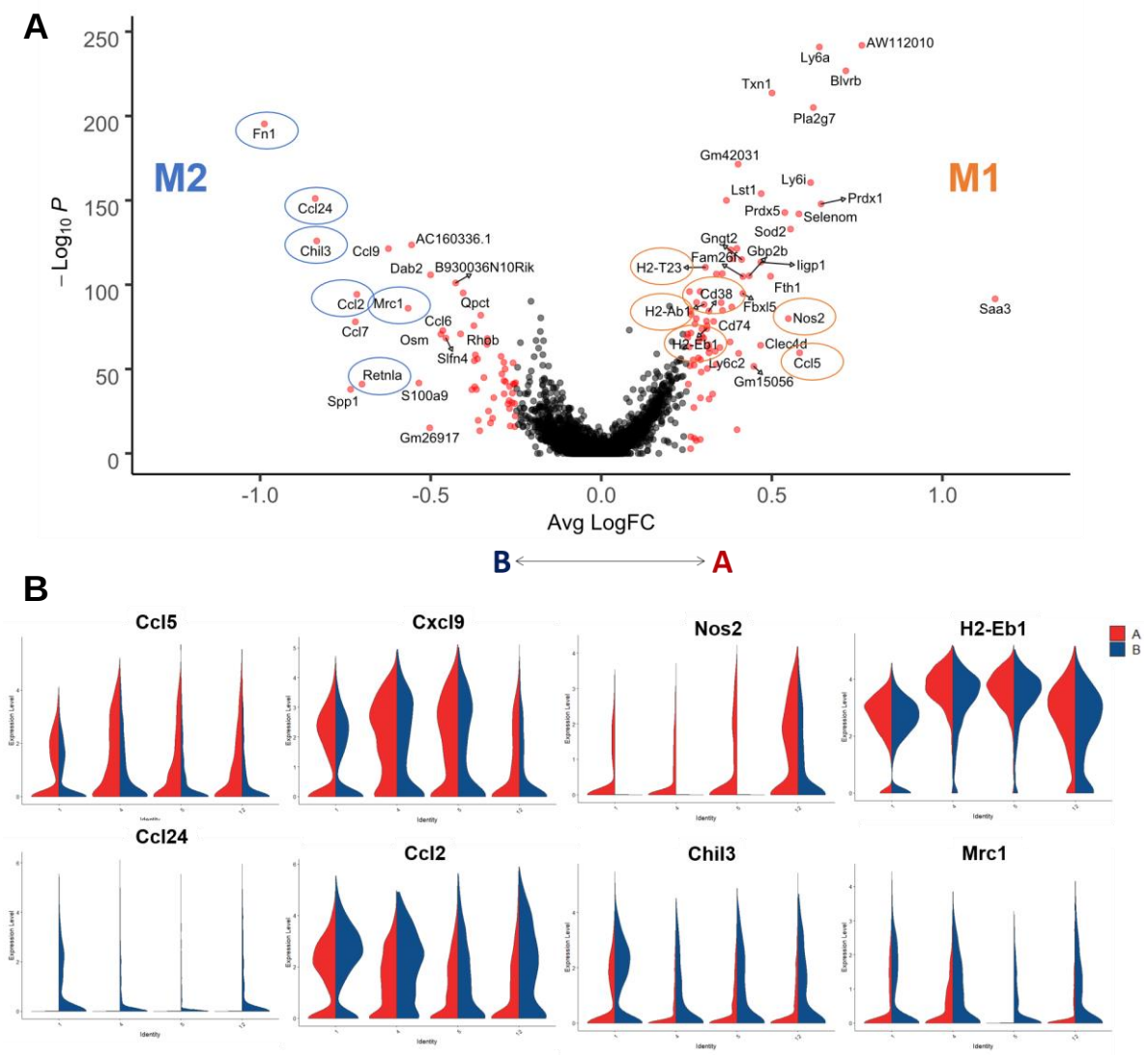

Figure 4.10 Tumor-associated macrophages in NR mice have more M2 gene expression profile vs M1 phenotype in R.
(A) Volcano plot of differentially expressed genes between models A and B in the four clusters comprising the MHC-II^{+} myeloid cells class. Highlighted are typical M2 (left, blue) and M1 (right, orange) associated gene expression markers. (B) Violin plots of normalized gene expression for select M1 (top) and M2 (bottom) genes across the four MHC-II^{high} myeloid cell clusters.

We next wanted to validate the differential M1/M2 polarization we observed via gene expression within the myeloid compartment by flow cytometry. We classified tumor-associated macrophages (TAMs) as live CD45^{+}CD3^{-}CD19^{-}NK1.1^{-}Ly6G^{-}Ly6C^{-}CD11b^{+}F4/80^{+}. Within this F4/80^{+} population we observed an MHC-II^{low} population and an MHC-II^{high} population. These flow data are consistent with our scRNAseq observations which identified two subclasses within

the larger myeloid cell type (MHC-II^{low} and MHC-II^{high}), as well as an MHC-II^{low} polymorphonuclear cell cluster. Based on our single cell data, we specifically analyzed MHC-II^{high} F4/80^{+} macrophages. We used the markers CD206 (Mrc1) and CD86 to distinguish between M1 macrophages (CD86^{+} CD206^{-}) and M2 macrophages (CD206^{+} CD86^{-}). Consistent from our scRNAseq data, we observed that macrophages in B mice expressed higher levels of CD206 and greater proportion were classified as M2 (Figure 4.11A-B). Conversely, TAMs in A mice expressed higher levels of CD86 and an increased percent were M1 macrophages (Figure 4.11C-D).

Because macrophage polarization is influenced by environmental cues, we assessed serum cytokine levels to determine whether there was evidence of cytokines capable of supporting macrophage differentiation towards either the M1 or M2 state. We found increased levels of IFN-γ in the serum of A mice compared to B, a cytokine which helps promote M1 polarization (Figure 4.11E). We also found higher levels of IL-12p70 as well as CXCL5 in A mice, both of which are M1-secreted factors (Figure 4.11F-G). These data are indicative of circulating factors which are conducive to M1 polarization in the A mice and are indicative of an overall more pro-inflammatory (anti-tumor) immune state.

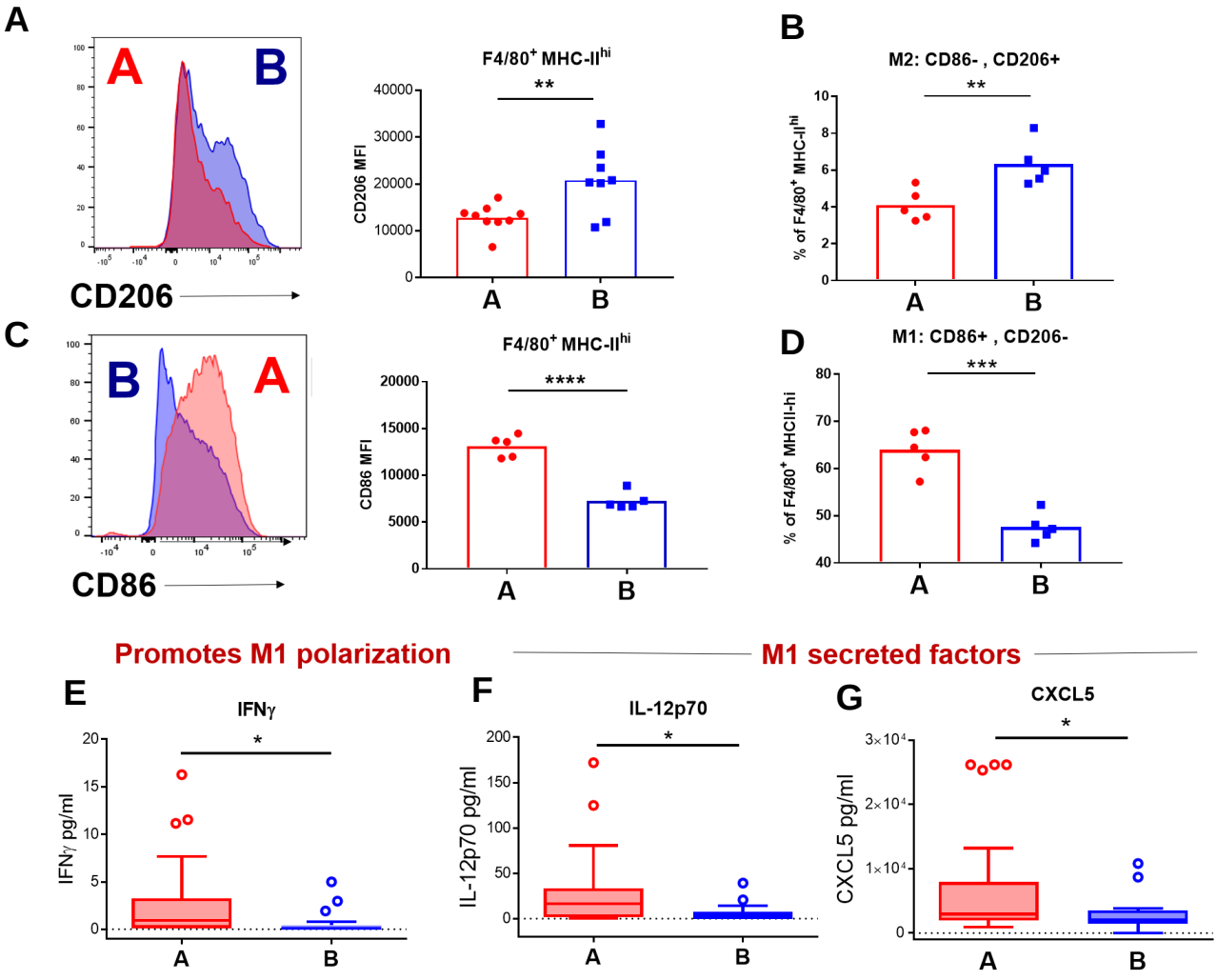

Figure 4.11 Increased M1 macrophage markers in TAMs and circulating levels of M1-associated cytokines in R mice compared to NR.
Flow and cytokine samples were collected from B16.SIY bearing mice treated with anti-PD-L1 at tumor endpoint (A-G). (A) Representative histogram of M2 associated marker CD206 (Mrc1) in TAMs and quantification by MFI in TAMs. (B) Percent of M2 macrophages in tumor. (C) Representative histogram of M1 associated marker CD86 in TAMs and quantification by MFI. (D) Percent of M1 macrophages in tumor. (E-G) Serum levels of indicated cytokines and chemokines.

4.7 The gut microbiome impacts the phenotype of granulocytic cells within the tumor microenvironment and alters numbers systemically

The neutrophil/granulocyte clusters were an unexpected population of interest, representing only about only 8% of total immune cells on average, but accounting for 15.4% and 29.3% of total DEGs in the baseline and anti-PD-L1 treated comparisons, respectively. As described previously (Chapter 1.1), tumor-associated neutrophils (TANs) can have both pro- or

anti-tumor functions, depending on their cell state and at different stages of tumor development. We asked whether neutrophils from the two models differed based on their gene programs towards either a pro-inflammatory neutrophil or a granulocytic myeloid-derived suppressive cell (G-MDSCs). Using a gene set developed using scRNAseq to distinguish between these two cell states (184), we observed TANs in B mice had increased expression of genes associated with G-MDSCs compared to A mice (Figure 4.12A). MDSC-related genes included Ptgs2 (or COX-2), Cebpb, S100a8 and S100a9 (185) (Figure 4.12B). Further confirming these findings, using an unrelated gene set including genes up-regulated in comparison of neutrophils versus G-MDSCs (186) we found that the neutrophils from A mice expressed higher levels of genes characteristic of typical neutrophils, compared to the immune-inhibitory MDSC phenotype (Figure 4.12C). Markers to distinguish classical neutrophils versus G-MDSCs have not been well established, however, CD44 gene expression has recently been associated with G-MDSC and was the most significant DEG with greater expression in B mice compared to A within the neutrophil clusters (Figure 4.12D). By flow cytometry we confirmed higher expression of CD44 in B16.SIY tumor-infiltrating $Ly6G^{+}$ neutrophils in B mice compared to A, confirming a more MDSC-like phenotype (Figure 4.12E). Collectively, these data indicate that both macrophages and neutrophils within the tumor microenvironment can be shifted by the microbiota, leading to either a more immune-suppressive state (as observed in B mice) or a more pro-inflammatory and anti-tumor state (as seen in A mice).

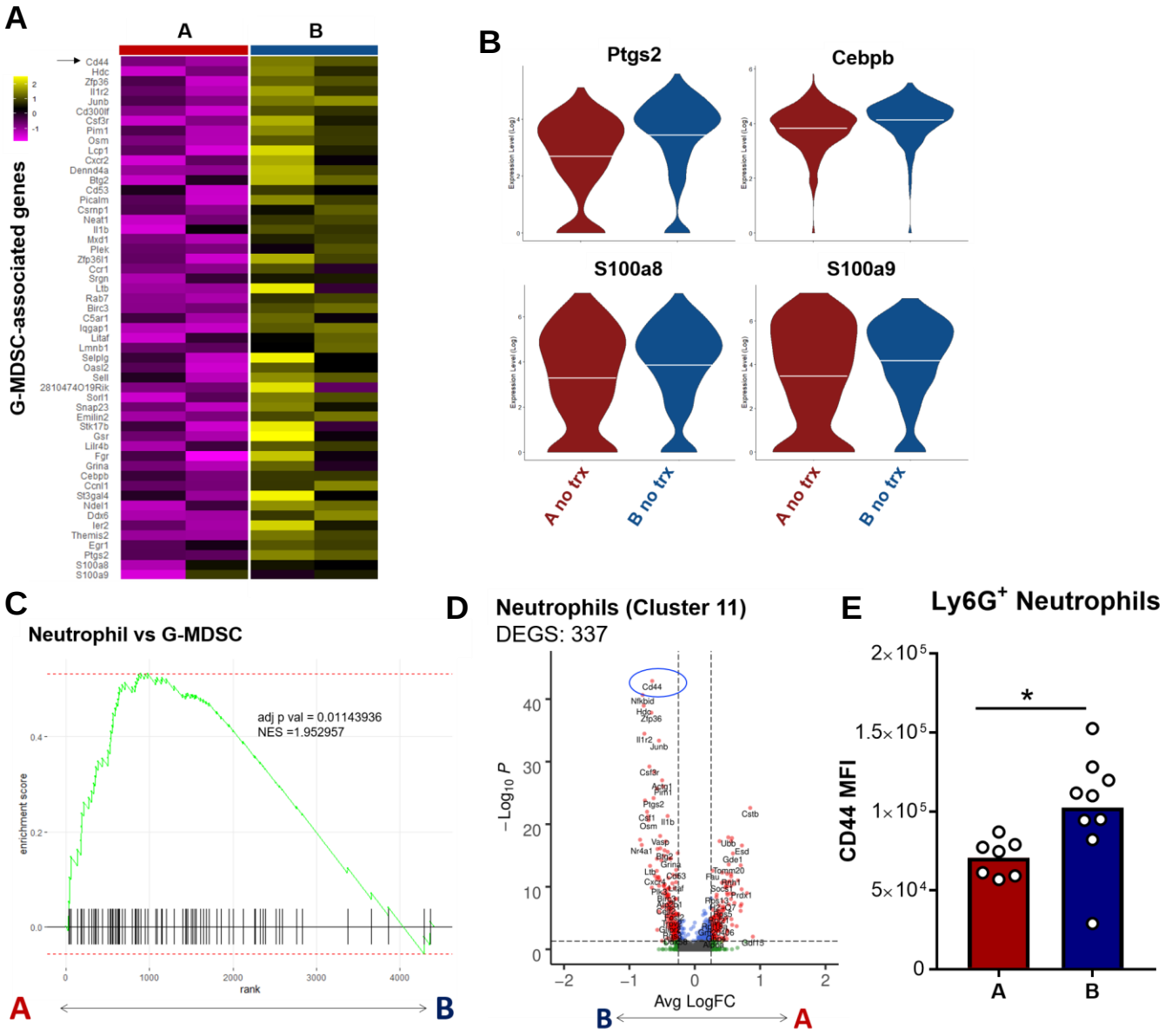

Figure 4.12 Increased MDSC-like gene expression in tumor-infiltrating granulocytes from NR mice compared to R.

(A) Normalized gene expression of G-MDSC specific gene set in combined neutrophil clusters. (B) Violin plot of common transcription targets associated with MDSC polarization. (C) GSEA of genes up-regulated in comparison of neutrophils vs G-MDSCs using genes ranked by fold change of A expression over B. (D) Volcano plot of differentially expressed genes between models A and B in neutrophil cluster 11 highlighting CD44. (E) MFI of CD44 on Ly6G^{+} neutrophils in B16.SIY tumors treated with anti-PD-L1 at endpoint.

Because we observed changes in the neutrophils within the tumor microenvironment, we next asked whether we could find evidence of alterations within this population systemically. A more global change among neutrophils between the two models would be supportive that these cells are directly influenced by the microbiome. We first looked within the circulation of naïve, non-tumor bearing mice to ascertain any effects of the microbiome in the absence of a tumor. It has been previously shown that tumors can lead to extramedullary hematopoiesis and increased peripheral polymorphonuclear cells (187). In the blood of germfree animals, we found very low levels of $Ly6G^+$ neutrophils initially, but post colonization with either A or B fecal material, observed a marked increase (Figure 4.13A) with a greater expansion of this population in B mice compared to A (Figure 4.13B). Similarly, in the circulation of naturally colonized A and B mice, we also saw an increased proportion of $Ly6G^+$ neutrophils in B mice compared to A (Figure 4.13C). These data are supportive of direct effects of the microbiota on granulocyte number and differentiation state.

We next wanted to evaluate changes among neutrophil numbers within immune organs in B16.SIY tumor-bearing animals. We found an increase in the percent of $Ly6G^+$ neutrophils in the spleen (Figure 4.13D) and in the mesenteric lymph nodes (Figure 4.13E) of B mice at endpoint. An increase within the intestinal-associated lymph nodes is suggestive of a direct link between the microbiota and expansion of $Ly6G^+$ neutrophils. There were no changes in the total number of neutrophils in the tumor, in line with scRNAseq results which find no difference in proportion, but rather phenotypic changes within these cells (Figure 4.13F).

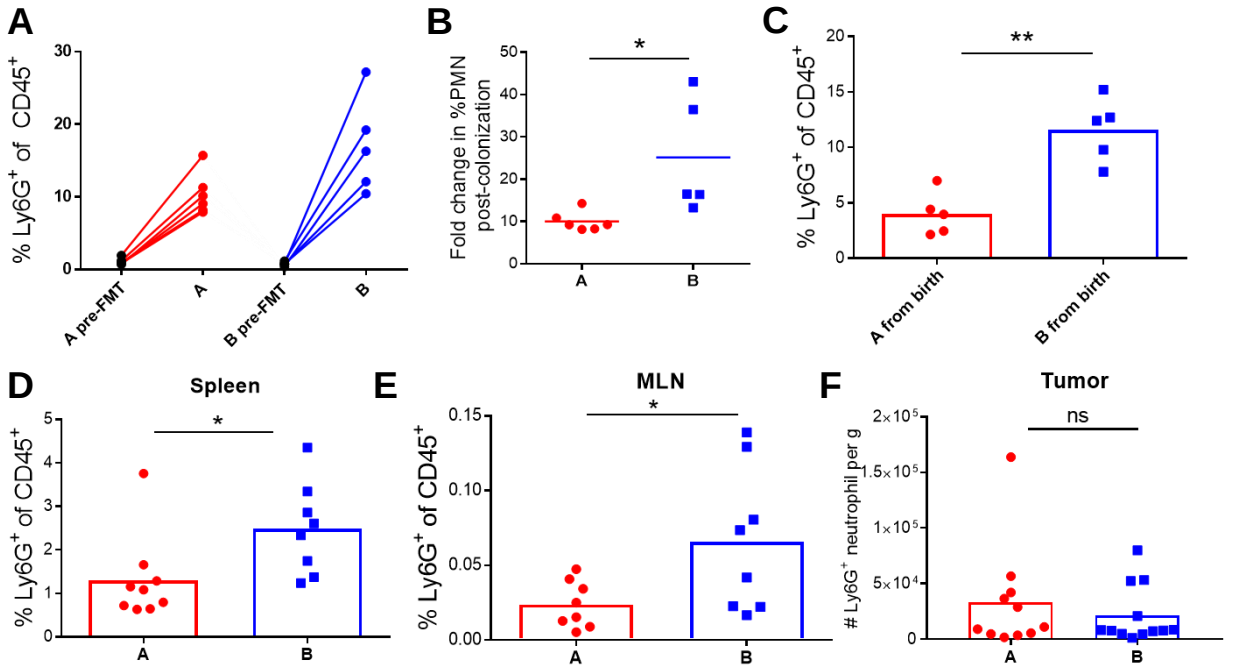

Figure 4.13 Increased frequency of Ly6G$^+$ granulocytes in the blood and lymphoid tissues of NR mice compared to R mice by flow cytometry.
(A) Percentage of Ly6G$^+$ neutrophils in the blood of germfree mice prior to colonization and 2 weeks post colonization with A or B fecal material. (B) Fold change increase in Ly6G$^+$neutrophils post colonization. (C) Percentage of Ly6G$^+$ neutrophils in the blood of non-tumor bearing naturally colonized A and B mice. (D-F) Quantification of Ly6G$^+$ neutrophils at B16.SIY tumor endpoint. Percent of Ly6G$^+$ neutrophils in the spleen (D) and mesenteric lymph nodes (E). Total number of Ly6G$^+$ neutrophils per gram tumor (F).

4.8 The gut microbiome differentially poises innate immune cells to produce type I IFNs globally and within the tumor microenvironment

We next wanted to determine what additional cell types, beyond neutrophils, were altered across the two models by analyzing immune cells within the gut associated lymphoid organs and in the spleen. We hypothesized that populations which were altered systemically were more likely directly modulated by the gut microbiota and made good candidates to compare to our analysis within the tumor to establish a logical link between the microbiota and tumor microenvironment. We identified an increase in the percent of CD8α$^+$ DCs in the spleen and in the mesenteric lymph nodes of A mice compared to B (Figure 4.14A-B). CD8α$^+$ DCs, in addition to CD103$^+$ DCs, are

classified as Batf3-lineage DCs, and are key immune mediators based on their superior capability for cross-presenting antigen to $CD8^+$ T cells.

Batf3 DCs play an essential role in the anti-tumor immune response via multiple mechanisms. They are essential for cross presenting tumor-derived antigen to $CD8^+$ T cells in the tumor draining lymph node and provide co-stimulation in the tumor. Additionally, Batf3 DCs contribute to the production of type I interferons (IFNs) in the tumor microenvironment which enhances the anti-tumor immune response in multiple ways, including through the activation and maturation of DCs and via the recruitment of $CD8^+$ T cells. Mirroring the changes observed in the spleen and MLNs, we found an increased proportion and density of both $CD103^+$ and $CD8\alpha^+$ DCs in B16.SIY tumors from A mice compared to B (Figure 4.14C-G).

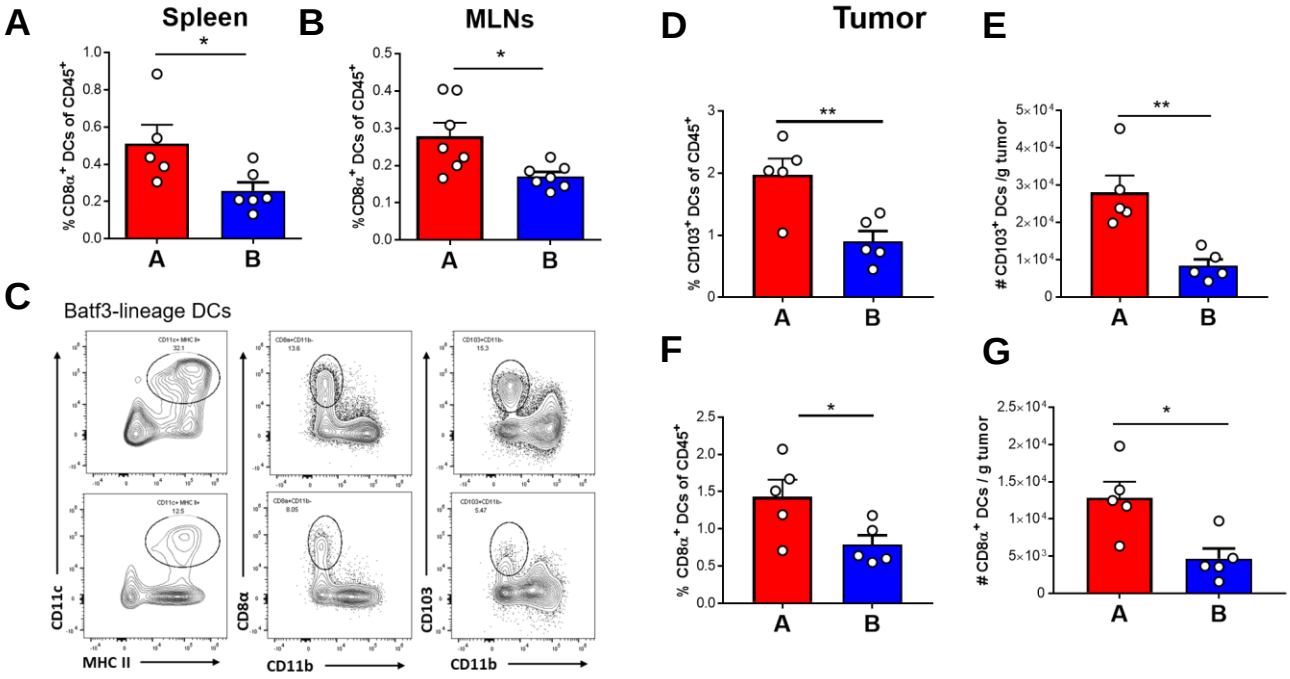

Figure 4.14 Batf3-lineage DCs are expanded peripherally and in the tumor microenvironment in R mice compared to NR.
Flow cytometric evaluation of DCs in A and B mice at B16.SIY tumor endpoint. (A-B) Proportion of $CD8\alpha^+$ DCs in the spleen (A) and mesenteric lymph nodes (B). (C) Representative gating of $CD103^+$ and $CD8\alpha^+$ DCs in the tumor. (D-G) Percent and absolute number per gram tumor of $CD103^+$ DCs (D, E) and $CD8\alpha^+$ DCs (F, G) in the tumor.

We next wanted to test how the gut microbiota might confer different anti-tumor properties to DCs within these two models. We first tested whether the gut microbiome influenced DCs ability to prime T cells. We isolated DCs from the spleen of A and B mice and tested their capacity to stimulate TCR transgenic T cells, 2C T cells, ex vivo. We found DCs from A and B mice resulted in equivalent T cell proliferation quantified by dilution of cell-trace violet (CTV), and that T cells produced equal levels of IFN-γ and TNF-α across all concentrations of cognate peptide tested (Figure 4.14A-B). This result suggested no intrinsic difference in the capacity of DCs to prime naïve T cells. We next tested T cell proliferation in vivo, by transferring CTV-labeled TCR-transgenic T cells (2C T cells), which recognize the tumor antigen SIY, to mice bearing B16.SIY tumors (Figure 4.14C). Three days later, the tumor draining lymph node was processed and resulting cell suspension re-stimulated with SIY peptide to assess T cell proliferation and function. We found equal dilution of CTV (Figure 4.14D-E) and equivalent capacity to produce IFN-γ and TNF-α (Figure 4.14F-G) in recovered 2C T cells isolated from A and B mice. These data support that there is no DC intrinsic difference in T cell priming, and that the magnitude of T cell priming appears to be equivalent in the two models, A and B. These results, in concert with our previous analysis of the tumor microenvironment, suggest that the gut microbiome in these model systems has the most profound effect within the tumor microenvironment during the effector phase of the anti-tumor immune response, downstream from T cell priming.

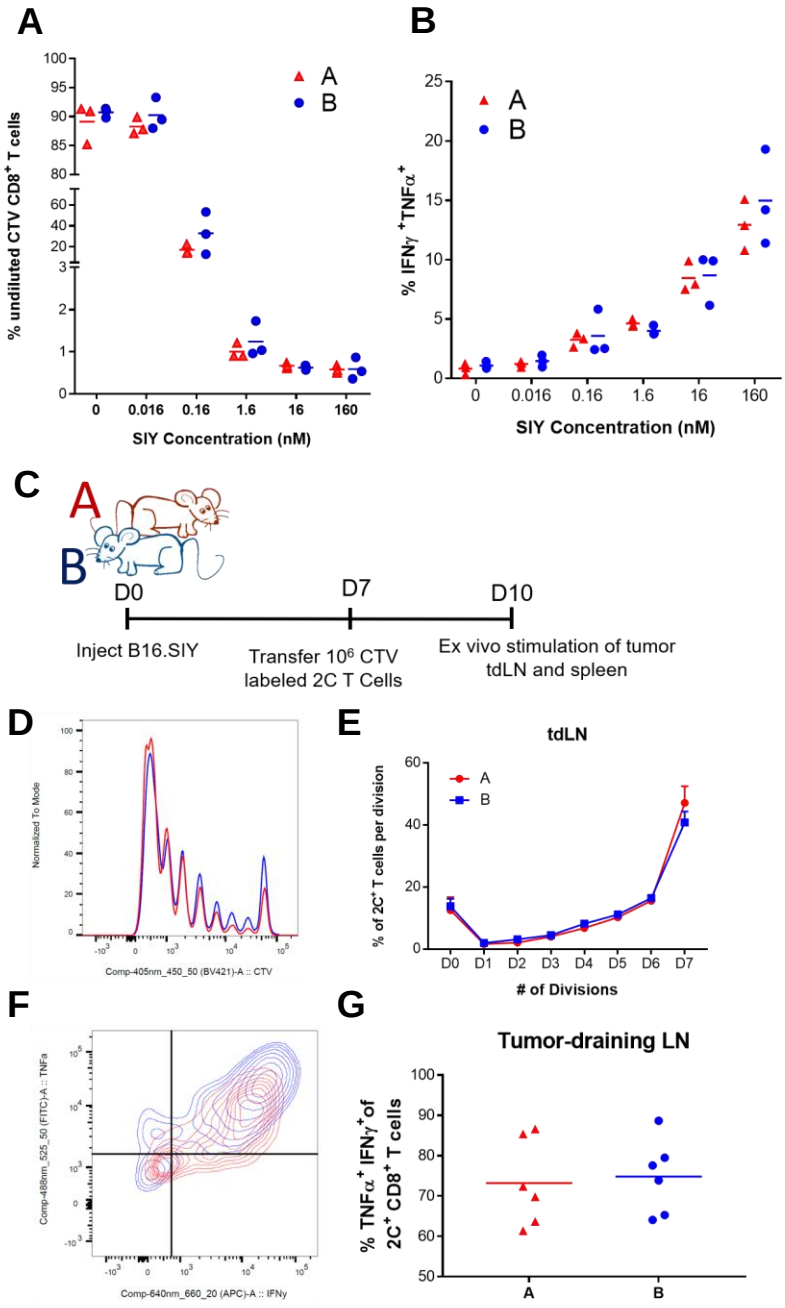

Figure 4.15 Equivalent T cell priming in vivo and in vitro suggests no intrinsic difference in DCs ability to prime T cells early in immune response.
(A) Percent of undiluted, or non-proliferated, 2C T cells stimulated with DCs isolated from the spleen of either A or B mice across varying peptide concentrations. (B) Percent of IFN-γ and TNF-α double positive cells of total 2C T cells. (C) Experimental approach to study microbiota effect on T cell priming in vivo, results shown in D-G. (D) Representative plot of 2C CTV dilution. (E) Quantification of D shows no difference in T cell proliferation in the tumor-draining lymph nodes. (F) Representative flow plot showing IFN-γ and TNF-α staining in ex-vivo stimulated 2C T cells. (G) Quantification of F shows no difference in T cell cytokine production.

Within the tumor microenvironment another key responsibility for DCs is to produce type I IFNs. As a readout of type I IFN signaling, we calculated an interferon-alpha/beta receptor (IFNAR) gene signature score, which integrates expression of multiple genes upregulated in response to type I IFN signaling. Using the single cell RNAseq data, we observed a higher IFNAR gene signature across all MHC-II^{high} and CD11b^{+} DC clusters in A mice compared to B, indicative of greater type I IFN signaling (Figure 4.16A). One of the effects of type I IFNs in the tumor microenvironment is increased activation and maturation of DCs. We assessed DCs activation in the tumor microenvironment based on the expression of co-stimulatory markers CD80 and CD86. DCs from A mice expressed higher levels of both CD80 and CD86, indicating that they are more activated (Figure 4.16B). Gene expression and flow cytometric analysis of immune infiltrate and activation status all support a stronger coordinated adaptive immune response in A mice compared to B, in part stemming from increased type I IFN production in the tumor microenvironment.

Based on our observations indicating increased type I IFN signaling in the tumor microenvironment of A mice compared to B, we next asked whether the microbiome could confer innate immune cells with differential capacity to produce type I IFNs. To test type I IFN production, we isolated bulk myeloid cells from the spleen of A and B mice and stimulated using the synthetic STING agonist, DMXAA (Figure 4.17A). We then measured the production of the type I IFN, IFN-β, by qPCR after 2 hours. In response to DMXAA, myeloid cells isolated from A mice expressed more IFN-β compared to those from B mice (Figure 4.17B). There was no difference in the basal levels of IFN-β expression (Figure 4.17C), pointing towards a distinct state where immune cells are differentially poised to sense and respond to STING agonists, rather than

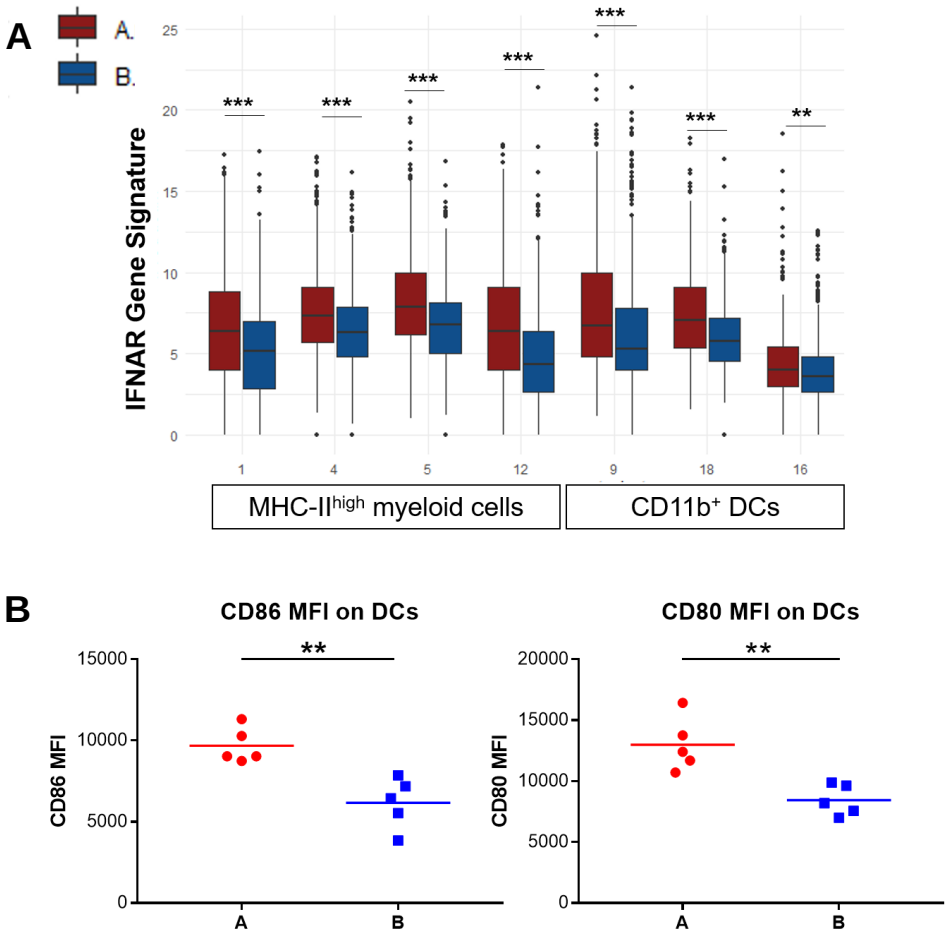

Figure 4.16 Increased IFNAR signaling in R mice compared to NR within the tumor microenvironment.
(A) IFNAR gene signature score in MHCII^{high} myeloid cells and CD11b^{+} DCs calculated from single cell RNAseq. (B) Higher activation status of in intra-tumoral DCs based on MFI of CD86 and CD80 on DCs in endpoint B16.SIY tumors by flow cytometry.

a non-specific difference in the general production of IFN-β. Upon myeloid cell isolation, we found no significant differences in cell types present (Figure 4.17D), suggesting that the difference in IFN-β expression is the product of cell-intrinsic differences between A and B, rather than a shift in the proportion of immune cells that might have a greater potential to produce IFN-β. Collectively, these data suggest that innate immune cells of A mice are preferentially positioned to produce greater amounts of IFN-β in response to endogenous STING signals within the tumor

microenvironment. Given that we observed the heightened capacity to produce IFN-β in cells isolated from the spleen, this result is suggestive of a global mechanism by which the microbiota can influence immune cell function in the periphery.

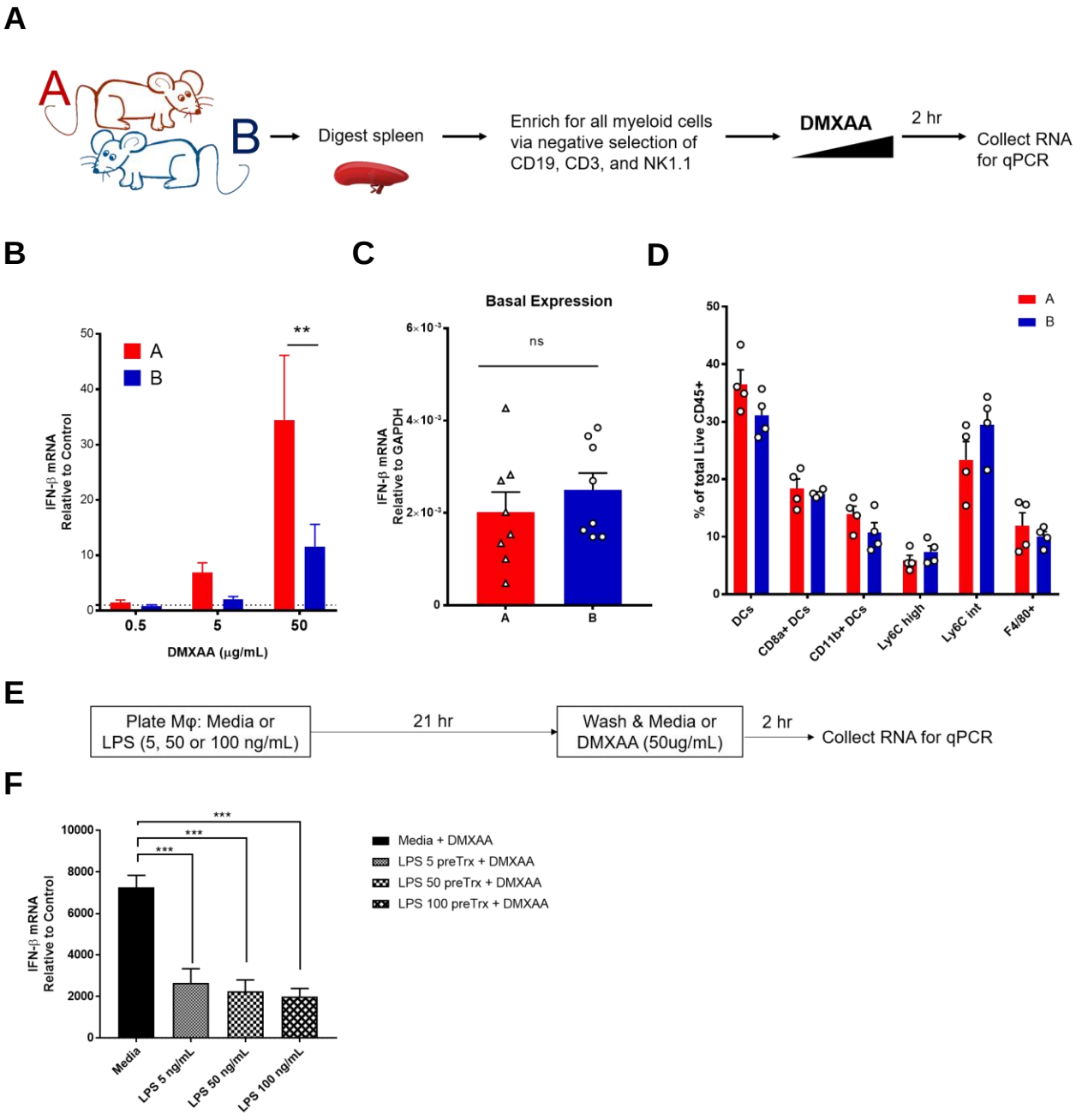

Figure 4.17 Splenic myeloid cells from A mice produce more IFN-β in response to a STING agonist compared to B mice.

Figure 4.17 (continued)
(A) Method used to evaluate STING signaling potential in innate immune cells from A and B mice. (B) Induction of IFN-β expression is greater in myeloid cells isolated from A mice compared to B after stimulation with STING agonist DMXAA. Combination of three independent experiments, N = 10. (B) No difference in baseline expression of IFN-β (without stimulation). (C) No difference in the percentage of immune cell subsets post-isolation. Tested by 2-way ANOVA. (D) Experimental method for evaluating the effect of LPS pre-treatment on IFN-β expression post DMXAA treatment. (E) Pre-treatment with LPS results in decreased IFN-β production after stimulation with DMXAA. (B-D,F) Error bars represent SEM.

We next wanted to test whether bacteria-derived products can directly influence STING signaling and impact the capacity for IFN-β production. As a proof of principle that signals derived from the gut microbiome might differentially poise immune cells to respond to subsequent stimulation, we pre-treated immortalized macrophages with varying levels of lipopolysaccharide (LPS), which is found in the outer membrane of gram-negative bacteria. One day later we removed the LPS, washed cells, and stimulated with DMXAA (Figure 4.17E). Macrophages which were pre-treated with even low levels of LPS (5 ng/mL) expressed significantly lower levels of IFN-β mRNA compared to macrophages which had not been pre-treated (Figure 4.17F). These results suggest that prolonged exposure to microbial products can impair subsequent responses critical to the anti-tumor immune response. While not definitively applicable in the case of models A and B, these data are suggestive that chronic stimulation provided by the gut microbiome have the potential to impede the ability of innate immune cells to produce type I IFNs, which would hamper anti-tumor immunity and potentially contribute to decreased immunotherapy efficacy.

4.9 Tumor kinetics and innate immune response share similar features in colon cancer model

We next wanted to investigate whether an unrelated tumor model would recapitulate the responder/non-responder phenotype in A versus B mice as had been seen with B16.SIY melanoma. We therefore turned to the MC38 colon cancer model, which also can be responsive to

immunotherapies when implanted subcutaneously in vivo. Indeed, using MC38 we also observed faster tumor growth in B mice compared to A with anti-PD-L1 therapy (Figure 4.18A), confirming the phenotypes observed with the melanoma model B16.SIY.

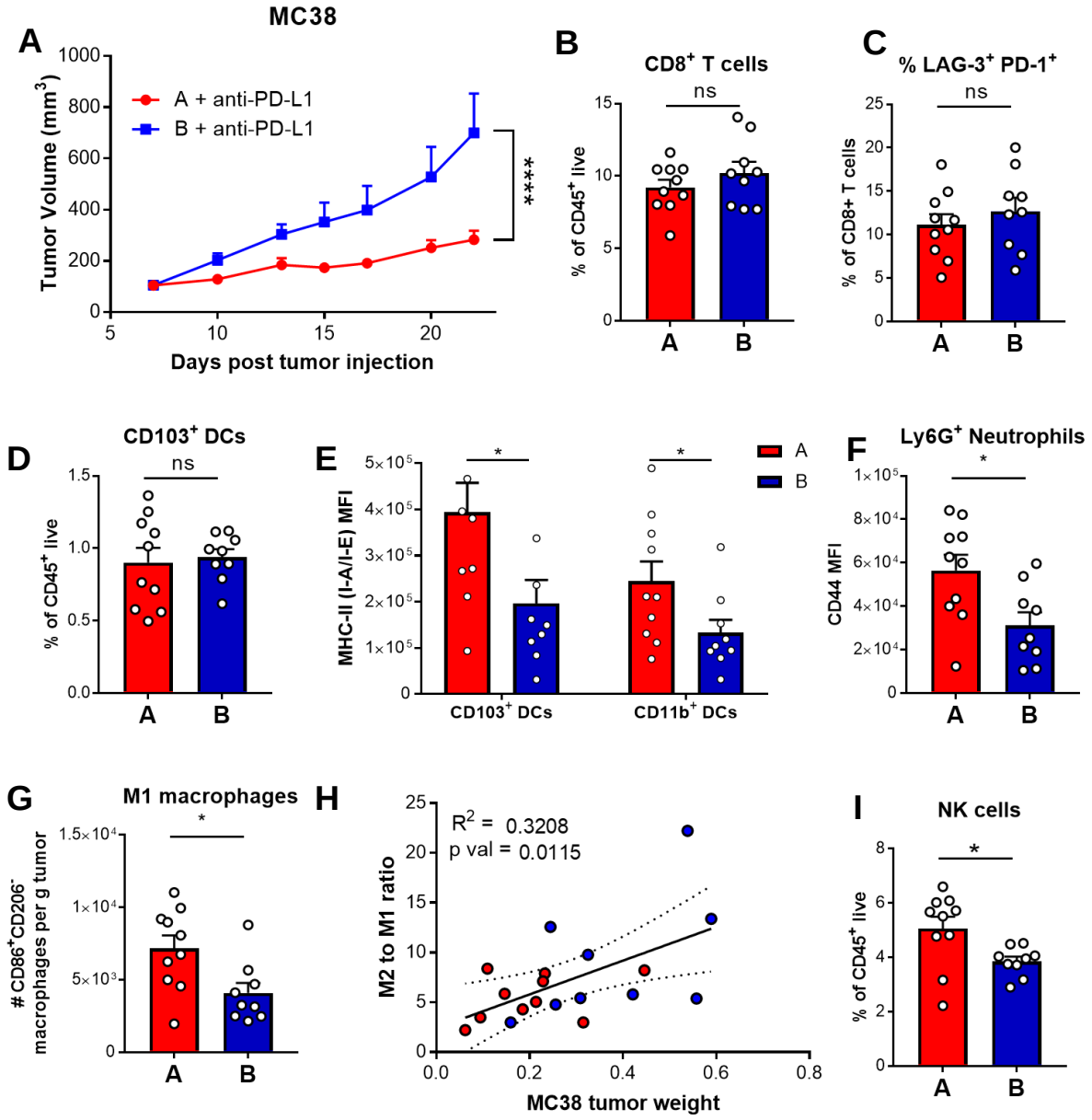

Figure 4.18 Tumor kinetics and innate immune response using colon cancer cell line shares features with melanoma model in A and B mice.
(A) Tumor growth with subcutaneous injection of MC38 cell line in naturally colonized A and B mice. (B-I) Analysis of MC38 tumor immune infiltrate at endpoint by flow cytometry. (B) No difference in percent of $CD8^+$ T cells. (C) No difference in the proportion of activated $LAG\text{-}3^+$ $PD\text{-}1^+$ $CD8^+$ T cells. (D) No difference in the percentage of $CD103^+$ DCs. (E) DCs from A mice express higher levels of MHC-II, associated with increased activation. (F) Neutrophils in A mice

Figure 4.18 (continued)
express higher levels of MDSC-associated marker, CD44. (G) Increased number of M1 macrophages in A mice compared to B. (H) Positive association between endpoint tumor weight and M2 to M1 ratio in the tumor. (I) Increased percentage of NK cells in A mice compared to B.

Given a similar tumor growth phenotype, we assessed whether the immune infiltrate in MC38 shared patterns with those observed in the B16.SIY model. At tumor endpoint, we did not see any difference in the percent of $CD8^+$ T cells in the tumor, or in the percentage of $PD\text{-}1^+LAG\text{-}3^+$ $CD8^+$ T cells (Figure 4.18B-C). In contrast to the B16.SIY model, this data suggests that $CD8^+$ T cells are less essential for the differences observed between A and B. We also observed no difference in the proportion of $CD103^+$ DCs in the tumor (Figure 4.18D), however, DCs within the tumor of A mice appeared more activated based on MHC-II expression (Figure 4.18E). Among the $Ly6G^+$ neutrophils, we saw a higher MFI of the MDSC-associated marker CD44 in A mice compared to B (Figure 4.18F). This differs with our previous observations in B16.SIY, where we had characterized more MDSC-like neutrophils in B compared to A (Figure 4.12). Within the tumor-associated macrophage population, we observed an increase in the number of M1, or anti-tumor, macrophages in A compared to B (Figure 4.18G). This follows the same pattern we observed in B16.SIY (Figure 4.11). Importantly, as the ratio of M2 to M1 macrophage in the tumor increased, tumor weight at endpoint similarly increased (Figure 4.18H). These data support that the ratio of M2 to M1, or the balance between pro- and anti-tumor macrophages, is related to tumor progression. Potentially contributing to the difference in tumor growth observed between A and B, the proportion of NK cells was greater in A mice compared to B mice (Figure 4.18I). Like their interaction with T cells, TAMs can either activate or inhibit NK cells in the tumor microenvironment depending on their polarization (188). Increased M1 macrophages in A mice may account for increased numbers of NK cells and contribute to slower tumor growth.

These data suggest that in this second tumor model, MC38, while A and B mice have similar differential tumor growth kinetics as seen with B16.SIY, the specific mechanisms responsible for the phenotype may be slightly different between tumor models. However, some features, including DC activation and increased M1 macrophages in A mice, are similar to the B16.SIY model.

4.10 A lower M2-to-M1 macrophage ratio in the tumor is associated with resistance to anti-PD-1 in metastatic melanoma patients

We reasoned that a shared immune feature across two cancer models increases its likelihood of being a more general immunological mechanism by which the microbiota can influence anti-tumor immunity. Therefore, given the consistent changes we saw in the TAM populations, we next investigated whether the ratio of M1 and M2 macrophages was associated with clinical response to anti-PD-1 in melanoma patients. Using a gene signature-based method used to infer immune cell types called xCell (167), we calculated an M1 macrophage and M2 macrophage enrichment score for each patient using RNA sequencing from pre-treatment tumor biopsies and divided these values to assign an M2 to M1 ratio.

Patients who showed progressive disease and did not benefit from anti-PD-1 tended to have tumors with a higher M2 to M1 ratio compared to those that responded to therapy, with a general trend of better outcomes being associated with a lower M2:M1 score (Figure 4.19A). By plotting the change in tumor size according to the M2:M1 ratio, we found that the degree of tumor shrinkage was negatively correlated with a higher M2:M1 ratio (Spearman's Rho = 0.5, p value = 0.06) (Figure 4.19B). Despite the small sample size (n = 15), these results suggest that TAM polarization in the tumor prior to treatment is associated with subsequent response to immunotherapy.

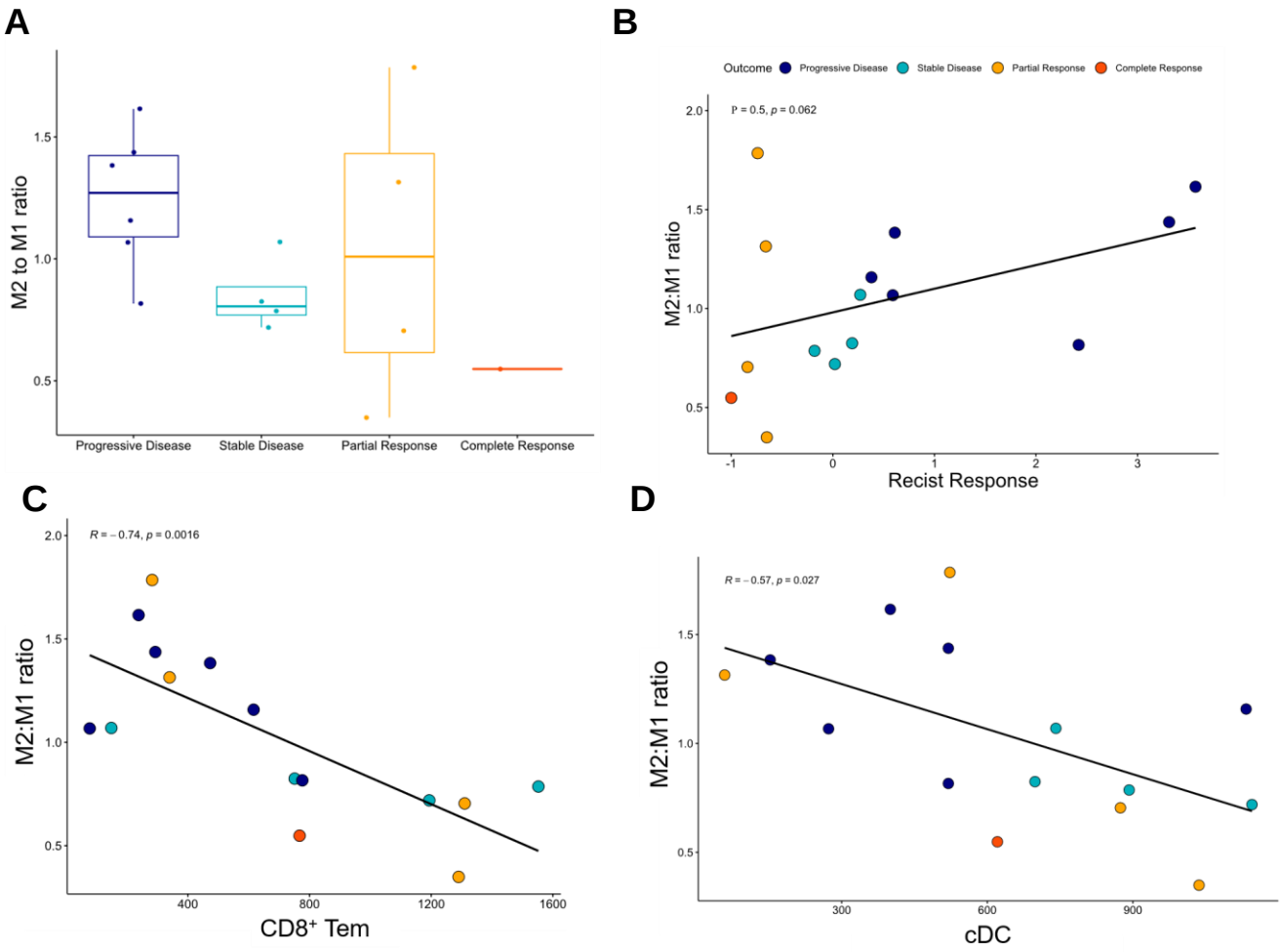

Figure 4.19 A higher M2:M1 gene signature ratio in baseline tumor samples is associated with worse response with immune checkpoint blockade and decreased tumor-infiltrating T cells and DCs.
(A) Ratio of M2 Macrophage to M1 Macrophage enrichment score in tumor biopsy samples prior to immunotherapy categorized by patient response to treatment. (B) Association between RECIST Response, or change in target lesion, and M2:M1 score. Rho and p value calculated using Spearman correlation. (C-D) Linear correlation between M2:M1 ratio and $CD8^+$ Tem (C) and cDC score (D). Calculated R and p value using Pearson correlation.

We additionally wanted to evaluate how M2:M1 ratio was related to other immune features within the tumor, including those which have been associated with treatment efficacy. Using the same method, xCell, to deconvolute bulk RNAseq into cell types we generated a $CD8^+$ T cell effector memory ($CD8^+$ Tem) score and a conventional DC (cDC) score. As the M2:M1 ratio decreased, the $CD8^+$ Tem and cDC score increased (Figure 4.19C-D). These data suggest the

higher the ratio of M2:M1 macrophages, the less permissive the tumor microenvironment is for a productive T cell response, likely accounting for worse outcomes with immunotherapy. Our preclinical data, which demonstrate that the microbiome can lead to variable myeloid immune states and alter macrophage polarization, underscores the importance of understanding the link between the gut microbiota and TAMs further.

4.11 Summary of findings

Motivated by our observations that the gut microbiome is associated with immunotherapy efficacy in patients, we have developed a clinically relevant mouse model to study the effect of the microbiome on anti-tumor immunity. We identified a prototypical responder microbiota model (A) and a non-responder (B) to use as the foundation of our studies. Our goal was to use the mouse model as a tractable system to interrogate mechanistic details to develop novel hypotheses to correlate back in patients. We established a system using exclusively human commensals and showed that our models are stable over multiple generations and exhibit no obvious physiological defects. We also established a bi-directional effect of the gut microbiome, where B mice, with poor tumor control, have detrimental microbes and conversely A mice, with strong tumor control, have beneficial commensals.

Using these models, we ascertained that the effect of the gut microbiome on tumor growth is T cell-dependent and identified key immune features which differ between our responder and non-responder model. Figure 4.19 summarizes the main findings in the B16.SIY model. Overall, we find that the gut microbiome alters anti-tumor immunity by shifting representation of immune populations systemically and differentially poising innate immune cells. In the B mice, this manifests as increased G-MDSC and increased proportion of M2, or pro-tumor, TAMs. This scenario results in an immune suppressive environment, inhibiting an initially equivalent $CD8^+$ T

cell response in the tumor microenvironment during the effector phase. In contrast, in A mice, the myeloid cells act collectively to create a stronger anti-tumor immune response resulting in greater $CD8^+$ T cell activation which is ultimately responsible for better tumor control. This includes greater numbers of Batf3 DCs and M1 TAMs, as well as increased type I IFN signaling, supporting a stronger adaptive immune response. Importantly, differences in the immune phenotype in a second tumor model, MC38, highlight that the precise effect of the microbiome is likely context dependent. Despite this, our findings offer insight into some of the key means by which the gut microbiome can influence anti-tumor immunity. Furthermore, these results support analyzing the polarization of TAMs in human tumors as it relates to the gut microbiome and immunotherapy efficacy.

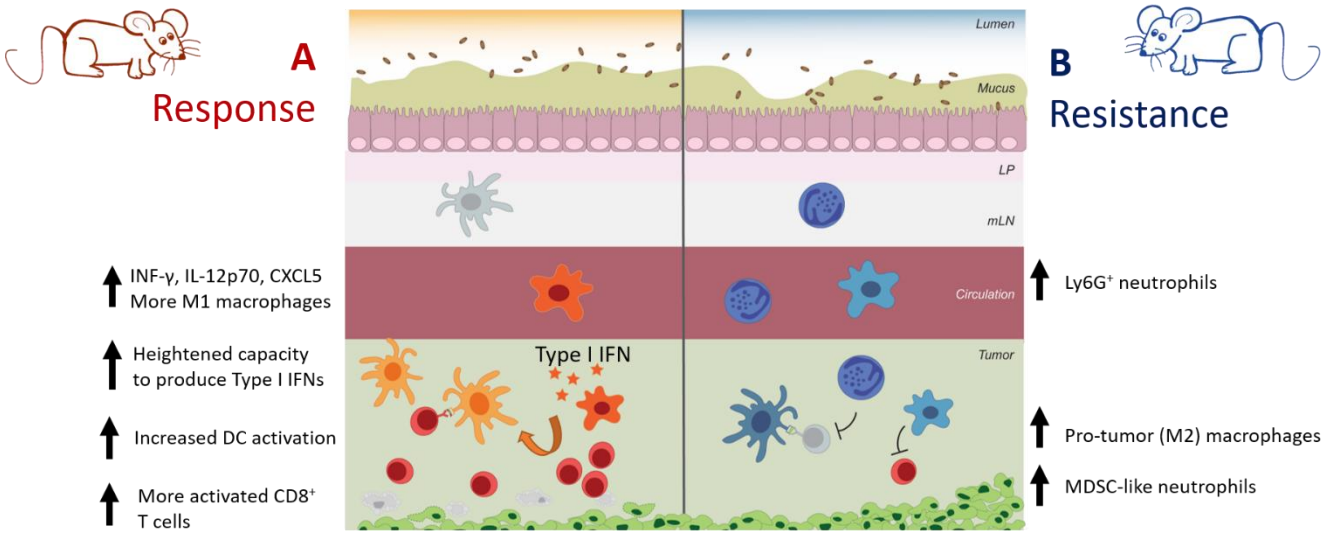

Figure 4.20 Immune populations altered in two microbiota models leading to different immunotherapy efficacy in B16.SIY.

Chapter 5: Discussion

5.1 Cross-study comparisons of the associations between the gut microbiome and immune checkpoint blockade efficacy

Our findings from Chapter 3 support that the gut microbiome is associated with response to immune checkpoint blockade in cancer patients. These findings join the results from other institutions which similarly find that the gut microbiome is linked to immunotherapy efficacy in cancer (110, 114, 189–191). Taking a similar approach to our study described in Chapter 3, stool samples were collected prior to checkpoint blockade therapy and analyzed via sequencing to assess the composition of the gut microbiome and to compare to patient outcome after immune checkpoint blockade therapy. Consistent with our findings, these groups identified distinct bacterial taxa overrepresented in responder (R) patients, whereas other bacterial sequences were over-represented in non-responder (NR) patients. Importantly, only some of these identified bacteria were consistent across multiple studies. While revelatory, these studies raise many questions and highlight knowledge gaps linking the gut microbiome and cancer immunotherapy. One major question which emerges: What accounts for the lack of overlap in the bacteria associated with response across studies?

One explanation is that this discrepancy reflects discordant biology. Different cancer types were included across the studies including metastatic melanoma, non-small cell lung, renal cell carcinoma, and urothelial carcinoma. In Routy et al. data from multiple cancer types were combined for analysis (110). In addition, across studies patient populations were from geographically distinct locations, with potentially dissimilar socioeconomic, genetic, and environmental factors, such as diet. These study-specific findings may also be explained by technical or analytical differences. Of note, the clinical definition of R and NR used in Gopalakrishnan et al. and Routy et al. differed from that used in our study (110, 114). Technical

details which may have differed between studies include methods for fecal collection and storage, DNA extraction, and sequencing. In addition, the specifics of the downstream bioinformatic analyses differed between studies, however this does not appear to be a major source for inter-study taxa disagreement. A meta-analysis which compared the data generated in our study, Gopalakrishnan et al., and Routy et al. concluded that the analytical pipelines alone were not responsible for the observed disparity in taxa associated with PD-1 response between studies (192).

While overall study differences may account for some variability, one possibility is that these discrepancies are explained by deeper, biological similarities beyond taxa identity. Supporting this notion, this meta-analysis also found that microbial gene content was a better predictor of response compared to bacterial taxa, and shared greater overlap between studies (192). Future analysis of the metagenome, as a means to evaluate the functional significance of the bacteria present, may lead to the identification of more universally impactful host-microbe interactions. If identified, these microbial genes and pathways will be top candidates to be therapeutically targeted.

Given the intricacy of the microbiome, it will be challenging to tease out the essential mechanistic elements in such a complex system from observational data alone. Even if two individuals harbor the same species of bacteria, there can be variation of each bacterium at the strain level, which could yield divergent functions upon interaction with the host. Moreover, two identical strains in two dissimilar communities may contribute differently to their collective consortium and thus function differently with respect to the host. As such, tremendous care will need to be taken when assigning specific functional attributes to given commensal bacteria. These limitations underscore the importance of using parallel models to experimentally test the functional role of human commensals.

5.2 Suppressive myeloid cells and immune checkpoint blockade efficacy

The data presented in Chapter 4 suggests that immune suppressive cells, M2 TAMs and G-MDSCs, may be responsible for insensitivity to anti-PD-L1 in mice harboring unfavorable gut microbes. Key next experiments will be establishing the relative importance of these cell types (macrophages and $Ly6G^+$ granulocytes) to tumor control. Depletion of these cells of interest using cell type-specific antibodies will help determine their contribution to the anti-tumor immune response. Alternatively, a more precise manipulation such as promoting differentiation of myeloid cells from a suppressive phenotype to a more anti-tumor or inflammatory state, will indicate whether it is possible to reverse this microbiota-mediated immune programming and regain efficacy to anti-PD-L1.

Macrophage polarization, the tumor microenvironment, and cancer immunotherapy

The patient data presented in Section 4.10 suggest that the ratio between pro- and anti-tumor TAMs may be one variable within the tumor microenvironment associated with response to anti-PD-1 therapy. While correlation does not prove causation, and other immune parameters previously associated with response, such as the number of infiltrating $CD8^+$ T cells, also appear to be tightly correlated with the M1:M2 ratio, these findings are still thought-provoking. Supporting these data, recent clinical studies investigating TAM polarization in relationship to the tumor microenvironment and ICB efficacy are coalescing around a common theme that the M1, pro-inflammatory macrophage signature is associated with improved outcomes. In a meta-analysis incorporating multiple cancer types, a gene signature of M1 polarization in patient tumor samples was associated with a T cell-inflamed tumor microenvironment (193). An analysis of 348 urothelial cancer samples prior to anti-PD-L1 found that M1 frequency was a strong predictor of response to treatment, surpassing the predictive power of $CD8^+$ T cells alone (194). Consistent

with the pan-cancer analysis completed in Oshi et al., this study also found that M1 infiltration was negatively correlated with immune exclusion (194).

Further supporting that TAMs play an important role in the tumor microenvironment as it relates to ICB, multiple pre-clinical and some clinical data find that macrophage-targeted therapy used in combination with checkpoint inhibitors can offer additional benefit (195). Depletion of TAMs through the inhibition and targeting of CSF-1/CSF-1R has improved the efficacy of numerous immune-modulating agents, including PD-1 and CTLA-4 antibodies in mouse models, which has encouraged several clinical trials testing CSF-1/CSF-1R inhibitors with ICB (196, 197). A drawback to total TAM depletion is the elimination of immune-potentiating macrophages from the host. A more nuanced approach may entail selective manipulation of TAMs to favor M1 over M2 TAMs, or to force M2 to M1 polarization. In a murine breast cancer model, an epigenetic inhibitor induced an anti-tumor (M1) macrophage phenotype which supported T cell responses and improved response to chemotherapy and anti-PD-1 (198).

G-MDSCs: Predictors of response and a new cancer immunotherapy target

The other major immune-suppressive cell type identified through studying these microbiota models was G-MDSCs. In addition to previously identified associations between MDSCs and overall worse prognosis, multiple lines of evidence point towards MDSCs as one possible source mediating resistance to ICB (199). Clinical data indicate that MDSCs may be used as a predictive marker in ICB. A lower frequency of MDSCs detected in the blood at baseline was correlated with response to anti-CTLA-4 in malignant melanoma patients (200–203). One study also found that higher MDSC levels appeared to prevent treatment-induced activation and expansion of tumor-specific T cells, leading to lower rates of clinical response (204).

Supporting MDSCs as one factor contributing to resistance to ICB, preclinical data find treatments aimed at reducing MDSC frequency or altering MDSC function can prove advantageous in combination with ICB. For example, mouse tumor models with little to no benefit with antibodies targeting CTLA-4 and PD-1 have increased T cell responses and better tumor control with the addition of biologics or small molecule inhibitors that decrease the number of MDSCs (205–207). Similarly, inhibiting MDSC immune suppression by blocking key MDSC signaling pathways has been used in combination with ICB leading to increased T cell activation and impaired tumor progression (208–210). For example, in mouse models inhibiting CSF-1R has been demonstrated to limit induction of suppressive myeloid cells, as well as functionally block MDSCs (208, 209). In addition, a selective PI3Kδ/γ isoform inhibitor can reverse splenic and tumor mouse MDSC suppressive capacity and when used in combination with anti-PD-L1 enhances $CD8^+$ T cell-dependent anti-tumor immunity (210).

5.3 Microbial signals associated with myeloid cell polarization

In Chapter 4, we used GF mice reconstituted with patient fecal material to study the effect of the gut microbiome on response to ICB. These findings illustrated how the human gut microbiome can alter the immune status of myeloid cells peripherally and in the tumor microenvironment. To continue building on our understanding of the gut microbiome and anti-tumor immunity, important next steps entail understanding which microbial signals are responsible for the myeloid cell phenotype observed in these microbiota avatar mice. These efforts will include identifying the cell types which sense these key microbial products leading to differential myeloid cell states, and drilling down even deeper, narrowing in on the specific cellular sensors that are required. On the bacteria side, identification of one, or a subset of bacteria which can confer these innate immune phenotypes can help elucidate the specific mechanisms behind observations made

in the tumor microenvironment. A complete understanding of the mechanisms involved will help illuminate the ways in which the gut microbiome interacts with anti-tumor immunity and may ultimately pave the way forward for related interventions.

The observations made in our R and NR microbiota avatar mice may be the product of microbial products acting either directly or indirectly on innate immune cells. Evidence from the literature suggests that metabolites from the gut microbiome can impact directly on myeloid cell polarization. Towards the goal of identifying key microbial products connected to myeloid cell phenotype, it may prove useful to use screen bacterial metabolites for their ability to modulate myeloid cells in vitro. In the R and NR pair we studied, the most prominent phenotypes we observed involved TAMs and G-MDSCs. Based on this, a logical experimental approach to would be to test various microbial metabolites and assess myeloid cell state using gene transcription and expression of receptors associated with either the M1/M2 state (for macrophages) or G-MDSC (for neutrophils).

There is some support in the literature that microbial metabolites may be able to directly act on macrophages and affect their activation status. As one example, several publications have implicated the aryl hydrocarbon receptor (AhR) as an important sensor for macrophage polarization (211, 212). Among the possible AhR ligands, of the most immunologically relevant are metabolites resulting from microbial metabolism of tryptophan (213). In addition, the gut microbiome is a source of prostaglandin (PGE_2) which is capable of promoting M2 macrophage polarization (214).

Additionally, there is precedent for development of MDSCs related to microbial products. While the origin of MDSCs is somewhat debated and will likely be context specific, MDSCs typically arise under pathological conditions with excess inflammation (187). Inflammatory cues

cause immature myeloid cells to expand in the bone marrow and migrate to the periphery, where are they believe to become functionally active MDSCs upon exposure to various inflammatory mediators. In particular, reprogramming of monocytes to monocytic MDSCs is believed to be trigged by TLR-signaling, likely initiated by pathogen-associated molecular patterns. As an example, LPS has been shown to induce the MDSCs accumulation at extramedullary sites, including the spleen (215). While published data support a possible role for microbial products directly affecting immune cell state, it will be imperative to determine within this system physiologically levels of microbial products and assess their immunological repercussions in vitro as well as in vivo.

5.4 Immune hyporesponsive state to STING

Among the data presented in Chapter 4, we found that innate immune cells isolated from the spleen of responder A mice produced more IFN-β in response to a synthetic STING agonist compared to non-responder B mice. Within the tumor microenvironment, we observed elevated transcripts associated with IFNAR signaling in A mice compared to B, and increased expression of DC activation markers, indicative of higher levels of type I IFNs in the tumor microenvironment. We posit that this is due to a heightened production of IFN-β in response to endogenous STING agonists in the tumor microenvironment of A mice versus B, similar to what we found with splenocytes stimulated ex vivo.

As a proof of principle that this phenotype could be the direct product of sensing differences in the gut microbiome, we evaluated whether microbial products could influence STING signaling. We selected LPS because of its ubiquitous presence in the gut microbiome, and its long studied and appreciated immunostimulatory properties. Using a macrophage cell line, we observed that prior exposure to LPS leads to decreased production of IFN-β in response to a STING

agonist. These findings demonstrate that encounter with an exclusively microbial entity can have ramifications on a signaling pathway essential to the anti-tumor immune response.

These findings are reminiscent of a well characterized phenomenon, initially identified in a mouse model of sepsis, known as “endotoxin tolerance” (216). In early observations that established the phenomenon, researchers found that administration of LPS prior to a second challenge with a lethal dose of LPS provided protection from septic shock (217). Following work in vitro and in vivo has demonstrated that through various mechanisms, pre-treatment with LPS can cause immune cells, primarily macrophages and DCs, to be hyporesponsive to subsequent LPS treatments (218). This phenomenon is not limited to LPS, but similar hyporesponsive states can occur after exposure to other innate agonists, as well as combinations of innate agonists which share common signaling pathways, such as TLR4 and TLR2 agonists, in a related phenomenon termed “heterotolerance” (219). We hypothesize that myeloid cells in B mice, with poor tumor control and less response to DMXAA, are in a similarly refractory state due to chronic exposure to immunostimulatory signals originating from the gut microbiome.

While we have not demonstrated that increased exposure to LPS is responsible for the defective type I IFN phenotype observed in microbiota model B, these observations open the door to future experiments studying the effect of other TLR agonists or other microbial associated molecular patterns and their effect on STING signaling, particularly as it relates to the anti-tumor immune response. Close study of the biologically active molecules originating from the gut microbiome of models A and B will likely facilitate the discovery of the culpable microbial factor(s).

5.5 Immune-altering components of the microbiome beyond bacteria

A large majority of focus on cancer immunotherapy and the microbiome has investigated the contribution of bacteria but has yet to thoroughly investigate non-bacterial components including viruses, fungi, and protozoa. Evidence in non-cancer disease models has indicated that the mycobiome (fungi) and the virome (viruses) can regulate systemic immunity. For example, manipulation of the mycobiome by oral antifungal drugs increased the severity of allergic airway disease in mice and was dependent on gut-resident $CX3CR1^{+}$ mononuclear phagocytes (220, 221). The virome, encompassing bacteriophages, mammalian viruses, and the endogenous retroviruses, is estimated to contain ten-fold more particles than bacterial microbes (222). Supporting the link between the intestinal virome and host immunity, alterations in viral communities have been observed in the context of human immunodeficiency virus (223), and inflammatory bowel disease (224) and have been associated with autoimmune disorders including Type 1 diabetes (225, 226). In a mouse tumor model, cross-reactivity between tumor MHC class I-restricted antigens and an enterococcal bacteriophage in the gut microbiome was capable of leading to stronger T cell responses after treatment with anti-PD-1 (227). Incorporating a pan-kingdom view of the microbiome will likely lead to a more holistic understanding of its impact on cancer treatment.

5.6 Clinical implications of the connection between the gut microbiome and anti-tumor immunity

Use of antibiotics in conjunction with immunotherapy

The collective evidence linking the gut microbiome to immunotherapy efficacy creates exciting opportunities to improve clinical treatment strategies. A straightforward implication is that antibiotics administration to patients receiving cancer immunotherapies should be pursued with caution. Routy et al. found that antibiotics administration to patients in conjunction with immunotherapy was associated with shorter PFS and shorter overall survival (OS) (110) and these

results have recently been supported by an additional retrospective analysis (228). Additionally, greater bacterial diversity was associated with higher response rates to anti-PD-1 therapy (110, 114). These data among others (reviewed in (229)) suggest that antibiotics may have detrimental effects on patient outcomes with checkpoint blockade immunotherapy, which should prompt discretion in their administration. However, one could also imagine that some patients may have an abundance of bacterial entities that dominantly mediate immune suppression. In these instances, appropriate antibiotics might decrease the abundance of such immune regulatory bacteria, perhaps allowing immune-potentiating bacteria to bloom and support improved tumor control. In the experimental system explored in Chapter 4, our data support this possible dual effect with antibiotics. Antibiotics improved tumor control in our non-responder B mice, while leading to impaired tumor control in our responder A mice. These data support the judicious use of antibiotics, but also suggest that they may be appropriate in certain applications. This includes possibly prior to the administration of therapeutic commensals in order to facilitate their engraftment.

Use of the microbiome as a prognostic/predictive biomarker

The modulatory effects of the microbiome could foreseeably offer multiple avenues of clinical intervention. Microbiome composition could be considered as a complementary prognostic or predictive biomarker for treatment outcomes. Higher bacterial diversity in the gut (but not the oral microbiome) was identified to be associated with better response rates to ICB (114). More specifically, certain bacteria were found to be enriched in anti-PD-1 responders while other species were enriched in non-responders. These data suggest that fecal DNA sequencing prior to therapy, by quantifying the community richness and the relative proportion of putatively identified “beneficial” or “detrimental” bacteria, may be suggestive of outcome and ultimately

help guide treatment decisions. Prospectively designed clinical studies to validate these associations will be key to define the utility of these approaches. In the future, the composition of the microbiome may be one parameter incorporated with other known correlates of outcome such as T cell infiltration and tumor mutational burden to 1) predict potential efficacy with a given immunotherapy and 2) inform additional interventions via the microbiota to improve immunotherapy potency or alternatively decrease treatment related toxicity.

Therapeutic interventions to modulate microbiome composition and function

Preclinical evidence extends the correlative relationship between the microbiome and response observed in patients to support a causal role. This scenario opens the exciting possibility to improve efficacy by manipulating the gut flora. Intervention strategies range from less precise or "blunt" approaches to more targeted therapeutic approaches. One such approach is fecal microbiota transplantation (FMT). For example, fecal samples could be prepared from anti-PD-1 responders that show a favorable composition of commensal bacteria, then transplanted endoscopically or prepared for oral delivery into patients who are anti-PD-1-resistant and show an unfavorable composition of gut microbes. This approach would parallel the strategies being used to treat refractory *Clostridium difficile* infection in patients (230). This approach delivers a complex community and the promise to transfer its beneficial effect. However, FMT is clouded by uncertainties related to the imprecise definition of a favorable microbiota, the possibility of delivering immune-regulatory bacteria, and the potential to transfer disease-promoting bacteria such as those contributing to obesity or even carcinogenesis. Despite the doubt, one recent study provides encouraging support that FMT may be a useful intervention (231). Ten metastatic melanoma patients that were refractory to anti-PD-1 were treated with FMT from one of two responders to anti-PD-1, followed by re-induction of anti-PD-1 immunotherapy. Three patients,

all of whom were received FMT from the same patient donor, experienced clinical responses accompanied by positive changes in the tumor-infiltrating immune populations.

A subtler means of intervention may include modulating the existing commensal community via prebiotics or dietary changes to favor the expansion of beneficial bacteria that require specific substrates, or conversely, "starving" detrimental bacteria of their required nutrients. For example, short-term changes in human macronutrient consumption towards a high fat, low fiber animal-based diet increased bile-tolerant microorganisms (*Alistipes*, *Bilophila* and Bacteroides) and decreased levels of Firmicutes that metabolize dietary plant polysaccharides (*Roseburia*, *Eubacterium rectale* and *Ruminococcus bromii*) (232). Similarly, antibiotics could be considered a means of targeting immune-regulatory bacteria. Both of these approaches lack the precision to modulate very specific bacterial populations, however, and may have variable effects depending on the starting state of the commensal community.

Alternatively, beneficial immune-potentiating bacteria could be prepared as a probiotic and provided as an immunotherapy adjuvant. Once molecular mechanisms are determined, genetic manipulation of the selected bacteria could be utilized to maximize beneficial effects. Historically, certain bacterial species have been some of the most amenable organisms to genetic manipulation, and the breadth of tools available to study and modify bacteria continues to expand. This technology allows the modification of a bacterium's existing function or the introduction of completely novel genes (233). For example, a *Bacteroides* strain modified to carry a gene cluster to utilize porphyran stabilized its engraftment into mice fed a porphyran-supplemented diet (234). This strategy effectively creates a unique metabolic niche for the exogenous microbe and presents a potential means to facilitate probiotic efficacy. Bacteria may also be genetically modified to drive expression of a metabolite of interest (235). For well-characterized bacteria such as *Escherichia*

coli, genetic manipulation is routine, but for many human commensals, incomplete genomic information leaves fewer tools available for these strategies currently. To circumvent this limitation, it is possible to express bacterial genes of interest heterologously in common laboratory hosts such as *E. coli* or *Bacillus subtilis* (235). An alternative approach to adding beneficial bacteria to the microbiota is selective depletion of harmful species from the community. Bacteriophages are viruses that can infect and kill bacteria and are naturally present in the microbiome where they play a key role in preserving community equilibrium. Some phages have been used preclinically to decrease pathogenic bacteria while leaving the commensal community intact, and could be further engineered to target certain bacterial species or strains (233).

Finally, if a bacterial metabolic pathway is identified along with defined metabolic products that mediate improved anti-tumor immunity and immunotherapy, then small molecule entities could be tested as candidate immune-potentiating drugs. In all cases, appropriately controlled clinical trials will be required to validate any potential microbiome-based therapy and to assess benefits and risks. Clinical trials to evaluate the impact of fecal microbiome transplant and probiotic administration with checkpoint inhibitors are already underway (236).

5.7 Future studies on the microbiome and immunotherapy

Looking forward, it is important to recognize that the microbiome contributes only one dimension to the many facets that govern the interface between cancer and the host immune response. Cancer cells grow and evolve under the selective pressure of therapy, and molecular evolution of the tumor could still occur when the microbiome is manipulated to maximize immunotherapy efficacy. In addition, it is conceivable that the composition of the microbiome similarly may evolve over the course of cancer progression and therapy administration. This variation offers additional research challenges, but with this pliability also comes exciting promise

for intervention and exploiting the host-microbiome interdependency to deliver more potent therapy. In the future, it will be important to consider the microbiota as one of several parameters to be incorporated into considerations of personalized cancer therapy.

Chapter 6: Publications

- Gajewski TF, **Fessler J.** PAK4 as a cancer immune-evasion target. *Nat Cancer*. 2020 Jan;1(1):18–9.

- **Fessler J*,** Matson V*, Gajewski TF. Exploring the emerging role of the microbiome in cancer immunotherapy. *J Immunother Cancer*. 2019 Apr 17;7(1):108.

- Ling A, Gruener RF, **Fessler J**, Huang RS. More than fishing for a cure: The promises and pitfalls of high throughput cancer cell line screens. *Pharmacol Ther*. 2018 Nov;191:178-189.

- Geeleher P, Nath A, Wang F, Zhang Z, Barbeira AN, **Fessler J,** Grossman RL, Seoighe C, Stephanie Huang R. Cancer expression quantitative trait loci (eQTLs) can be determined from heterogeneous tumor gene expression data by modeling variation in tumor purity. *Genome Biol*. 2018 Sep 11;19(1):130

- Matson V*, **Fessler J***, Bao R*, Chongsuwat T, Zha Y, Alegre ML, Luke JJ, Gajewski TF. The commensal microbiome is associated with anti-PD-1 efficacy in metastatic melanoma patients. *Science*. 2018 Jan 5;359(6371):104-108.

- **Fessler JL,** Gajewski TF. The Microbiota: A New Variable Impacting Cancer Treatment Outcomes. *Clin Cancer Res.* 2017 Jul 1;23(13):3229-3231.

* Authors contributed equally

References

1. Hanahan, D. and Weinberg, R. A. (2011) Hallmarks of Cancer: The Next Generation. *Cell* **144**, 646–674

2. Houghton, A. N. (1994) Cancer antigens: immune recognition of self and altered self. *J. Exp. Med.* **180**, 1–4

3. Cao, Y., Wang, X., Jin, T., Tian, Y., Dai, C., Widarma, C., Song, R., and Xu, F. (2020) Immune checkpoint molecules in natural killer cells as potential targets for cancer immunotherapy. *Signal Transduct. Target. Ther.* **5**, 1–19

4. Dunn, G. P., Old, L. J., and Schreiber, R. D. (2004) The Three Es of Cancer Immunoediting. *Annu. Rev. Immunol.* **22**, 329–360

5. Chen, D. S. and Mellman, I. (2017) Elements of cancer immunity and the cancer–immune set point. *Nature* **541**, 321–330

6. Roberts, E. W., Broz, M. L., Binnewies, M., Headley, M. B., Nelson, A. E., Wolf, D. M., Kaisho, T., Bogunovic, D., Bhardwaj, N., and Krummel, M. F. (2016) Critical Role for CD103+/CD141+ Dendritic Cells Bearing CCR7 for Tumor Antigen Trafficking and Priming of T Cell Immunity in Melanoma. *Cancer Cell* **30**, 324–336

7. Whiteside, T. L. (2006) Immune suppression in cancer: Effects on immune cells, mechanisms and future therapeutic intervention. *Semin. Cancer Biol.* **16**, 3–15

8. Munn, D. H. and Mellor, A. L. (2016) IDO in the Tumor Microenvironment: Inflammation, Counter-regulation and Tolerance. *Trends Immunol.* **37**, 193–207

9. Ruffell, B. and Coussens, L. M. (2015) Macrophages and therapeutic resistance in cancer. *Cancer Cell* **27**, 462–472

10. Martinez, F. O. and Gordon, S. (2014) The M1 and M2 paradigm of macrophage activation: time for reassessment. *F1000Prime Rep.* **6**

11. Jayasingam, S. D., Citartan, M., Thang, T. H., Mat Zin, A. A., Ang, K. C., and Ch'ng, E. S. (2020) Evaluating the Polarization of Tumor-Associated Macrophages Into M1 and M2 Phenotypes in Human Cancer Tissue: Technicalities and Challenges in Routine Clinical Practice. *Front. Oncol.* **9**

12. Mukaida, N., Sasaki, S., and Baba, T. (2020) Two-Faced Roles of Tumor-Associated Neutrophils in Cancer Development and Progression. *Int. J. Mol. Sci.* **21**

13. Ng, L. G., Ostuni, R., and Hidalgo, A. (2019) Heterogeneity of neutrophils. *Nat. Rev. Immunol.* **19**, 255–265

14. Templeton, A. J., McNamara, M. G., Šeruga, B., Vera-Badillo, F. E., Aneja, P., Ocaña, A., Leibowitz-Amit, R., Sonpavde, G., Knox, J. J., Tran, B., Tannock, I. F., and Amir, E. (2014) Prognostic Role of Neutrophil-to-Lymphocyte Ratio in Solid Tumors: A Systematic Review and Meta-Analysis. *JNCI J. Natl. Cancer Inst.* **106**

15. Berkow, R. L., Wang, D., Larrick, J. W., Dodson, R. W., and Howard, T. H. (1987) Enhancement of neutrophil superoxide production by preincubation with recombinant human tumor necrosis factor. *J. Immunol. Baltim. Md 1950* **139**, 3783–3791

16. Kushner, B. H. and Cheung, N. K. (1992) Absolute requirement of CD11/CD18 adhesion molecules, FcRII and the phosphatidylinositol-linked FcRIII for monoclonal antibody-mediated neutrophil antihuman tumor cytotoxicity. *Blood* **79**, 1484–1490

17. Mishalian, I., Bayuh, R., Eruslanov, E., Michaeli, J., Levy, L., Zolotarov, L., Singhal, S., Albelda, S. M., Granot, Z., and Fridlender, Z. G. (2014) Neutrophils recruit regulatory T-cells into tumors via secretion of CCL17--a new mechanism of impaired anti-tumor immunity. *Int. J. Cancer* **135**, 1178–1186

18. Rodriguez, P. C., Quiceno, D. G., Zabaleta, J., Ortiz, B., Zea, A. H., Piazuelo, M. B., Delgado, A., Correa, P., Brayer, J., Sotomayor, E. M., Antonia, S., Ochoa, J. B., and Ochoa, A. C. (2004) Arginase I production in the tumor microenvironment by mature myeloid cells inhibits T-cell receptor expression and antigen-specific T-cell responses. *Cancer Res.* **64**, 5839–5849

19. Yang, T.-H., St John, L. S., Garber, H. R., Kerros, C., Ruisaard, K. E., Clise-Dwyer, K., Alatrash, G., Ma, Q., and Molldrem, J. J. (2018) Membrane-Associated Proteinase 3 on Granulocytes and Acute Myeloid Leukemia Inhibits T Cell Proliferation. *J. Immunol. Baltim. Md 1950* **201**, 1389–1399

20. Walunas, T. L., Lenschow, D. J., Bakker, C. Y., Linsley, P. S., Freeman, G. J., Green, J. M., Thompson, C. B., and Bluestone, J. A. (1994) CTLA-4 can function as a negative regulator of T cell activation. *Immunity* **1**, 405–413

21. Brunner, M. C., Chambers, C. A., Chan, F. K.-M., Hanke, J., Winoto, A., and Allison, J. P. (1999) CTLA-4-Mediated Inhibition of Early Events of T Cell Proliferation. *J. Immunol.* **162**, 5813–5820

22. Simpson, T. R., Li, F., Montalvo-Ortiz, W., Sepulveda, M. A., Bergerhoff, K., Arce, F., Roddie, C., Henry, J. Y., Yagita, H., Wolchok, J. D., Peggs, K. S., Ravetch, J. V., Allison, J. P., and Quezada, S. A. (2013) Fc-dependent depletion of tumor-infiltrating regulatory T cells co-defines the efficacy of anti–CTLA-4 therapy against melanoma. *J. Exp. Med.* **210**, 1695–1710

23. Selby, M. J., Engelhardt, J. J., Quigley, M., Henning, K. A., Chen, T., Srinivasan, M., and Korman, A. J. (2013) Anti-CTLA-4 Antibodies of IgG2a Isotype Enhance Anti-tumor Activity through Reduction of Intratumoral Regulatory T Cells. *Cancer Immunol. Res.* **1**, 32–42

24. Agata, Y., Kawasaki, A., Nishimura, H., Ishida, Y., Tsubata, T., Yagita, H., and Honjo, T. (1996) Expression of the PD-1 antigen on the surface of stimulated mouse T and B lymphocytes. *Int. Immunol.* **8**, 765–772

25. Keir, M. E., Liang, S. C., Guleria, I., Latchman, Y. E., Qipo, A., Albacker, L. A., Koulmanda, M., Freeman, G. J., Sayegh, M. H., and Sharpe, A. H. (2006) Tissue expression of PD-L1 mediates peripheral T cell tolerance. *J. Exp. Med.* **203**, 883–895

26. Loke, P. and Allison, J. P. (2003) PD-L1 and PD-L2 are differentially regulated by Th1 and Th2 cells. *Proc. Natl. Acad. Sci.* **100**, 5336–5341

27. Robert, C., Ribas, A., Hamid, O., Daud, A., Wolchok, J. D., Joshua, A. M., Hwu, W.-J., Weber, J. S., Gangadhar, T. C., Joseph, R. W., Dronca, R., Patnaik, A., Zarour, H., Kefford, R., Hersey, P., Zhang, J., Anderson, J., Diede, S. J., Ebbinghaus, S., and Hodi, F. S. (2017) Durable Complete Response After Discontinuation of Pembrolizumab in Patients With Metastatic Melanoma. *J. Clin. Oncol.* **36**, 1668–1674

28. Larkin, J., Chiarion-Sileni, V., Gonzalez, R., Grob, J.-J., Rutkowski, P., Lao, C. D., Cowey, C. L., Schadendorf, D., Wagstaff, J., Dummer, R., Ferrucci, P. F., Smylie, M., Hogg, D., Hill, A., Márquez-Rodas, I., Haanen, J., Guidoboni, M., Maio, M., Schöffski, P., Carlino, M. S., Lebbé, C., McArthur, G., Ascierto, P. A., Daniels, G. A., Long, G. V., Bastholt, L., Rizzo, J. I., Balogh, A., Moshyk, A., Hodi, F. S., and Wolchok, J. D. (2019) Five-Year Survival with Combined Nivolumab and Ipilimumab in Advanced Melanoma. *N. Engl. J. Med.*

29. Robert, C. (2020) A decade of immune-checkpoint inhibitors in cancer therapy. *Nat. Commun.* **11**, 3801

30. Gaynor, N., Crown, J., and Collins, D. M. (2020) Immune checkpoint inhibitors: Key trials and an emerging role in breast cancer. *Semin. Cancer Biol.*

31. Grzywa, T. M., Paskal, W., and Włodarski, P. K. (2017) Intratumor and Intertumor Heterogeneity in Melanoma. *Transl. Oncol.* **10**, 956–975

32. Pagès, F., Galon, J., Dieu-Nosjean, M.-C., Tartour, E., Sautès-Fridman, C., and Fridman, W.-H. (2010) Immune infiltration in human tumors: a prognostic factor that should not be ignored. *Oncogene* **29**, 1093–1102

33. Ayers, M., Lunceford, J., Nebozhyn, M., Murphy, E., Loboda, A., Kaufman, D. R., Albright, A., Cheng, J. D., Kang, S. P., Shankaran, V., Piha-Paul, S. A., Yearley, J., Seiwert, T. Y., Ribas, A., and McClanahan, T. K. (2017) IFN-γ-related mRNA profile predicts clinical response to PD-1 blockade. *J. Clin. Invest.* **127**, 2930–2940

34. Jochems, C. and Schlom, J. (2011) Tumor-infiltrating immune cells and prognosis: the potential link between conventional cancer therapy and immunity. *Exp. Biol. Med. Maywood NJ* **236**, 567–579

35. Tumeh, P. C., Harview, C. L., Yearley, J. H., Shintaku, I. P., Taylor, E. J. M., Robert, L., Chmielowski, B., Spasic, M., Henry, G., Ciobanu, V., West, A. N., Carmona, M., Kivork, C., Seja, E., Cherry, G., Gutierrez, A. J., Grogan, T. R., Mateus, C., Tomasic, G., Glaspy, J. A., Emerson, R. O., Robins, H., Pierce, R. H., Elashoff, D. A., Robert, C., and Ribas, A. (2014) PD-1 blockade induces responses by inhibiting adaptive immune resistance. *Nature* **515**, 568–571

36. Brown, S. D., Warren, R. L., Gibb, E. A., Martin, S. D., Spinelli, J. J., Nelson, B. H., and Holt, R. A. (2014) Neo-antigens predicted by tumor genome meta-analysis correlate with increased patient survival. *Genome Res.* **24**, 743–750

37. Spranger, S. and Gajewski, T. F. (2018) Impact of oncogenic pathways on evasion of antitumour immune responses. *Nat. Rev. Cancer*

38. Spranger, S., Bao, R., and Gajewski, T. F. (2015) Melanoma-intrinsic β-catenin signalling prevents anti-tumour immunity. *Nature* **523**, 231–235

39. Casey, S. C., Tong, L., Li, Y., Do, R., Walz, S., Fitzgerald, K. N., Gouw, A., Baylot, V., Gutgemann, I., Eilers, M., and Felsher, D. W. (2016) MYC Regulates the Anti-Tumor Immune Response through CD47 and PD-L1. *Science* **352**, 227–231

40. Peng, W., Chen, J. Q., Liu, C., Malu, S., Creasy, C., Tetzlaff, M. T., Xu, C., McKenzie, J. A., Zhang, C., Liang, X., Williams, L. J., Deng, W., Chen, G., Mbofung, R., Lazar, A. J., Torres-Cabala, C. A., Cooper, Z. A., Chen, P.-L., Tieu, T. N., Spranger, S., Yu, X., Bernatchez, C., Forget, M.-A., Haymaker, C., Amaria, R., McQuade, J. L., Glitza, I. C., Cascone, T., Li, H. S., Kwong, L. N., Heffernan, T. P., Hu, J., Bassett, R. L., Bosenberg, M. W., Woodman, S. E., Overwijk, W. W., Lizée, G., Roszik, J., Gajewski, T. F., Wargo, J. A., Gershenwald, J. E., Radvanyi, L., Davies, M. A., and Hwu, P. (2016) Loss of PTEN Promotes Resistance to T Cell-Mediated Immunotherapy. *Cancer Discov.* **6**, 202–216

41. Chowell, D., Morris, L. G. T., Grigg, C. M., Weber, J. K., Samstein, R. M., Makarov, V., Kuo, F., Kendall, S. M., Requena, D., Riaz, N., Greenbaum, B., Carroll, J., Garon, E., Hyman, D. M., Zehir, A., Solit, D., Berger, M., Zhou, R., Rizvi, N. A., and Chan, T. A. (2018) Patient HLA class I genotype influences cancer response to checkpoint blockade immunotherapy. *Science* **359**, 582–587

42. Chat, V., Ferguson, R., Simpson, D., Kazlow, E., Lax, R., Moran, U., Pavlick, A., Frederick, D., Boland, G., Sullivan, R., Ribas, A., Flaherty, K., Osman, I., Weber, J., and Kirchhoff, T. (2019) Autoimmune genetic risk variants as germline biomarkers of response to melanoma immune-checkpoint inhibition. *Cancer Immunol. Immunother.* **68**, 897–905

43. Steck, S. E. and Murphy, E. A. (2020) Dietary patterns and cancer risk. *Nat. Rev. Cancer* **20**, 125–138

44. Soldati, L., Di Renzo, L., Jirillo, E., Ascierto, P. A., Marincola, F. M., and De Lorenzo, A. (2018) The influence of diet on anti-cancer immune responsiveness. *J. Transl. Med.* **16**

45. Fuerst, M. L. (2019) Gut Microbiome Affects Response to Immunotherapy. *Oncol. Times* **41**, 32

46. Pedersen, L., Idorn, M., Olofsson, G. H., Lauenborg, B., Nookaew, I., Hansen, R. H., Johannesen, H. H., Becker, J. C., Pedersen, K. S., Dethlefsen, C., Nielsen, J., Gehl, J., Pedersen, B. K., thor Straten, P., and Hojman, P. (2016) Voluntary Running Suppresses Tumor Growth through Epinephrine- and IL-6-Dependent NK Cell Mobilization and Redistribution. *Cell Metab.* **23**, 554–562

47. Kamada, N., Seo, S.-U., Chen, G. Y., and Núñez, G. (2013) Role of the gut microbiota in immunity and inflammatory disease. *Nat. Rev. Immunol.* **13**, 321–335

48. Sender, R., Fuchs, S., and Milo, R. (2016) Revised Estimates for the Number of Human and Bacteria Cells in the Body. *PLoS Biol.* **14**

49. Lepage, P., Leclerc, M. C., Joossens, M., Mondot, S., Blottière, H. M., Raes, J., Ehrlich, D., and Doré, J. (2013) A metagenomic insight into our gut's microbiome. *Gut* **62**, 146–158

50. Vernocchi, P., Del Chierico, F., and Putignani, L. (2016) Gut Microbiota Profiling: Metabolomics Based Approach to Unravel Compounds Affecting Human Health. *Front. Microbiol.* **7**, 1144

51. Tai, N., Wong, F. S., and Wen, L. (2015) The role of gut microbiota in the development of type 1, obesity and type 2 diabetes mellitus. *Rev. Endocr. Metab. Disord.* **16**, 55–65

52. Matsuoka, K. and Kanai, T. (2015) The gut microbiota and inflammatory bowel disease. *Semin. Immunopathol.* **37**, 47–55

53. Geuking, M. B., Köller, Y., Rupp, S., and McCoy, K. D. (2014) The interplay between the gut microbiota and the immune system. *Gut Microbes* **5**, 411–418

54. Fujimura, K. E. and Lynch, S. V. (2015) Microbiota in Allergy and Asthma and the Emerging Relationship with the Gut Microbiome. *Cell Host Microbe* **17**, 592–602

55. Collins, S. M. (2014) A role for the gut microbiota in IBS. *Nat. Rev. Gastroenterol. Hepatol.* **11**, 497–505

56. Zhang, X., Zhang, D., Jia, H., Feng, Q., Wang, D., Liang, D., Wu, X., Li, J., Tang, L., Li, Y., Lan, Z., Chen, B., Li, Y., Zhong, H., Xie, H., Jie, Z., Chen, W., Tang, S., Xu, X., Wang, X., Cai, X., Liu, S., Xia, Y., Li, J., Qiao, X., Al-Aama, J. Y., Chen, H., Wang, L., Wu, Q., Zhang, F., Zheng, W., Li, Y., Zhang, M., Luo, G., Xue, W., Xiao, L., Li, J., Chen, W., Xu, X., Yin, Y., Yang, H., Wang, J., Kristiansen, K., Liu, L., Li, T., Huang, Q., Li, Y., and Wang, J. (2015) The oral and gut microbiomes are perturbed in rheumatoid arthritis and partly normalized after treatment. *Nat. Med.* **21**, 895–905

57. Vieira, S. M., Pagovich, O. E., and Kriegel, M. A. (2014) Diet, Microbiota and Autoimmune Diseases. *Lupus* **23**, 518–526

58. Miele, L., Giorgio, V., Alberelli, M. A., De Candia, E., Gasbarrini, A., and Grieco, A. (2015) Impact of Gut Microbiota on Obesity, Diabetes, and Cardiovascular Disease Risk. *Curr. Cardiol. Rep.* **17**, 120

59. Torres-Fuentes, C., Schellekens, H., Dinan, T. G., and Cryan, J. F. (2017) The microbiota–gut–brain axis in obesity. *Lancet Gastroenterol. Hepatol.* **2**, 747–756

60. Mulak, A. and Bonaz, B. (2015) Brain-gut-microbiota axis in Parkinson's disease. *World J. Gastroenterol. WJG* **21**, 10609–10620

61. Blanton, L. V., Barratt, M. J., Charbonneau, M. R., Ahmed, T., and Gordon, J. I. (2016) Childhood undernutrition, the gut microbiota, and microbiota-directed therapeutics. *Science* **352**, 1533–1533

62. Zhang, H. and Sun, L. (2018) When human cells meet bacteria: precision medicine for cancers using the microbiota. *Am. J. Cancer Res.* **8**, 1157–1175

63. Browne, H. P., Forster, S. C., Anonye, B. O., Kumar, N., Neville, B. A., Stares, M. D., Goulding, D., and Lawley, T. D. (2016) Culturing of 'unculturable' human microbiota reveals novel taxa and extensive sporulation. *Nature* **533**, 543–546

64. Goodman, A. L., Kallstrom, G., Faith, J. J., Reyes, A., Moore, A., Dantas, G., and Gordon, J. I. (2011) Extensive personal human gut microbiota culture collections characterized and manipulated in gnotobiotic mice. *Proc. Natl. Acad. Sci. U. S. A.* **108**, 6252–6257

65. Lagier, J.-C., Hugon, P., Khelaifia, S., Fournier, P.-E., La Scola, B., and Raoult, D. (2015) The Rebirth of Culture in Microbiology through the Example of Culturomics To Study Human Gut Microbiota. *Clin. Microbiol. Rev.* **28**, 237–264

66. Bilen, M., Dufour, J.-C., Lagier, J.-C., Cadoret, F., Daoud, Z., Dubourg, G., and Raoult, D. (2018) The contribution of culturomics to the repertoire of isolated human bacterial and archaeal species. *Microbiome* **6**

67. Woese, C. R. and Fox, G. E. (1977) Phylogenetic structure of the prokaryotic domain: the primary kingdoms. *Proc. Natl. Acad. Sci. U. S. A.* **74**, 5088–5090

68. Cole, J. R., Wang, Q., Fish, J. A., Chai, B., McGarrell, D. M., Sun, Y., Brown, C. T., Porras-Alfaro, A., Kuske, C. R., and Tiedje, J. M. (2014) Ribosomal Database Project: data and tools for high throughput rRNA analysis. *Nucleic Acids Res.* **42**, D633–D642

69. DeSantis, T. Z., Hugenholtz, P., Larsen, N., Rojas, M., Brodie, E. L., Keller, K., Huber, T., Dalevi, D., Hu, P., and Andersen, G. L. (2006) Greengenes, a Chimera-Checked 16S rRNA Gene Database and Workbench Compatible with ARB. *Appl. Environ. Microbiol.* **72**, 5069–5072

70. Quast, C., Pruesse, E., Yilmaz, P., Gerken, J., Schweer, T., Yarza, P., Peplies, J., and Glöckner, F. O. (2013) The SILVA ribosomal RNA gene database project: improved data processing and web-based tools. *Nucleic Acids Res.* **41**, D590–D596

71. Nguyen, N.-P., Warnow, T., Pop, M., and White, B. (2016) A perspective on 16S rRNA operational taxonomic unit clustering using sequence similarity. *NPJ Biofilms Microbiomes* **2**, 16004

72. Edgar, R. C. (2016) UNOISE2: improved error-correction for Illumina 16S and ITS amplicon sequencing. *bioRxiv* 081257

73. Amir, A., McDonald, D., Navas-Molina, J. A., Kopylova, E., Morton, J. T., Zech Xu, Z., Kightley, E. P., Thompson, L. R., Hyde, E. R., Gonzalez, A., and Knight, R. (2017) Deblur Rapidly Resolves Single-Nucleotide Community Sequence Patterns. *mSystems* **2**

74. Callahan, B. J., McMurdie, P. J., Rosen, M. J., Han, A. W., Johnson, A. J. A., and Holmes, S. P. (2016) DADA2: High resolution sample inference from Illumina amplicon data. *Nat. Methods* **13**, 581–583

75. Ma, J., Prince, A., and Aagaard, K. M. (2014) Use of Whole Genome Shotgun Metagenomics: A Practical Guide for the Microbiome-Minded Physician Scientist. *Semin. Reprod. Med.* **32**, 005–013

76. Kembel, S. W., Wu, M., Eisen, J. A., and Green, J. L. (2012) Incorporating 16S Gene Copy Number Information Improves Estimates of Microbial Diversity and Abundance. *PLoS Comput. Biol.* **8**

77. Prakash, T. and Taylor, T. D. (2012) Functional assignment of metagenomic data: challenges and applications. *Brief. Bioinform.* **13**, 711–727

78. D'Argenio, V. (2018) Human Microbiome Acquisition and Bioinformatic Challenges in Metagenomic Studies. *Int. J. Mol. Sci.* **19**

79. Langille, M. G. I., Zaneveld, J., Caporaso, J. G., McDonald, D., Knights, D., Reyes, J. A., Clemente, J. C., Burkepile, D. E., Vega Thurber, R. L., Knight, R., Beiko, R. G., and Huttenhower, C. (2013) Predictive functional profiling of microbial communities using 16S rRNA marker gene sequences. *Nat. Biotechnol.* **31**, 814–821

80. Aßhauer, K. P., Wemheuer, B., Daniel, R., and Meinicke, P. (2015) Tax4Fun: predicting functional profiles from metagenomic 16S rRNA data. *Bioinformatics* **31**, 2882–2884

81. Iwai, S., Weinmaier, T., Schmidt, B. L., Albertson, D. G., Poloso, N. J., Dabbagh, K., and DeSantis, T. Z. (2016) Piphillin: Improved Prediction of Metagenomic Content by Direct Inference from Human Microbiomes. *PLoS ONE* **11**

82. Al-Asmakh, M. and Zadjali, F. (2015) Use of Germ-Free Animal Models in Microbiota-Related Research. *J. Microbiol. Biotechnol.* **25**, 1583–1588

83. Luczynski, P., McVey Neufeld, K.-A., Oriach, C. S., Clarke, G., Dinan, T. G., and Cryan, J. F. (2016) Growing up in a Bubble: Using Germ-Free Animals to Assess the Influence of the Gut Microbiota on Brain and Behavior. *Int. J. Neuropsychopharmacol.* **19**

84. Gorjifard, S. and Goldszmid, R. S. (2016) Microbiota—myeloid cell crosstalk beyond the gut. *J. Leukoc. Biol.* **100**, 865–879

85. Trompette, A., Gollwitzer, E. S., Yadava, K., Sichelstiel, A. K., Sprenger, N., Ngom-Bru, C., Blanchard, C., Junt, T., Nicod, L. P., Harris, N. L., and Marsland, B. J. (2014) Gut microbiota metabolism of dietary fiber influences allergic airway disease and hematopoiesis. *Nat. Med.* **20**, 159–166

86. Bauer, H., Horowitz, R. E., Levenson, S. M., and Popper, H. (1963) The response of the lymphatic tissue to the microbial flora. Studies on germfree mice. *Am. J. Pathol.* **42**, 471–483

87. Benveniste, J., Lespinats, G., Adam, C., and Salomon, J. C. (1971) Immunoglobulins in intact, immunized, and contaminated axenic mice: study of serum IgA. *J. Immunol. Baltim. Md 1950* **107**, 1647–1655

88. Mazmanian, S. K., Liu, C. H., Tzianabos, A. O., and Kasper, D. L. (2005) An Immunomodulatory Molecule of Symbiotic Bacteria Directs Maturation of the Host Immune System. *Cell* **122**, 107–118

89. Ivanov, I. I., Atarashi, K., Manel, N., Brodie, E. L., Shima, T., Karaoz, U., Wei, D., Goldfarb, K. C., Santee, C. A., Lynch, S. V., Tanoue, T., Imaoka, A., Itoh, K., Takeda, K., Umesaki, Y., Honda, K., and Littman, D. R. (2009) Induction of intestinal Th17 cells by segmented filamentous bacteria. *Cell* **139**, 485–498

90. Atarashi, K., Tanoue, T., Ando, M., Kamada, N., Nagano, Y., Narushima, S., Suda, W., Imaoka, A., Setoyama, H., Nagamori, T., Ishikawa, E., Shima, T., Hara, T., Kado, S., Jinnohara, T., Ohno, H., Kondo, T., Toyooka, K., Watanabe, E., Yokoyama, S., Tokoro, S., Mori, H., Noguchi, Y., Morita, H., Ivanov, I. I., Sugiyama, T., Nuñez, G., Camp, J. G., Hattori, M., Umesaki, Y., and Honda, K. (2015) Th17 Cell Induction by Adhesion of Microbes to Intestinal Epithelial Cells. *Cell* **163**, 367–380

91. Tan, T. G., Sefik, E., Geva-Zatorsky, N., Kua, L., Naskar, D., Teng, F., Pasman, L., Ortiz-Lopez, A., Jupp, R., Wu, H.-J. J., Kasper, D. L., Benoist, C., and Mathis, D. (2016) Identifying species of symbiont bacteria from the human gut that, alone, can induce intestinal Th17 cells in mice. *Proc. Natl. Acad. Sci. U. S. A.* **113**, E8141–E8150

92. Geva-Zatorsky, N., Sefik, E., Kua, L., Pasman, L., Tan, T. G., Ortiz-Lopez, A., Yanortsang, T. B., Yang, L., Jupp, R., Mathis, D., Benoist, C., and Kasper, D. L. (2017) Mining the Human Gut Microbiota for Immunomodulatory Organisms. *Cell* **168**, 928-943.e11

93. Round, J. L. and Mazmanian, S. K. (2010) Inducible Foxp3+ regulatory T-cell development by a commensal bacterium of the intestinal microbiota. *Proc. Natl. Acad. Sci. U. S. A.* **107**, 12204–12209

94. Atarashi, K., Tanoue, T., Shima, T., Imaoka, A., Kuwahara, T., Momose, Y., Cheng, G., Yamasaki, S., Saito, T., Ohba, Y., Taniguchi, T., Takeda, K., Hori, S., Ivanov, I. I., Umesaki, Y., Itoh, K., and Honda, K. (2011) Induction of Colonic Regulatory T Cells by Indigenous Clostridium Species. *Science* **331**, 337–341

95. Atarashi, K., Tanoue, T., Oshima, K., Suda, W., Nagano, Y., Nishikawa, H., Fukuda, S., Saito, T., Narushima, S., Hase, K., Kim, S., Fritz, J. V., Wilmes, P., Ueha, S., Matsushima, K., Ohno, H., Olle, B., Sakaguchi, S., Taniguchi, T., Morita, H., Hattori, M., and Honda, K. (2013) T_{reg} induction by a rationally selected mixture of Clostridia strains from the human microbiota. *Nature* **500**, 232–236

96. Nguyen, T. L. A., Vieira-Silva, S., Liston, A., and Raes, J. (2015) How informative is the mouse for human gut microbiota research? *Dis. Model. Mech.* **8**, 1–16

97. Hugenholtz, F. and de Vos, W. M. (2018) Mouse models for human intestinal microbiota research: a critical evaluation. *Cell. Mol. Life Sci.* **75**, 149–160

98. Xiao, L., Feng, Q., Liang, S., Sonne, S. B., Xia, Z., Qiu, X., Li, X., Long, H., Zhang, J., Zhang, D., Liu, C., Fang, Z., Chou, J., Glanville, J., Hao, Q., Kotowska, D., Colding, C., Licht, T. R., Wu, D., Yu, J., Sung, J. J. Y., Liang, Q., Li, J., Jia, H., Lan, Z., Tremaroli, V., Dworzynski, P., Nielsen, H. B., Bäckhed, F., Doré, J., Chatelier, E. L., Ehrlich, S. D., Lin, J. C., Arumugam, M., Wang, J., Madsen, L., and Kristiansen, K. (2015) A catalog of the mouse gut metagenome. *Nat. Biotechnol.* **33**, 1103–1108

99. Lundberg, R., Bahl, M. I., Licht, T. R., Toft, M. F., and Hansen, A. K. (2017) Microbiota composition of simultaneously colonized mice housed under either a gnotobiotic isolator or individually ventilated cage regime. *Sci. Rep.* **7**, 42245

100. Macpherson, A. J. and McCoy, K. D. (2015) Standardised animal models of host microbial mutualism. *Mucosal Immunol.* **8**, 476–486

101. Lagkouvardos, I., Pukall, R., Abt, B., Foesel, B. U., Meier-Kolthoff, J. P., Kumar, N., Bresciani, A., Martínez, I., Just, S., Ziegler, C., Brugiroux, S., Garzetti, D., Wenning, M., Bui, T. P. N., Wang, J., Hugenholtz, F., Plugge, C. M., Peterson, D. A., Hornef, M. W., Baines, J. F., Smidt, H., Walter, J., Kristiansen, K., Nielsen, H. B., Haller, D., Overmann, J., Stecher, B., and Clavel, T. (2016) The Mouse Intestinal Bacterial Collection (miBC) provides host-specific insight into cultured diversity and functional potential of the gut microbiota. *Nat. Microbiol.* **1**, 16131

102. Desai, M. S., Seekatz, A. M., Koropatkin, N. M., Kamada, N., Hickey, C. A., Wolter, M., Pudlo, N. A., Kitamoto, S., Terrapon, N., Muller, A., Young, V. B., Henrissat, B., Wilmes, P., Stappenbeck, T. S., Núñez, G., and Martens, E. C. (2016) A Dietary Fiber-Deprived Gut Microbiota Degrades the Colonic Mucus Barrier and Enhances Pathogen Susceptibility. *Cell* **167**, 1339-1353.e21

103. Sivan, A., Corrales, L., Hubert, N., Williams, J. B., Aquino-Michaels, K., Earley, Z. M., Benyamin, F. W., Lei, Y. M., Jabri, B., Alegre, M.-L., Chang, E. B., and Gajewski, T. F. (2015) Commensal Bifidobacterium promotes anti-tumor immunity and facilitates anti–PD-L1 efficacy. *Science* **350**, 1084–1089

104. Vétizou, M., Pitt, J. M., Daillère, R., Lepage, P., Waldschmitt, N., Flament, C., Rusakiewicz, S., Routy, B., Roberti, M. P., Duong, C. P. M., Poirier-Colame, V., Roux, A., Becharef, S., Formenti, S., Golden, E., Cording, S., Eberl, G., Schlitzer, A., Ginhoux, F., Mani, S., Yamazaki, T., Jacquelot, N., Enot, D. P., Bérard, M., Nigou, J., Opolon, P., Eggermont, A., Woerther, P.-L., Chachaty, E., Chaput, N., Robert, C., Mateus, C., Kroemer, G., Raoult, D., Boneca, I. G., Carbonnel, F., Chamaillard, M., and Zitvogel, L. (2015) Anticancer immunotherapy by CTLA-4 blockade relies on the gut microbiota. *Science* **350**, 1079–1084

105. Iida, N., Dzutsev, A., Stewart, C. A., Smith, L., Bouladoux, N., Weingarten, R. A., Molina, D. A., Salcedo, R., Back, T., Cramer, S., Dai, R.-M., Kiu, H., Cardone, M., Naik, S., Patri, A. K., Wang, E., Marincola, F. M., Frank, K. M., Belkaid, Y., Trinchieri, G., and Goldszmid, R. S. (2013) Commensal bacteria control cancer response to therapy by modulating the tumor microenvironment. *Science* **342**, 967–970

106. Viaud, S., Saccheri, F., Mignot, G., Yamazaki, T., Daillère, R., Hannani, D., Enot, D. P., Pfirschke, C., Engblom, C., Pittet, M. J., Schlitzer, A., Ginhoux, F., Apetoh, L., Chachaty, E., Woerther, P.-L., Eberl, G., Bérard, M., Ecobichon, C., Clermont, D., Bizet, C., Gaboriau-Routhiau, V., Cerf-Bensussan, N., Opolon, P., Yessaad, N., Vivier, E., Ryffel, B., Elson, C. O., Doré, J., Kroemer, G., Lepage, P., Boneca, I. G., Ghiringhelli, F., and Zitvogel, L. (2013) The Intestinal Microbiota Modulates the Anticancer Immune Effects of Cyclophosphamide. *Science* **342**, 971–976

107. Paulos, C. M., Wrzesinski, C., Andrew Kaiser, Hinrichs, C. S., Chieppa, M., Cassard, L., Palmer, D. C., Boni, A., Muranski, P., Yu, Z., Gattinoni, L., Antony, P. A., Rosenberg, S. A., and Restifo, N. P. (2007) Microbial translocation augments the function of adoptively transferred self/tumor-specific $CD8^+$ T cells via TLR4 signaling. *J. Clin. Invest.* **117**, 2197–2204

108. Geller, L. T., Barzily-Rokni, M., Danino, T., Jonas, O. H., Shental, N., Nejman, D., Gavert, N., Zwang, Y., Cooper, Z. A., Shee, K., Thaiss, C. A., Reuben, A., Livny, J., Avraham, R., Frederick, D. T., Ligorio, M., Chatman, K., Johnston, S. E., Mosher, C. M., Brandis, A., Fuks, G., Gurbatri, C., Gopalakrishnan, V., Kim, M., Hurd, M. W., Katz, M., Fleming, J., Maitra, A., Smith, D. A., Skalak, M., Bu, J., Michaud, M., Trauger, S. A., Barshack, I., Golan, T., Sandbank, J., Flaherty, K. T., Mandinova, A., Garrett, W. S., Thayer, S. P., Ferrone, C. R., Huttenhower, C., Bhatia, S. N., Gevers, D., Wargo, J. A., Golub, T. R., and Straussman, R. (2017) Potential role of intratumor bacteria in mediating tumor resistance to the chemotherapeutic drug gemcitabine. *Science* **357**, 1156–1160

109. Nejman, D., Livyatan, I., Fuks, G., Gavert, N., Zwang, Y., Geller, L. T., Rotter-Maskowitz, A., Weiser, R., Mallel, G., Gigi, E., Meltser, A., Douglas, G. M., Kamer, I., Gopalakrishnan, V., Dadosh, T., Levin-Zaidman, S., Avnet, S., Atlan, T., Cooper, Z. A., Arora, R., Cogdill, A. P., Khan, M. A. W., Ologun, G., Bussi, Y., Weinberger, A., Lotan-Pompan, M., Golani, O., Perry, G., Rokah, M., Bahar-Shany, K., Rozeman, E. A., Blank, C. U., Ronai, A., Shaoul, R., Amit, A., Dorfman, T., Kremer, R., Cohen, Z. R., Harnof, S., Siegal, T., Yehuda-Shnaidman, E., Gal-Yam, E. N., Shapira, H., Baldini, N., Langille, M. G. I., Ben-Nun, A., Kaufman, B., Nissan, A., Golan, T., Dadiani, M., Levanon, K., Bar, J., Yust-Katz, S., Barshack, I., Peeper, D. S., Raz, D. J., Segal, E., Wargo, J. A., Sandbank, J., Shental, N., and Straussman, R. (2020) The human tumor microbiome is composed of tumor type–specific intracellular bacteria. *Science* **368**, 973–980

110. Routy, B., Chatelier, E. L., Derosa, L., Duong, C. P. M., Alou, M. T., Daillère, R., Fluckiger, A., Messaoudene, M., Rauber, C., Roberti, M. P., Fidelle, M., Flament, C., Poirier-Colame, V., Opolon, P., Klein, C., Iribarren, K., Mondragón, L., Jacquelot, N., Qu, B., Ferrere, G., Clémenson, C., Mezquita, L., Masip, J. R., Naltet, C., Brosseau, S., Kaderbhai, C., Richard, C., Rizvi, H., Levenez, F., Galleron, N., Quinquis, B., Pons, N., Ryffel, B., Minard-Colin, V., Gonin, P., Soria, J.-C., Deutsch, E., Loriot, Y., Ghiringhelli, F., Zalcman, G., Goldwasser, F., Escudier, B., Hellmann, M. D., Eggermont, A., Raoult, D., Albiges, L., Kroemer, G., and Zitvogel, L. (2017) Gut microbiome influences efficacy of PD-1–based immunotherapy against epithelial tumors. *Science* eaan3706

111. Balachandran, V. P., Łuksza, M., Zhao, J. N., Makarov, V., Moral, J. A., Remark, R., Herbst, B., Askan, G., Bhanot, U., Senbabaoglu, Y., Wells, D. K., Cary, C. I. O., Grbovic-Huezo, O., Attiyeh, M., Medina, B., Zhang, J., Loo, J., Saglimbeni, J., Abu-Akeel, M., Zappasodi, R., Riaz, N., Smoragiewicz, M., Kelley, Z. L., Basturk, O., Initiative, A. P. C. G., Gönen, M., Levine, A. J., Allen, P. J., Fearon, D. T., Merad, M., Gnjatic, S., Iacobuzio-Donahue, C. A., Wolchok, J. D., DeMatteo, R. P., Chan, T. A., Greenbaum, B. D., Merghoub, T., and Leach, S. D. (2017) Identification of unique neoantigen qualities in long-term survivors of pancreatic cancer. *Nature* **551**, 512–516

112. Thaiss, C. A., Levy, M., Grosheva, I., Zheng, D., Soffer, E., Blacher, E., Braverman, S., Tengeler, A. C., Barak, O., Elazar, M., Ben-Zeev, R., Lehavi-Regev, D., Katz, M. N., Pevsner-Fischer, M., Gertler, A., Halpern, Z., Harmelin, A., Aamar, S., Serradas, P., Grosfeld, A., Shapiro, H., Geiger, B., and Elinav, E. (2018) Hyperglycemia drives intestinal barrier dysfunction and risk for enteric infection. *Science* **359**, 1376–1383

113. Hall, J. A., Bouladoux, N., Sun, C. M., Wohlfert, E. A., Blank, R. B., Zhu, Q., Grigg, M. E., Berzofsky, J. A., and Belkaid, Y. (2008) Commensal DNA Limits Regulatory T Cell Conversion and Is a Natural Adjuvant of Intestinal Immune Responses. *Immunity* **29**, 637–649

114. Gopalakrishnan, V., Spencer, C. N., Nezi, L., Reuben, A., Andrews, M. C., Karpinets, T. V., Prieto, P. A., Vicente, D., Hoffman, K., Wei, S. C., Cogdill, A. P., Zhao, L., Hudgens, C. W., Hutchinson, D. S., Manzo, T., Macedo, M. P. de, Cotechini, T., Kumar, T., Chen, W. S., Reddy, S. M., Sloane, R. S., Galloway-Pena, J., Jiang, H., Chen, P. L., Shpall, E. J., Rezvani, K., Alousi, A. M., Chemaly, R. F., Shelburne, S., Vence, L. M., Okhuysen, P. C., Jensen, V. B., Swennes, A. G., McAllister, F., Sanchez, E. M. R., Zhang, Y., Chatelier, E. L., Zitvogel, L., Pons, N., Austin-Breneman, J. L., Haydu, L. E., Burton, E. M., Gardner, J. M., Sirmans, E., Hu, J., Lazar, A. J., Tsujikawa, T., Diab, A., Tawbi, H., Glitza, I. C., Hwu, W. J., Patel, S. P., Woodman, S. E., Amaria, R. N., Davies, M. A., Gershenwald, J. E., Hwu, P., Lee, J. E., Zhang, J., Coussens, L. M., Cooper, Z. A., Futreal, P. A., Daniel, C. R., Ajami, N. J., Petrosino, J. F., Tetzlaff, M. T., Sharma, P., Allison, J. P., Jenq, R. R., and Wargo, J. A. (2017) Gut microbiome modulates response to anti–PD-1 immunotherapy in melanoma patients. *Science* eaan4236

115. Rooks, M. G. and Garrett, W. S. (2016) Gut microbiota, metabolites and host immunity. *Nat. Rev. Immunol.* **16**, 341–352

116. Morrison, D. J. and Preston, T. (2016) Formation of short chain fatty acids by the gut microbiota and their impact on human metabolism. *Gut Microbes* **7**, 189–200

117. Besten, G. den, Eunen, K. van, Groen, A. K., Venema, K., Reijngoud, D.-J., and Bakker, B. M. (2013) The role of short-chain fatty acids in the interplay between diet, gut microbiota, and host energy metabolism. *J. Lipid Res.* **54**, 2325–2340

118. Iraporda, C., Errea, A., Romanin, D. E., Cayet, D., Pereyra, E., Pignataro, O., Sirard, J. C., Garrote, G. L., Abraham, A. G., and Rumbo, M. (2015) Lactate and short chain fatty acids produced by microbial fermentation downregulate proinflammatory responses in intestinal epithelial cells and myeloid cells. *Immunobiology* **220**, 1161–1169

119. Gurav, A., Sivaprakasam, S., Bhutia, Y. D., Boettger, T., Singh, N., and Ganapathy, V. (2015) Slc5a8, a Na+-coupled high-affinity transporter for short-chain fatty acids, is a conditional tumor suppressor in colon that protects against colitis and colon cancer under low-fiber dietary conditions. *Biochem. J.* **469**, 267–278

120. White, C. A., Pone, E. J., Lam, T., Tat, C., Hayama, K. L., Li, G., Zan, H., and Casali, P. (2014) HDAC Inhibitors Upregulate B Cell microRNAs that Silence AID and Blimp-1 Expression for Epigenetic Modulation of Antibody and Autoantibody Responses. *J. Immunol. Baltim. Md 1950* **193**, 5933–5950

121. Arpaia, N., Campbell, C., Fan, X., Dikiy, S., van der Veeken, J., deRoos, P., Liu, H., Cross, J. R., Pfeffer, K., Coffer, P. J., and Rudensky, A. Y. (2013) Metabolites produced by commensal bacteria promote peripheral regulatory T-cell generation. *Nature* **504**, 451–455

122. Cohen, L. J., Esterhazy, D., Kim, S.-H., Lemetre, C., Aguilar, R. R., Gordon, E. A., Pickard, A. J., Cross, J. R., Emiliano, A. B., Han, S. M., Chu, J., Vila-Farres, X., Kaplitt, J., Rogoz, A., Calle, P. Y., Hunter, C., Bitok, J. K., and Brady, S. F. (2017) Commensal bacteria make GPCR ligands that mimic human signalling molecules. *Nature* **549**, 48–53

123. Levy, M., Thaiss, C. A., and Elinav, E. (2016) Metabolites: messengers between the microbiota and the immune system. *Genes Dev.* **30**, 1589–1597

124. Sano, T., Huang, W., Hall, J. A., Yang, Y., Chen, A., Gavzy, S. J., Lee, J.-Y., Ziel, J., Miraldi, E. R., Bonneau, R., and Littman, D. R. (2015) An IL-23R/IL-22 circuit regulates epithelial serum amyloid A to promote local effector Th17 responses. *Cell* **163**, 381–393

125. Uribe-Herranz, M., Bittinger, K., Rafail, S., Guedan, S., Pierini, S., Tanes, C., Ganetsky, A., Morgan, M. A., Gill, S., Tanyi, J. L., Bushman, F. D., June, C. H., and Facciabene, A. (2018) Gut microbiota modulates adoptive cell therapy via CD8α dendritic cells and IL-12. *JCI Insight* **3**

126. Tanoue, T., Morita, S., Plichta, D. R., Skelly, A. N., Suda, W., Sugiura, Y., Narushima, S., Vlamakis, H., Motoo, I., Sugita, K., Shiota, A., Takeshita, K., Yasuma-Mitobe, K., Riethmacher, D., Kaisho, T., Norman, J. M., Mucida, D., Suematsu, M., Yaguchi, T., Bucci, V., Inoue, T., Kawakami, Y., Olle, B., Roberts, B., Hattori, M., Xavier, R. J., Atarashi, K., and Honda, K. (2019) A defined commensal consortium elicits CD8 T cells and anti-cancer immunity. *Nature* 1

127. Morton, A. M., Sefik, E., Upadhyay, R., Weissleder, R., Benoist, C., and Mathis, D. (2014) Endoscopic photoconversion reveals unexpectedly broad leukocyte trafficking to and from the gut. *Proc. Natl. Acad. Sci.* **111**, 6696–6701

128. Wolchok, J. D., Chiarion-Sileni, V., Gonzalez, R., Rutkowski, P., Grob, J.-J., Cowey, C. L., Lao, C. D., Wagstaff, J., Schadendorf, D., Ferrucci, P. F., Smylie, M., Dummer, R., Hill, A., Hogg, D., Haanen, J., Carlino, M. S., Bechter, O., Maio, M., Marquez-Rodas, I., Guidoboni, M., McArthur, G., Lebbé, C., Ascierto, P. A., Long, G. V., Cebon, J., Sosman, J., Postow, M. A., Callahan, M. K., Walker, D., Rollin, L., Bhore, R., Hodi, F. S., and Larkin, J. (2017) Overall Survival with Combined Nivolumab and Ipilimumab in Advanced Melanoma. *N. Engl. J. Med.* **377**, 1345–1356

129. Arques, J. L., Hautefort, I., Ivory, K., Bertelli, E., Regoli, M., Clare, S., Hinton, J. C. D., and Nicoletti, C. (2009) Salmonella Induces Flagellin- and MyD88-Dependent Migration of Bacteria-Capturing Dendritic Cells Into the Gut Lumen. *Gastroenterology* **137**, 579-587.e2

130. McDole, J. R., Wheeler, L. W., McDonald, K. G., Wang, B., Konjufca, V., Knoop, K. A., Newberry, R. D., and Miller, M. J. (2012) Goblet cells deliver luminal antigen to $CD103^+$ dendritic cells in the small intestine. *Nature* **483**, 345–349

131. Mowat, A. M. and Agace, W. W. (2014) Regional specialization within the intestinal immune system. *Nat. Rev. Immunol.* **14**, 667–685

132. Queirolo, P., Morabito, A., Laurent, S., Lastraioli, S., Piccioli, P., Ascierto, P. A., Gentilcore, G., Serra, M., Marasco, A., Tornari, E., Dozin, B., and Pistillo, M. P. (2013) Association of CTLA-4 Polymorphisms with Improved Overall Survival in Melanoma Patients Treated with CTLA-4 Blockade: A Pilot Study. *Cancer Invest.* **31**, 336–345

133. Caporaso, J. G., Lauber, C. L., Walters, W. A., Berg-Lyons, D., Huntley, J., Fierer, N., Owens, S. M., Betley, J., Fraser, L., Bauer, M., Gormley, N., Gilbert, J. A., Smith, G., and Knight, R. (2012) Ultra-high-throughput microbial community analysis on the Illumina HiSeq and MiSeq platforms. *ISME J.* **6**, 1621–1624

134. Caporaso, J. G., Lauber, C. L., Walters, W. A., Berg-Lyons, D., Lozupone, C. A., Turnbaugh, P. J., Fierer, N., and Knight, R. (2011) Global patterns of 16S rRNA diversity at a depth of millions of sequences per sample. *Proc. Natl. Acad. Sci.* **108**, 4516–4522

135. Caporaso, J. G., Kuczynski, J., Stombaugh, J., Bittinger, K., Bushman, F. D., Costello, E. K., Fierer, N., Peña, A. G., Goodrich, J. K., Gordon, J. I., Huttley, G. A., Kelley, S. T., Knights, D., Koenig, J. E., Ley, R. E., Lozupone, C. A., McDonald, D., Muegge, B. D., Pirrung, M., Reeder, J., Sevinsky, J. R., Turnbaugh, P. J., Walters, W. A., Widmann, J., Yatsunenko, T., Zaneveld, J., and Knight, R. (2010) QIIME allows analysis of high-throughput community sequencing data. *Nat. Methods* **7**, 335–336

136. McDonald, D., Price, M. N., Goodrich, J., Nawrocki, E. P., DeSantis, T. Z., Probst, A., Andersen, G. L., Knight, R., and Hugenholtz, P. (2012) An improved Greengenes taxonomy with explicit ranks for ecological and evolutionary analyses of bacteria and archaea. *ISME J.* **6**, 610–618

137. Caporaso, J. G., Bittinger, K., Bushman, F. D., DeSantis, T. Z., Andersen, G. L., and Knight, R. (2010) PyNAST: a flexible tool for aligning sequences to a template alignment. *Bioinforma. Oxf. Engl.* **26**, 266–267

138. Edgar, R. C. (2010) Search and clustering orders of magnitude faster than BLAST. *Bioinforma. Oxf. Engl.* **26**, 2460–2461

139. Bolyen, E., Rideout, J. R., Dillon, M. R., Bokulich, N. A., Abnet, C. C., Al-Ghalith, G. A., Alexander, H., Alm, E. J., Arumugam, M., Asnicar, F., Bai, Y., Bisanz, J. E., Bittinger, K., Brejnrod, A., Brislawn, C. J., Brown, C. T., Callahan, B. J., Caraballo-Rodríguez, A. M., Chase, J., Cope, E. K., Da Silva, R., Diener, C., Dorrestein, P. C., Douglas, G. M., Durall, D. M., Duvallet, C., Edwardson, C. F., Ernst, M., Estaki, M., Fouquier, J., Gauglitz, J. M., Gibbons, S. M., Gibson, D. L., Gonzalez, A., Gorlick, K., Guo, J., Hillmann, B., Holmes, S., Holste, H., Huttenhower, C., Huttley, G. A., Janssen, S., Jarmusch, A. K., Jiang, L., Kaehler, B. D., Kang, K. B., Keefe, C. R., Keim, P., Kelley, S. T., Knights, D., Koester, I., Kosciolek, T., Kreps, J., Langille, M. G. I., Lee, J.,

Ley, R., Liu, Y.-X., Loftfield, E., Lozupone, C., Maher, M., Marotz, C., Martin, B. D., McDonald, D., McIver, L. J., Melnik, A. V., Metcalf, J. L., Morgan, S. C., Morton, J. T., Naimey, A. T., Navas-Molina, J. A., Nothias, L. F., Orchanian, S. B., Pearson, T., Peoples, S. L., Petras, D., Preuss, M. L., Pruesse, E., Rasmussen, L. B., Rivers, A., Robeson, M. S., Rosenthal, P., Segata, N., Shaffer, M., Shiffer, A., Sinha, R., Song, S. J., Spear, J. R., Swafford, A. D., Thompson, L. R., Torres, P. J., Trinh, P., Tripathi, A., Turnbaugh, P. J., Ul-Hasan, S., van der Hooft, J. J. J., Vargas, F., Vázquez-Baeza, Y., Vogtmann, E., von Hippel, M., Walters, W., Wan, Y., Wang, M., Warren, J., Weber, K. C., Williamson, C. H. D., Willis, A. D., Xu, Z. Z., Zaneveld, J. R., Zhang, Y., Zhu, Q., Knight, R., and Caporaso, J. G. (2019) Reproducible, interactive, scalable and extensible microbiome data science using QIIME 2. *Nat. Biotechnol.* **37**, 852–857

140. Katoh, K., Misawa, K., Kuma, K., and Miyata, T. (2002) MAFFT: a novel method for rapid multiple sequence alignment based on fast Fourier transform. *Nucleic Acids Res.* **30**, 3059–3066

141. Price, M. N., Dehal, P. S., and Arkin, A. P. (2010) FastTree 2--approximately maximum-likelihood trees for large alignments. *PloS One* **5**, e9490

142. Faith, D. P. (2007) The Role of the Phylogenetic Diversity Measure, PD, in Bio-informatics: Getting the Definition Right. *Evol. Bioinforma. Online* **2**, 277–283

143. Lozupone, C. and Knight, R. (2005) UniFrac: a new phylogenetic method for comparing microbial communities. *Appl. Environ. Microbiol.* **71**, 8228–8235

144. Lozupone, C. A., Stombaugh, J. I., Gordon, J. I., Jansson, J. K., and Knight, R. (2012) Diversity, stability and resilience of the human gut microbiota. *Nature* **489**, 220–230

145. Bokulich, N. A., Kaehler, B. D., Rideout, J. R., Dillon, M., Bolyen, E., Knight, R., Huttley, G. A., and Gregory Caporaso, J. (2018) Optimizing taxonomic classification of marker-gene amplicon sequences with QIIME 2's q2-feature-classifier plugin. *Microbiome* **6**, 90

146. Benjamini, Y. and Hochberg, Y. (1995) Controlling the False Discovery Rate: A Practical and Powerful Approach to Multiple Testing. *J. R. Stat. Soc. Ser. B Methodol.* **57**, 289–300

147. Segata, N., Waldron, L., Ballarini, A., Narasimhan, V., Jousson, O., and Huttenhower, C. (2012) Metagenomic microbial community profiling using unique clade-specific marker genes. *Nat. Methods* **9**, 811–814

148. Methé, B. A., Nelson, K. E., Pop, M., Creasy, H. H., Giglio, M. G., Huttenhower, C., Gevers, D., Petrosino, J. F., Abubucker, S., Badger, J. H., Chinwalla, A. T., Earl, A. M., FitzGerald, M. G., Fulton, R. S., Hallsworth-Pepin, K., Lobos, E. A., Madupu, R., Magrini, V., Martin, J. C., Mitreva, M., Muzny, D. M., Sodergren, E. J., Versalovic, J., Wollam, A. M., Worley, K. C., Wortman, J. R., Young, S. K., Zeng, Q., Aagaard, K. M., Abolude, O. O., Allen-Vercoe, E., Alm, E. J., Alvarado, L., Andersen, G. L., Anderson, S., Appelbaum, E., Arachchi, H. M., Armitage, G., Arze, C. A., Ayvaz, T., Baker, C. C., Begg, L., Belachew, T., Bhonagiri, V., Bihan, M., Blaser, M. J., Bloom, T., Bonazzi, V. R., Brooks, P., Buck, G. A., Buhay, C. J., Busam, D. A., Campbell, J. L., Canon, S. R., Cantarel, B. L., Chain, P. S., Chen, I.-M. A., Chen, L., Chhibba, S., Chu, K., Ciulla, D. M., Clemente, J. C., Clifton, S. W., Conlan, S., Crabtree, J., Cutting, M. A., Davidovics, N. J., Davis, C. C., DeSantis, T. Z., Deal, C., Delehaunty, K. D., Dewhirst, F. E., Deych, E., Ding, Y., Dooling, D. J., Dugan, S. P., Michael Dunne, W., Scott Durkin, A., Edgar, R. C., Erlich, R. L., Farmer, C. N., Farrell, R. M., Faust, K., Feldgarden, M., Felix, V. M., Fisher, S., Fodor, A. A., Forney, L., Foster, L., Di Francesco, V., Friedman, J., Friedrich, D. C., Fronick, C. C., Fulton, L. L., Gao, H., Garcia,

N., Giannoukos, G., Giblin, C., Giovanni, M. Y., Goldberg, J. M., Goll, J., Gonzalez, A., Griggs, A., Gujja, S., Haas, B. J., Hamilton, H. A., Harris, E. L., Hepburn, T. A., Herter, B., Hoffmann, D. E., Holder, M. E., Howarth, C., Huang, K. H., Huse, S. M., Izard, J., Jansson, J. K., Jiang, H., Jordan, C., Joshi, V., Katancik, J. A., Keitel, W. A., Kelley, S. T., Kells, C., Kinder-Haake, S., King, N. B., Knight, R., Knights, D., Kong, H. H., Koren, O., Koren, S., Kota, K. C., Kovar, C. L., Kyrpides, N. C., La Rosa, P. S., Lee, S. L., Lemon, K. P., Lennon, N., Lewis, C. M., Lewis, L., Ley, R. E., Li, K., Liolios, K., Liu, B., Liu, Y., Lo, C.-C., Lozupone, C. A., Dwayne Lunsford, R., Madden, T., Mahurkar, A. A., Mannon, P. J., Mardis, E. R., Markowitz, V. M., Mavrommatis, K., McCorrison, J. M., McDonald, D., McEwen, J., McGuire, A. L., McInnes, P., Mehta, T., Mihindukulasuriya, K. A., Miller, J. R., Minx, P. J., Newsham, I., Nusbaum, C., O'Laughlin, M., Orvis, J., Pagani, I., Palaniappan, K., Patel, S. M., Pearson, M., Peterson, J., Podar, M., Pohl, C., Pollard, K. S., Priest, M. E., Proctor, L. M., Qin, X., Raes, J., Ravel, J., Reid, J. G., Rho, M., Rhodes, R., Riehle, K. P., Rivera, M. C., Rodriguez-Mueller, B., Rogers, Y.-H., Ross, M. C., Russ, C., Sanka, R. K., Sankar, P., Fah Sathirapongsasuti, J., Schloss, J. A., Schloss, P. D., Schmidt, T. M., Scholz, M., Schriml, L., Schubert, A. M., Segata, N., Segre, J. A., Shannon, W. D., Sharp, R. R., Sharpton, T. J., Shenoy, N., Sheth, N. U., Simone, G. A., Singh, I., Smillie, C. S., Sobel, J. D., Sommer, D. D., Spicer, P., Sutton, G. G., Sykes, S. M., Tabbaa, D. G., Thiagarajan, M., Tomlinson, C. M., Torralba, M., Treangen, T. J., Truty, R. M., Vishnivetskaya, T. A., Walker, J., Wang, L., Wang, Z., Ward, D. V., Warren, W., Watson, M. A., Wellington, C., Wetterstrand, K. A., White, J. R., Wilczek-Boney, K., Qing Wu, Y., Wylie, K. M., Wylie, T., Yandava, C., Ye, L., Ye, Y., Yooseph, S., Youmans, B. P., Zhang, L., Zhou, Y., Zhu, Y., Zoloth, L., Zucker, J. D., Birren, B. W., Gibbs, R. A., Highlander, S. K., Weinstock, G. M., Wilson, R. K., White, O., and The Human Microbiome Project Consortium. (2012) A framework for human microbiome research. *Nature* **486**, 215–221

149. Collado, M. C., Derrien, M., Isolauri, E., Vos, W. M. de, and Salminen, S. (2007) Intestinal Integrity and Akkermansia muciniphila, a Mucin-Degrading Member of the Intestinal Microbiota Present in Infants, Adults, and the Elderly. *Appl. Environ. Microbiol.* **73**, 7767–7770

150. Junick, J. and Blaut, M. (2012) Quantification of Human Fecal Bifidobacterium Species by Use of Quantitative Real-Time PCR Analysis Targeting the groEL Gene. *Appl. Environ. Microbiol.* **78**, 2613–2622

151. Malinen, E., Kassinen, A., Rinttilä, T., and Palva, A. (2003) Comparison of real-time PCR with SYBR Green I or 5'-nuclease assays and dot-blot hybridization with rDNA-targeted oligonucleotide probes in quantification of selected faecal bacteria. *Microbiol. Read. Engl.* **149**, 269–277

152. Matsuki, T., Watanabe, K., Tanaka, R., and Oyaizu, H. (1998) Rapid identification of human intestinal bifidobacteria by 16S rRNA-targeted species- and group-specific primers. *FEMS Microbiol. Lett.* **167**, 113–121

153. Kassinen, A., Krogius-Kurikka, L., Mäkivuokko, H., Rinttilä, T., Paulin, L., Corander, J., Malinen, E., Apajalahti, J., and Palva, A. (2007) The fecal microbiota of irritable bowel syndrome patients differs significantly from that of healthy subjects. *Gastroenterology* **133**, 24–33

154. Rathnayake, I. U., Hargreaves, M., and Huygens, F. (2011) Genotyping of Enterococcus faecalis and Enterococcus faecium Isolates by Use of a Set of Eight Single Nucleotide Polymorphisms. *J. Clin. Microbiol.* **49**, 367–372

155. Rinttilä, T., Kassinen, A., Malinen, E., Krogius, L., and Palva, A. (2004) Development of an extensive set of 16S rDNA-targeted primers for quantification of pathogenic and indigenous bacteria in faecal samples by real-time PCR. *J. Appl. Microbiol.* **97**, 1166–1177

156. Sun, Z., Chen, Z., Hou, X., Li, S., Zhu, H., Qian, J., Lu, D., and Liu, W. (2008) Locked nucleic acid pentamers as universal PCR primers for genomic DNA amplification. *PloS One* **3**, e3701

157. Matsuda, K., Tsuji, H., Asahara, T., Matsumoto, K., Takada, T., and Nomoto, K. (2009) Establishment of an Analytical System for the Human Fecal Microbiota, Based on Reverse Transcription-Quantitative PCR Targeting of Multicopy rRNA Molecules. *Appl. Environ. Microbiol.* **75**, 1961–1969

158. Louis, P., McCrae, S. I., Charrier, C., and Flint, H. J. (2007) Organization of butyrate synthetic genes in human colonic bacteria: phylogenetic conservation and horizontal gene transfer. *FEMS Microbiol. Lett.* **269**, 240–247

159. Huijsdens, X. W., Linskens, R. K., Mak, M., Meuwissen, S. G. M., Vandenbroucke-Grauls, C. M. J. E., and Savelkoul, P. H. M. (2002) Quantification of Bacteria Adherent to Gastrointestinal Mucosa by Real-Time PCR. *J. Clin. Microbiol.* **40**, 4423–4427

160. Tong, J., Liu, C., Summanen, P., Xu, H., and Finegold, S. M. (2011) Application of quantitative real-time PCR for rapid identification of Bacteroides fragilis group and related organisms in human wound samples. *Anaerobe* **17**, 64–68

161. Yampara-Iquise, H., Zheng, G., Jones, J. E., and Carson, C. A. (2008) Use of a Bacteroides thetaiotaomicron-specific alpha-1-6, mannanase quantitative PCR to detect human faecal pollution in water. *J. Appl. Microbiol.* **105**, 1686–1693

162. Song, S. J., Lauber, C., Costello, E. K., Lozupone, C. A., Humphrey, G., Berg-Lyons, D., Caporaso, J. G., Knights, D., Clemente, J. C., Nakielny, S., Gordon, J. I., Fierer, N., and Knight, R. (2013) Cohabiting family members share microbiota with one another and with their dogs. *eLife* **2**, e00458

163. Buffie, C. G., Jarchum, I., Equinda, M., Lipuma, L., Gobourne, A., Viale, A., Ubeda, C., Xavier, J., and Pamer, E. G. (2012) Profound Alterations of Intestinal Microbiota following a Single Dose of Clindamycin Results in Sustained Susceptibility to Clostridium difficile-Induced Colitis. *Infect. Immun.* **80**, 62–73

164. Andrews, S., Krueger, F., Segonds-Pichon, A., Biggins, L., Krueger, C., and Wingett, S. (2012) FastQC. Babraham, UK

165. Bray, N. L., Pimentel, H., Melsted, P., and Pachter, L. (2016) Near-optimal probabilistic RNA-seq quantification. *Nat. Biotechnol.* **34**, 525–527

166. Soneson, C., Love, M. I., and Robinson, M. D. (2015) Differential analyses for RNA-seq: transcript-level estimates improve gene-level inferences. *F1000Research* **4**, 1521

167. Aran, D., Hu, Z., and Butte, A. J. (2017) xCell: digitally portraying the tissue cellular heterogeneity landscape. *Genome Biol.* **18**

168. Blank, C., Brown, I., Peterson, A. C., Spiotto, M., Iwai, Y., Honjo, T., and Gajewski, T. F. (2004) PD-L1/B7H-1 Inhibits the Effector Phase of Tumor Rejection by T Cell Receptor (TCR) Transgenic CD8+ T Cells. *Cancer Res.* **64**, 1140–1145

169. Furuta, G. T., Turner, J. R., Taylor, C. T., Hershberg, R. M., Comerford, K., Narravula, S., Podolsky, D. K., and Colgan, S. P. (2001) Hypoxia-Inducible Factor 1–Dependent Induction of Intestinal Trefoil Factor Protects Barrier Function during Hypoxia. *J. Exp. Med.* **193**, 1027–1034

170. Stuart, T., Butler, A., Hoffman, P., Hafemeister, C., Papalexi, E., Mauck, W. M., Hao, Y., Stoeckius, M., Smibert, P., and Satija, R. (2019) Comprehensive Integration of Single-Cell Data. *Cell* **177**, 1888-1902.e21

171. Hafemeister, C. and Satija, R. (2019) Normalization and variance stabilization of single-cell RNA-seq data using regularized negative binomial regression. *Genome Biol.* **20**, 296

172. Butler, A., Hoffman, P., Smibert, P., Papalexi, E., and Satija, R. (2018) Integrating single-cell transcriptomic data across different conditions, technologies, and species. *Nat. Biotechnol.* **36**, 411–420

173. Zappia, L. and Oshlack, A. (2018) Clustering trees: a visualization for evaluating clusterings at multiple resolutions. *GigaScience* **7**

174. Finak, G., McDavid, A., Yajima, M., Deng, J., Gersuk, V., Shalek, A. K., Slichter, C. K., Miller, H. W., McElrath, M. J., Prlic, M., Linsley, P. S., and Gottardo, R. (2015) MAST: a flexible statistical framework for assessing transcriptional changes and characterizing heterogeneity in single-cell RNA sequencing data. *Genome Biol.* **16**, 278

175. Ourthiague, D. R., Birnbaum, H., Ortenlöf, N., Vargas, J. D., Wollman, R., and Hoffmann, A. (2015) Limited specificity of IRF3 and ISGF3 in the transcriptional innate-immune response to double-stranded RNA. *J. Leukoc. Biol.* **98**, 119–128

176. Roberson, S. M. and Walker, W. S. (1988) Immortalization of cloned mouse splenic macrophages with a retrovirus containing the v-raf/mil and v-myc oncogenes. *Cell. Immunol.* **116**, 341–351

177. Corrales, L., Matson, V., Flood, B., Spranger, S., and Gajewski, T. F. (2017) Innate immune signaling and regulation in cancer immunotherapy. *Cell Res.* **27**, 96–108

178. Topalian, S. L., Hodi, F. S., Brahmer, J. R., Gettinger, S. N., Smith, D. C., McDermott, D. F., Powderly, J. D., Carvajal, R. D., Sosman, J. A., Atkins, M. B., Leming, P. D., Spigel, D. R., Antonia, S. J., Horn, L., Drake, C. G., Pardoll, D. M., Chen, L., Sharfman, W. H., Anders, R. A., Taube, J. M., McMiller, T. L., Xu, H., Korman, A. J., Jure-Kunkel, M., Agrawal, S., McDonald, D., Kollia, G. D., Gupta, A., Wigginton, J. M., and Sznol, M. (2012) Safety, activity, and immune correlates of anti-PD-1 antibody in cancer. *N. Engl. J. Med.* **366**, 2443–2454

179. Robert, C., Schachter, J., Long, G. V., Arance, A., Grob, J. J., Mortier, L., Daud, A., Carlino, M. S., McNeil, C., Lotem, M., Larkin, J., Lorigan, P., Neyns, B., Blank, C. U., Hamid, O., Mateus, C., Shapira-Frommer, R., Kosh, M., Zhou, H., Ibrahim, N., Ebbinghaus, S., Ribas, A., and KEYNOTE-006 investigators. (2015) Pembrolizumab versus Ipilimumab in Advanced Melanoma. *N. Engl. J. Med.* **372**, 2521–2532

180. Daillère, R., Vétizou, M., Waldschmitt, N., Yamazaki, T., Isnard, C., Poirier-Colame, V., Duong, C. P. M., Flament, C., Lepage, P., Roberti, M. P., Routy, B., Jacquelot, N., Apetoh, L., Becharef, S., Rusakiewicz, S., Langella, P., Sokol, H., Kroemer, G., Enot, D., Roux, A., Eggermont, A., Tartour, E., Johannes, L., Woerther, P.-L., Chachaty, E., Soria, J.-C., Golden, E., Formenti, S., Plebanski, M., Madondo, M., Rosenstiel, P., Raoult, D., Cattoir, V., Boneca, I. G., Chamaillard, M., and

Zitvogel, L. (2016) Enterococcus hirae and Barnesiella intestinihominis Facilitate Cyclophosphamide-Induced Therapeutic Immunomodulatory Effects. *Immunity* **45**, 931–943

181. Ugurel, S., Schrama, D., Keller, G., Schadendorf, D., Bröcker, E.-B., Houben, R., Zapatka, M., Fink, W., Kaufman, H. L., and Becker, J. C. (2008) Impact of the CCR5 gene polymorphism on the survival of metastatic melanoma patients receiving immunotherapy. *Cancer Immunol. Immunother. CII* **57**, 685–691

182. Elkrief, A., Derosa, L., Kroemer, G., Zitvogel, L., and Routy, B. (2019) The negative impact of antibiotics on outcomes in cancer patients treated with immunotherapy: a new independent prognostic factor? *Ann. Oncol.* **30**, 1572–1579

183. Maier, B., Leader, A. M., Chen, S. T., Tung, N., Chang, C., LeBerichel, J., Chudnovskiy, A., Maskey, S., Walker, L., Finnigan, J. P., Kirkling, M. E., Reizis, B., Ghosh, S., D'Amore, N. R., Bhardwaj, N., Rothlin, C. V., Wolf, A., Flores, R., Marron, T., Rahman, A. H., Kenigsberg, E., Brown, B. D., and Merad, M. (2020) A conserved dendritic-cell regulatory program limits antitumour immunity. *Nature* **580**, 257–262

184. Alshetaiwi, H., Pervolarakis, N., McIntyre, L. L., Ma, D., Nguyen, Q., Rath, J. A., Nee, K., Hernandez, G., Evans, K., Torosian, L., Silva, A., Walsh, C., and Kessenbrock, K. (2020) Defining the emergence of myeloid-derived suppressor cells in breast cancer using single-cell transcriptomics. *Sci. Immunol.* **5**

185. Gabrilovich, D. I. and Nagaraj, S. (2009) Myeloid-derived suppressor cells as regulators of the immune system. *Nat. Rev. Immunol.* **9**, 162–174

186. Youn, J.-I., Collazo, M., Shalova, I. N., Biswas, S. K., and Gabrilovich, D. I. (2012) Characterization of the nature of granulocytic myeloid-derived suppressor cells in tumor-bearing mice. *J. Leukoc. Biol.* **91**, 167–181

187. Millrud, C. R., Bergenfelz, C., and Leandersson, K. (2017) On the origin of myeloid-derived suppressor cells. *Oncotarget* **8**, 3649

188. M, M., D, S., D, M., A, S., L, M., A, M., and C, G. (2018) The yin-yang of the interaction between myelomonocytic cells and NK cells. *Scand. J. Immunol.* **88**, e12705–e12705

189. Matson, V., Fessler, J., Bao, R., Chongsuwat, T., Zha, Y., Alegre, M.-L., Luke, J. J., and Gajewski, T. F. (2018) The commensal microbiome is associated with anti-PD-1 efficacy in metastatic melanoma patients. *Science* **359**, 104–108

190. Frankel, A. E., Coughlin, L. A., Kim, J., Froehlich, T. W., Xie, Y., Frenkel, E. P., and Koh, A. Y. (2017) Metagenomic Shotgun Sequencing and Unbiased Metabolomic Profiling Identify Specific Human Gut Microbiota and Metabolites Associated with Immune Checkpoint Therapy Efficacy in Melanoma Patients. *Neoplasia N. Y. N* **19**, 848–855

191. Chaput, N., Lepage, P., Coutzac, C., Soularue, E., Le Roux, K., Monot, C., Boselli, L., Routier, E., Cassard, L., Collins, M., Vaysse, T., Marthey, L., Eggermont, A., Asvatourian, V., Lanoy, E., Mateus, C., Robert, C., and Carbonnel, F. (2017) Baseline gut microbiota predicts clinical response and colitis in metastatic melanoma patients treated with ipilimumab. *Ann. Oncol.* **28**, 1368–1379

192. Gharaibeh, R. Z. and Jobin, C. (2019) Microbiota and cancer immunotherapy: in search of microbial signals. *Gut* **68**, 385–388

193. Oshi, M., Tokumaru, Y., Asaoka, M., Yan, L., Satyananda, V., Matsuyama, R., Matsuhashi, N., Futamura, M., Ishikawa, T., Yoshida, K., Endo, I., and Takabe, K. (2020) M1 Macrophage and M1/M2 ratio defined by transcriptomic signatures resemble only part of their conventional clinical characteristics in breast cancer. *Sci. Rep.* **10**, 16554

194. Zeng, D., Ye, Z., Wu, J., Zhou, R., Fan, X., Wang, G., Huang, Y., Wu, J., Sun, H., Wang, M., Bin, J., Liao, Y., Li, N., Shi, M., and Liao, W. (2020) Macrophage correlates with immunophenotype and predicts anti-PD-L1 response of urothelial cancer. *Theranostics* **10**, 7002–7014

195. DeNardo, D. G. and Ruffell, B. (2019) Macrophages as regulators of tumor immunity and immunotherapy. *Nat. Rev. Immunol.* **19**, 369–382

196. Peranzoni, E., Lemoine, J., Vimeux, L., Feuillet, V., Barrin, S., Kantari-Mimoun, C., Bercovici, N., Guérin, M., Biton, J., Ouakrim, H., Régnier, F., Lupo, A., Alifano, M., Damotte, D., and Donnadieu, E. (2018) Macrophages impede CD8 T cells from reaching tumor cells and limit the efficacy of anti–PD-1 treatment. *Proc. Natl. Acad. Sci. U. S. A.* **115**, E4041–E4050

197. Zhu, Y., Herndon, J. M., Sojka, D. K., Kim, K.-W., Knolhoff, B. L., Zuo, C., Cullinan, D. R., Luo, J., Bearden, A. R., Lavine, K. J., Yokoyama, W. M., Hawkins, W. G., Fields, R. C., Randolph, G. J., and DeNardo, D. G. (2017) Tissue Resident Macrophages in Pancreatic Ductal Adenocarcinoma Originate from Embryonic Hematopoiesis and Promote Tumor Progression. *Immunity* **47**, 323-338.e6

198. Guerriero, J. L., Sotayo, A., Ponichtera, H. E., Castrillon, J. A., Pourzia, A. L., Schad, S., Johnson, S. F., Carrasco, R. D., Lazo, S., Bronson, R. T., Davis, S. P., Lobera, M., Nolan, M. A., and Letai, A. (2017) Class IIa HDAC inhibition reduces breast tumours and metastases through anti-tumour macrophages. *Nature* **543**, 428–432

199. Weber, R., Fleming, V., Hu, X., Nagibin, V., Groth, C., Altevogt, P., Utikal, J., and Umansky, V. (2018) Myeloid-Derived Suppressor Cells Hinder the Anti-Cancer Activity of Immune Checkpoint Inhibitors. *Front. Immunol.* **9**

200. Gebhardt, C., Sevko, A., Jiang, H., Lichtenberger, R., Reith, M., Tarnanidis, K., Holland-Letz, T., Umansky, L., Beckhove, P., Sucker, A., Schadendorf, D., Utikal, J., and Umansky, V. (2015) Myeloid Cells and Related Chronic Inflammatory Factors as Novel Predictive Markers in Melanoma Treatment with Ipilimumab. *Clin. Cancer Res.* **21**, 5453–5459

201. Martens, A., Wistuba-Hamprecht, K., Foppen, M. G., Yuan, J., Postow, M. A., Wong, P., Romano, E., Khammari, A., Dreno, B., Capone, M., Ascierto, P. A., Giacomo, A. M. D., Maio, M., Schilling, B., Sucker, A., Schadendorf, D., Hassel, J. C., Eigentler, T. K., Martus, P., Wolchok, J. D., Blank, C., Pawelec, G., Garbe, C., and Weide, B. (2016) Baseline Peripheral Blood Biomarkers Associated with Clinical Outcome of Advanced Melanoma Patients Treated with Ipilimumab. *Clin. Cancer Res.* **22**, 2908–2918

202. Meyer, C., Cagnon, L., Costa-Nunes, C. M., Baumgaertner, P., Montandon, N., Leyvraz, L., Michielin, O., Romano, E., and Speiser, D. E. (2014) Frequencies of circulating MDSC correlate with clinical outcome of melanoma patients treated with ipilimumab. *Cancer Immunol. Immunother. CII* **63**, 247–257

203. Sade-Feldman, M., Kanterman, J., Klieger, Y., Ish-Shalom, E., Olga, M., Saragovi, A., Shtainberg, H., Lotem, M., and Baniyash, M. (2016) Clinical Significance of Circulating CD33+CD11b+HLA-DR- Myeloid Cells in Patients with Stage IV Melanoma Treated with Ipilimumab. *Clin. Cancer Res. Off. J. Am. Assoc. Cancer Res.* **22**, 5661–5672

204. Weide, B., Martens, A., Zelba, H., Stutz, C., Derhovanessian, E., Di Giacomo, A. M., Maio, M., Sucker, A., Schilling, B., Schadendorf, D., Büttner, P., Garbe, C., and Pawelec, G. (2014) Myeloid-derived suppressor cells predict survival of patients with advanced melanoma: comparison with regulatory T cells and NY-ESO-1- or melan-A-specific T cells. *Clin. Cancer Res. Off. J. Am. Assoc. Cancer Res.* **20**, 1601–1609

205. Kim, K., Skora, A. D., Li, Z., Liu, Q., Tam, A. J., Blosser, R. L., Diaz, L. A., Papadopoulos, N., Kinzler, K. W., Vogelstein, B., and Zhou, S. (2014) Eradication of metastatic mouse cancers resistant to immune checkpoint blockade by suppression of myeloid-derived cells. *Proc. Natl. Acad. Sci. U. S. A.* **111**, 11774–11779

206. Orillion, A., Hashimoto, A., Damayanti, N., Shen, L., Adelaiye-Ogala, R., Arisa, S., Chintala, S., Ordentlich, P., Kao, C., Elzey, B., Gabrilovich, D., and Pili, R. (2017) Entinostat Neutralizes Myeloid-Derived Suppressor Cells and Enhances the Anti-tumor Effect of PD-1 Inhibition in Murine Models of Lung and Renal Cell Carcinoma. *Clin. Cancer Res. Off. J. Am. Assoc. Cancer Res.* **23**, 5187–5201

207. Clavijo, P. E., Moore, E. C., Chen, J., Davis, R. J., Friedman, J., Kim, Y., Van Waes, C., Chen, Z., and Allen, C. T. (2017) Resistance to CTLA-4 checkpoint inhibition reversed through selective elimination of granulocytic myeloid cells. *Oncotarget* **8**, 55804–55820

208. Holmgaard, R. B., Zamarin, D., Lesokhin, A., Merghoub, T., and Wolchok, J. D. (2016) Targeting myeloid-derived suppressor cells with colony stimulating factor-1 receptor blockade can reverse immune resistance to immunotherapy in indoleamine 2,3-dioxygenase-expressing tumors. *EBioMedicine* **6**, 50–58

209. Mao, Y., Eissler, N., Blanc, K. L., Johnsen, J. I., Kogner, P., and Kiessling, R. (2016) Targeting Suppressive Myeloid Cells Potentiates Checkpoint Inhibitors to Control Spontaneous Neuroblastoma. *Clin. Cancer Res. Off. J. Am. Assoc. Cancer Res.* **22**, 3849–3859

210. Davis, R. J., Moore, E. C., Clavijo, P. E., Friedman, J., Cash, H., Chen, Z., Silvin, C., Van Waes, C., and Allen, C. (2017) Anti-PD-L1 Efficacy Can Be Enhanced by Inhibition of Myeloid-Derived Suppressor Cells with a Selective Inhibitor of PI3Kδ/γ. *Cancer Res.* **77**, 2607–2619

211. Climaco-Arvizu, S., Domínguez-Acosta, O., Cabañas-Cortés, M. A., Rodríguez-Sosa, M., Gonzalez, F. J., Vega, L., and Elizondo, G. (2016) Aryl hydrocarbon receptor influences nitric oxide and arginine production and alters M1/M2 macrophage polarization. *Life Sci.* **155**, 76–84

212. Krishnan, S., Ding, Y., Saedi, N., Choi, M., Sridharan, G. V., Sherr, D. H., Yarmush, M. L., Alaniz, R. C., Jayaraman, A., and Lee, K. (2018) Gut Microbiota-Derived Tryptophan Metabolites Modulate Inflammatory Response in Hepatocytes and Macrophages. *Cell Rep.* **23**, 1099–1111

213. Rothhammer, V. and Quintana, F. J. (2019) The aryl hydrocarbon receptor: an environmental sensor integrating immune responses in health and disease. *Nat. Rev. Immunol.* **19**, 184–197

214. Kim, Y.-G., Udayanga, K. G. S., Totsuka, N., Weinberg, J. B., Núñez, G., and Shibuya, A. (2014) Gut dysbiosis promotes M2 macrophage polarization and allergic airway inflammation via fungi-induced PGE2. *Cell Host Microbe* **15**, 95–102

215. Massberg, S., Schaerli, P., Knezevic-Maramica, I., Köllnberger, M., Tubo, N., Moseman, E. A., Huff, I. V., Junt, T., Wagers, A. J., Mazo, I. B., and von Andrian, U. H. (2007) Immunosurveillance by hematopoietic progenitor cells trafficking through blood, lymph, and peripheral tissues. *Cell* **131**, 994–1008

216. Biswas, S. K. and Lopez-Collazo, E. (2009) Endotoxin tolerance: new mechanisms, molecules and clinical significance. *Trends Immunol.* **30**, 475–487

217. Watson, D. W. and Kim, Y. B. (1963) MODIFICATION OF HOST RESPONSES TO BACTERIAL ENDOTOXINS. I. SPECIFICITY OF PYROGENIC TOLERANCE AND THE ROLE OF HYPERSENSITIVITY IN PYROGENICITY, LETHALITY, AND SKIN REACTIVITY. *J. Exp. Med.* **118**, 425–446

218. Mages, J., Dietrich, H., and Lang, R. (2007) A genome-wide analysis of LPS tolerance in macrophages. *Immunobiology* **212**, 723–737

219. Dobrovolskaia, M. A., Medvedev, A. E., Thomas, K. E., Cuesta, N., Toshchakov, V., Ren, T., Cody, M. J., Michalek, S. M., Rice, N. R., and Vogel, S. N. (2003) Induction of In Vitro Reprogramming by Toll-Like Receptor (TLR)2 and TLR4 Agonists in Murine Macrophages: Effects of TLR "Homotolerance" Versus "Heterotolerance" on NF-κB Signaling Pathway Components. *J. Immunol.* **170**, 508–519

220. Wheeler, M. L., Limon, J. J., Bar, A. S., Leal, C. A., Gargus, M., Tang, J., Brown, J., Funari, V. A., Wang, H. L., Crother, T. R., Arditi, M., Underhill, D. M., and Iliev, I. D. (2016) Immunological Consequences of Intestinal Fungal Dysbiosis. *Cell Host Microbe* **19**, 865–873

221. Li, X., Leonardi, I., Semon, A., Doron, I., Gao, I. H., Putzel, G. G., Kim, Y., Kabata, H., Artis, D., Fiers, W. D., Ramer-Tait, A. E., and Iliev, I. D. (2018) Response to Fungal Dysbiosis by Gut-Resident CX3CR1+ Mononuclear Phagocytes Aggravates Allergic Airway Disease. *Cell Host Microbe* **24**, 847-856.e4

222. Filyk, H. A. and Osborne, L. C. (2016) The Multibiome: The Intestinal Ecosystem's Influence on Immune Homeostasis, Health, and Disease. *EBioMedicine* **13**, 46–54

223. Monaco, C. L., Gootenberg, D. B., Zhao, G., Handley, S. A., Ghebremichael, M. S., Lim, E. S., Lankowski, A., Baldridge, M. T., Wilen, C. B., Flagg, M., Norman, J. M., Keller, B. C., Luévano, J. M., Wang, D., Boum, Y., Martin, J. N., Hunt, P. W., Bangsberg, D. R., Siedner, M. J., Kwon, D. S., and Virgin, H. W. (2016) Altered Virome and Bacterial Microbiome in Human Immunodeficiency Virus-Associated Acquired Immunodeficiency Syndrome. *Cell Host Microbe* **19**, 311–322

224. Norman, J. M., Handley, S. A., Baldridge, M. T., Droit, L., Liu, C. Y., Keller, B. C., Kambal, A., Monaco, C. L., Zhao, G., Fleshner, P., Stappenbeck, T. S., McGovern, D. P. B., Keshavarzian, A., Mutlu, E. A., Sauk, J., Gevers, D., Xavier, R. J., Wang, D., Parkes, M., and Virgin, H. W. (2015) Disease-Specific Alterations in the Enteric Virome in Inflammatory Bowel Disease. *Cell* **160**, 447–460

225. Richardson, S. J. and Horwitz, M. S. (2014) Is Type 1 Diabetes "Going Viral"? *Diabetes* **63**, 2203–2205

226. Zhao, G., Vatanen, T., Droit, L., Park, A., Kostic, A. D., Poon, T. W., Vlamakis, H., Siljander, H., Härkönen, T., Hämäläinen, A. M., Peet, A., Tillmann, V., Ilonen, J., Wang, D., Knip, M., Xavier, R. J., and Virgin, H. W. (2017) Intestinal virome changes precede autoimmunity in type I diabetes-susceptible children. *Proc. Natl. Acad. Sci. U. S. A.* **114**, E6166–E6175

227. Fluckiger, A., Daillère, R., Sassi, M., Sixt, B. S., Liu, P., Loos, F., Richard, C., Rabu, C., Alou, M. T., Goubet, A.-G., Lemaitre, F., Ferrere, G., Derosa, L., Duong, C. P. M., Messaoudene, M., Gagné, A., Joubert, P., Sordi, L. D., Debarbieux, L., Simon, S., Scarlata, C.-M., Ayyoub, M., Palermo, B., Facciolo, F., Boidot, R., Wheeler, R., Boneca, I. G., Sztupinszki, Z., Papp, K., Csabai, I., Pasolli, E., Segata, N., Lopez-Otin, C., Szallasi, Z., Andre, F., Iebba, V., Quiniou, V., Klatzmann, D., Boukhalil, J., Khelaifia, S., Raoult, D., Albiges, L., Escudier, B., Eggermont, A., Mami-Chouaib, F., Nistico, P., Ghiringhelli, F., Routy, B., Labarrière, N., Cattoir, V., Kroemer, G., and Zitvogel, L. (2020) Cross-reactivity between tumor MHC class I–restricted antigens and an enterococcal bacteriophage. *Science* **369**, 936–942

228. Derosa, L., Hellmann, M. D., Spaziano, M., Halpenny, D., Fidelle, M., Rizvi, H., Long, N., Plodkowski, A. J., Arbour, K. C., Chaft, J. E., Rouche, J. A., Zitvogel, L., Zalcman, G., Albiges, L., Escudier, B., and Routy, B. (2018) Negative association of antibiotics on clinical activity of immune checkpoint inhibitors in patients with advanced renal cell and non-small-cell lung cancer. *Ann. Oncol.* **29**, 1437–1444

229. Galloway-Peña, J. R., Jenq, R. R., and Shelburne, S. A. (2017) Can Consideration of the Microbiome Improve Antimicrobial Utilization and Treatment Outcomes in the Oncology Patient? *Clin. Cancer Res.* **23**, 3263–3268

230. Rohlke, F. and Stollman, N. (2012) Fecal microbiota transplantation in relapsing Clostridium difficile infection. *Ther. Adv. Gastroenterol.* **5**, 403–420

231. Baruch, E. N., Youngster, I., Ben-Betzalel, G., Ortenberg, R., Lahat, A., Katz, L., Adler, K., Dick-Necula, D., Raskin, S., Bloch, N., Rotin, D., Anafi, L., Avivi, C., Melnichenko, J., Steinberg-Silman, Y., Mamtani, R., Harati, H., Asher, N., Shapira-Frommer, R., Brosh-Nissimov, T., Eshet, Y., Ben-Simon, S., Ziv, O., Khan, M. A. W., Amit, M., Ajami, N. J., Barshack, I., Schachter, J., Wargo, J. A., Koren, O., Markel, G., and Boursi, B. (2020) Fecal microbiota transplant promotes response in immunotherapy-refractory melanoma patients. *Science*

232. David, L. A., Maurice, C. F., Carmody, R. N., Gootenberg, D. B., Button, J. E., Wolfe, B. E., Ling, A. V., Devlin, A. S., Varma, Y., Fischbach, M. A., Biddinger, S. B., Dutton, R. J., and Turnbaugh, P. J. (2014) Diet rapidly and reproducibly alters the human gut microbiome. *Nature* **505**, 559–563

233. Lim, B., Zimmermann, M., Barry, N. A., and Goodman, A. L. (2017) Engineered Regulatory Systems Modulate Gene Expression of Human Commensals in the Gut. *Cell* **169**, 547-558.e15

234. Shepherd, E. S., DeLoache, W. C., Pruss, K. M., Whitaker, W. R., and Sonnenburg, J. L. (2018) An exclusive metabolic niche enables strain engraftment in the gut microbiota. *Nature* **557**, 434–438

235. Guo, C.-J., Chang, F.-Y., Wyche, T. P., Backus, K. M., Acker, T. M., Funabashi, M., Taketani, M., Donia, M. S., Nayfach, S., Pollard, K. S., Craik, C. S., Cravatt, B. F., Clardy, J., Voigt, C. A., and

Fischbach, M. A. (2017) Discovery of Reactive Microbiota-Derived Metabolites that Inhibit Host Proteases. *Cell* **168**, 517-526.e18

236. Mullard, A. (2018) Oncologists tap the microbiome in bid to improve immunotherapy outcomes. *Nat. Rev. Drug Discov.*